

**MICROBIAL USAGE OF DIVERSE ELECTRON DONORS IN
MARINE NITROGEN LOSS**

A Dissertation
Presented to
The Academic Faculty

by

Claire Elise Elbon

In Partial Fulfillment
of the Requirements for the Degree
of Doctor of Philosophy in the
Program of Ocean Science and Engineering
in the School of Earth and Atmospheric Sciences

Georgia Institute of Technology
May 2025

COPYRIGHT © 2025 BY CLAIRE ELISE ELBON

MICROBIAL USAGE OF DIVERSE ELECTRON DONORS IN MARINE NITROGEN LOSS

Approved by:

Dr. Jennifer Glass, Advisor
School of Earth and Atmospheric Sciences
Georgia Institute of Technology

Dr. Frank Stewart
Department of Microbiology
& Cell Biology
Montana State University

Dr. Joel Kostka
School of Biological Sciences
Georgia Institute of Technology

Dr. Laura Bristow
Department of Marine Sciences
University of Gothenburg

Dr. Ameet Pinto
School of Civil and Environmental
Engineering
Georgia Institute of Technology

Date Approved: [03, 11, 2025]

“Even in the vast and mysterious reaches of the sea we are brought back to the
fundamental truth that nothing lives to itself”

-Rachel Carson, *Silent Spring*

ACKNOWLEDGEMENTS

A massive thank you to my advisor, Jennifer Glass. I would not be writing this thesis without her unwavering support, mentorship, and commitment to diversity, equity, and inclusion over the past 5 years. I will continue to look up to her to be a better scientist throughout the rest of my career as she leads by example. Thank you for always being in my corner.

Thank you and merci beaucoup to all of my wonderful lab siblings through this journey. Thank you to my “big sisters” and “little sisters” in the Glass lab for their incredible support, especially while I started during COVID-19. Thank you all for lunch check-ins, assistance/dance parties in the lab, and feedback on talks, research papers, and this thesis.

Thank you to the rest of my committee members, Joel Kostka, Ameet Pinto, Frank Stewart, and Laura Bristow, for their mentorship in class, in the lab, and at sea. Thank you to Joel Kostka for mentorship in the classroom and collaboration with his student, Gabby Krueger and research assistant, Michael Stone, by providing *Marinobacter* samples and access to growth plate readers. Thank you to Ameet Pinto for their excitement in this thesis and wealth of knowledge contributing to these projects. Thank you to Frank Stewart for the seawater samples full of fun microbes, and his continued collaboration and invaluable input for the duration of this PhD. Thank you to Laura Bristow for her mentorship, abundance of paper suggestions, and support both at sea and on land.

Thank you to all my collaborators over this PhD. Thank you to all the folks in the Oceans Across Space and Time project for research opportunities and support (OAST). Massive thanks to undergraduate research assistants Hector, Helen, Emma, Aya, and high school research student Amy for their enthusiasm and hard work growing microbes and imaging them. Thank you to the R/V *Atlantis* science team and crew as well as the R/V *Point Sur* science team and crew for supporting the science and scientists onboard. Thank you to Ashley Kleinman of the GLOW project at Cornell and providing high quality metagenomic sequences and MAGs of *Marinobacter pacificus* sp. nov. Thank you to Brook Nunn, Michael Riffle, and Emma Timmins-Schiffman of the Environmental Proteomics Center/University of Washington for your incredible generosity, enthusiasm for this project, and expertise in proteomics on *Marinobacter pacificus* sp. nov.

Thank you to my funding sources. Thanks to the Presidents Fellowship at Georgia Tech for continued support over 4 years. Thanks to the OAST grant for the ability to focus on research during my 1st and 2nd summer and opportunities for field research. Thank you to the National Science Foundation for a Graduate Research Fellowship to focus on this thesis. Thank you to the Center for Promoting Inclusive and Equity in Science for funds to assist with travel to University of Washington to learn proteomics.

Thank you and merci beaucoup to all my friends and family. Thank you to Richard and Roska for everything.

TABLE OF CONTENTS

ACKNOWLEDGEMENTS	iv
LIST OF TABLES	ix
LIST OF FIGURES	x
LIST OF SYMBOLS AND ABBREVIATIONS	xvi
SUMMARY	xviii
CHAPTER 1. Anoxic marine systems and their biogeochemistry: zones of intense nitrogen loss	1
1.1 Abstract	1
1.2 Physical oceanography of anoxic marine systems	1
1.2.1 Intermediate water anoxic marine systems: oxygen deficient zones	2
1.2.2 Deep water anoxic marine systems: deep hypersaline anoxic basins	4
1.3 Biogeochemistry of electron acceptors in two anoxic marine systems	6
1.3.1 Oxygen	6
1.3.2 Nitrogen	7
1.4 Biogeochemistry of electron donors in two anoxic marine systems	11
1.4.1 Methane	12
1.4.2 Manganese	14
1.5 Potential for denitrification concurrent with methane and manganese oxidation	16
1.5.1 Nitrate/nitrite reduction coupled to methane oxidation	16
1.5.2 Nitrate reduction coupled to manganese oxidation	17
1.6 Research scopes and objectives	18
CHAPTER 2. Novel Alphaproteobacteria transcribe genes for nitric oxide transformation at high levels in a marine oxygen deficient zone	19
2.1 Abstract	19
2.2 Introduction	20
2.3 Methods	21
2.3.1 Nod phylogeny and gene neighborhood	22
2.3.2 Transcription of nod genes in ETNP ODZ depth profiles	22
2.3.3 Metagenomic binning	22
2.3.4 Alphaproteobacterial NuoL phylogeny	23
2.3.5 Mapping transcripts to metagenomic bins	24
2.3.6 Cellular localization and heme numbers	24
2.4 Data availability	24
2.5 Results	25
2.5.1 Transcribed nod sequences in the ETNP ODZ belong to Alphaproteobacteria, Gammaproteobacteria, and Planctomycetia	25
2.5.2 Alphaproteobacterial nod is highly transcribed in anoxic waters.	28

2.5.3	MAGs with highly transcribed nod gene represent a new order of Alphaproteobacteria.	30
2.5.4	Alphaproteobacteria transcribe genes for formate metabolism, aerobic respiration, and a multiheme cytochrome complex	31
2.6	Discussion	35
2.7	Conclusion	38
CHAPTER 3. Denitrifying <i>Marinobacter pacificus</i> sp. nov. from an oxygen deficient zone grows under a methane headspace and oxidizes ethanol, methanol, and formate		40
3.1	Abstract	40
3.2	Introduction	41
3.3	Methods	44
3.3.1	Culture enrichment and transfers	44
3.3.2	Nutrient quantification	50
3.3.3	Microbial identification and activity	52
3.4	Results	57
3.4.1	Methane stimulates bacterial growth in long term enrichments	57
3.4.2	Secondary transfers of bottle 69 produce nitrous oxide under methane	59
3.4.3	<i>Marinobacter</i> spp. dominate in transfers with nitrate	61
3.4.4	Cellular autofluorescence emits at 465 nm in unstained cells	63
3.4.5	Autofluorescence in related bacteria	65
3.4.6	Consistent nitrate reduction supports growth both aerobically and anaerobically over enrichment of <i>Marinobacter</i>	66
3.4.7	<i>Marinobacter pacificus</i> sp. nov. forms a clade with two uncultured strains	68
3.4.8	Alcohol and formate dehydrogenase, ATP synthase for cell division are significantly abundant under methane and denitrifying conditions	69
3.4.9	<i>Marinobacter pacificus</i> sp. nov grows on formate, ethanol, and methanol as the sole carbon source	74
3.4.10	95% methane bottle cultures contain methanol and formaldehyde in the headspace	75
3.5	Discussion	77
3.6	Conclusion	81
CHAPTER 4. Identification and characterization of manganese-oxide associated microbes above a deep hypersaline anoxic basin		83
4.1	Abstract	83
4.2	Introduction	84
4.3	Methods	86
4.3.1	Field geochemical sampling	86
4.3.2	Field anoxic water sampling for cultures and filter sampling	88
4.3.3	Simul-staining and imaging of manganese oxides and microbial cells	89
4.3.4	Sterile Orca Basin media	90
4.3.5	Anoxic enrichment cultures	90
4.3.6	Scanning electron microscopy coupled with energy dispersive x-ray spectroscopy	91
4.3.7	X-ray Absorption Spectroscopy	91

4.3.8	Nitrate, nitrite, and nitrous oxide quantification	92
4.3.9	Manganese oxide quantification	93
4.3.10	Oxygen measurements	93
4.3.11	16S rRNA Sequencing	94
4.3.12	Metagenomics	94
4.3.13	Metatranscriptomics	98
4.4	Results	98
4.4.1	Orca Basin redoxcline geochemistry	98
4.4.2	Manganese particles co-located with cells are only detected at 2200 m	99
4.4.3	Manganese particles produced by culture transfers are likely δ -MnO ₂ and coated in cellular biofilms	102
4.4.4	Low-suboxic enrichments from 2200 meters consume nitrate and produce manganese oxides	104
4.4.5	MnO _x producing transfers from ~2200 meters are dominated by <i>Marinobacter</i> and <i>Idiomarina</i> spp	108
4.4.6	Nitrospirota are present and transcriptionally active at ~2200 meters	110
4.5	Discussion	112
4.6	Conclusion	115
CHAPTER 5.	Conclusions and future directions	117
5.1	Novel bacteria contribute to nitrogen loss in anoxic marine systems	117
5.2	Methanol, formaldehyde and formate utilization in the ETNP ODZ	118
5.3	Manganese oxidation in Orca Basin	119
5.4	Low-suboxic seawater amended with nitrate selects for <i>Marinobacter</i> spp.	119
5.5	Future directions	120
REFERENCES		121

LIST OF TABLES

Table 1	Bottle IDs for primary enrichments from May 2017.	44
Table 2	Respiration and growth proteins that are highly abundant in both methane and helium headspaces. Significantly different abundance is reported as log fold change (logFC), log-transformed change in proteomic abundance between the two conditions (methane versus helium) where negative LogFC is significant expression under methane and positive logFC is significant expression under helium. Average expression log fold change (Ave Expr Log) is the log transformed average protein expression across both conditions and all duplicates. T-test numbers (t) represent significant differences between methane and helium conditions.	73
Table 3	Transcription of Mn ²⁺ -oxidizing genes in Orca Basin. Protein-type and transcription per million (TPM) for each depth where proteins were detected with metatranscriptomics.	111

LIST OF FIGURES

- Figure 1 Marine Nod clades, gene neighborhoods, and depth profiles of transcription. (A) Maximum likelihood phylogeny of nitric oxide dismutase (Nod) amino acid sequences in marine (blue) and select terrestrial (brown) taxa, primarily from marine MAGs (Tully et al., 2018; Cabello-Yeves et al., 2021; Lin et al., 2021) and ETNP ODZ metagenomes (Ruiz-Perez et al., 2021). Branch support was evaluated using 1000 rapid bootstrap replicates, with bootstrap values shown for deep branches. The tree is drawn to scale, with branch lengths in number of substitutions per site. Bold sequences represent those present in multiple ETNP ODZ metagenomes. “PF” indicates genes from the particle fraction (>1.6 μm fraction) of filters. “FL” indicates genes from the free-living fraction (0.2-1.6 micron) collected on Sterivex filters. The most highly transcribed ETNP ODZ sequence is indicated with an asterisk. The qNor sequence *Geobacillus stearothermophilus* was used as the outgroup. (B) Gene neighborhoods surrounding *nod* genes in select taxa. GenBank contigs: *Cecembia calfontis* SGXG01000001, *Scalindua japonica* BAOS01000045, Gammaproteobacteria NP964 PBRC01000062, Gammaproteobacterium HdN1 FP929140, Deltaproteobacteria NZCL01000067, *Candidatus Methyloirabilis oxyfera* FP565575, and *Rhodospirillaceae* NP1106 PCBZ01000014. Unlabeled gray genes are hypothetical. (C, D) Oxygen and nitrite concentrations (circles), and *nod* transcripts (squares, as reads per kilobase per million mapped reads (RKPM)) with depth in ETNP ODZ P1 (onshore) and P2 (offshore) sites.
- Figure 2 Figure 2. Phylogeny of Alphaproteobacteria showing order UBA11136, with *nod*-containing MAGs. The phylogeny was constructed using the Alphaproteobacterial phylogenetic marker NADH ubiquinone oxidoreductase subunit L as in Cevallos and Esposti (2022). Order UBA11136 is expanded, and *nod*-containing MAGs are bolded. Taxonomic names are from Cevallos and Esposti (2022) and GTDB Release 08-RS214. The scale bar represents amino acid substitutions per site.
- Figure 3 Schematic of the electron transport chain in *nod*-containing ODZ Alphaproteobacteria. Enzymes were included based on presence and transcriptional activity of metagenome-assembled genomes (MAGs) assigned to Alphaproteobacteria (GTDB taxonomy: UBA11136 sp002686135; see text). The color of each protein is chosen according to transcriptional activity and represented from 0-100, 100-1,000, 1,000-10,000, and 10,000-100,000 FPKM in gradient from lighter to darker blue. Heme proteins are indicated by red

circular hemes with the cartoon number corresponding to the number of actual hemes present on each protein. Hypothetical Ptd proteins are labelled A, B, C, D, E, F, and G, and location within the cell is determined using Psort bacterial localization prediction tool. ETC complexes I-V found in Alphaproteobacteria MAGs are labelled with proposed interactions between formate oxidation and complex I NADH electron transfer. Highly transcribed NOD protein and predicted O₂ generation is shown as feeding into A1 type CCO complex IV reduction. Additional electrons for CytC and the ETC are proposed to come from sulfur oxidation carried out by the flavocytochrome c sulfide dehydrogenase (FccAB, FCC), and sulfane-sulfur dehydrogenase (SoxCD) with the multi-enzyme carrier complex (SoxYZ).

- Figure 4 **Gene neighborhoods of pentaheme-tetraheme-decaheme genes from** select organisms. Depicted heme spacing is approximate. All organisms are from saline environments (seawater, marine sediment, or saline spring). 35
- Figure 5 SYBR-stained cell images from enrichment bottles imaged in 2021 and corresponding triplicate cell count values of each condition. No DAPI stain was used. Numbers in panels A-D correspond to Table 1. SYBR-stained cells imaged under GFP filter channel are shown are green. Blue autofluorescence imaged in DAPI filter aligns with SYBR-stained cells. Scalebar is 10 μ m. 58
- Figure 6 Stacked microscopy images of the same section of a filter stained with SYBR (green) DNA stain and imaged under the DAPI (blue) channel with no DAPI stain from 2° transfers. (a) Microscopy of cell morphology from 71 bottle 2° transfers. (b) 2° overlaid image of SYBR (green) stained cells and DAPI (blue) under 95% CH₄/5% CO₂ headspace. Gray scale bar is 2 microns for both images. 60
- Figure 7 Nitrous oxide production in bottle 69 enrichment cultures for 2° and 3° triplicate transfers over time in days. 2° transfers with sterile ETNP culture and a 95% CH₄/5% CO₂ headspace are plotted with black squares. 3° transfers with sterile ETNP culture and a 95% CH₄/5% CO₂ headspace are plotted with pink upward arrows. 60
- Figure 8 Microscopy of cells hybridized with *Marinobacter* (Mrb-0625-a) probe (red), SYBR (green) DNA stain, and imaged under the DAPI (blue) channel with no DAPI stain from 69 bottle and transfers. (a,b,c) 1° bottle contain a microbial community that hybridize with *Marinobacter* probe ~50%. (d,e) 2° transfer cultures hybridize with *Marinobacter* probe ~70%. (f,g,h) 3° transfers cultures hybridize ~98% with gam42 CARD-FISH probe. Approximately 90% of autofluorescent cells also hybridize with gammaproteobacteria 62

probe in 3° transfers which glow under DAPI wavelength excitation. Gray scale bar is 5 microns for all images.

- Figure 9 Overlaid image of microscopy of cells hybridized with CARD-FISH Flavobacteriales probe (CF998) probe (red) from 1° 69 bottle culture. SYBR (green) DNA stain image and cellular autofluorescence under DAPI-filter (blue) excitation overlaid with CARD-FISH image. No DAPI stain was used. Gray scale bar is 10 microns. 63
- Figure 10 Intensity versus wavelength plotted for emission spectra from 405 nm excitation of unstained cells. Inset image taken from unstained 1° bottle 69 using structured illumination microscopy (SIM) during concurrent spectral analysis. Gray scale bar is 5 microns. 65
- Figure 11 Images of unstained bacteria under DAPI-filter microscopy. (a) *Methylobacterium extorquens* AM1 strain under DAPI filter imaging with 5 µm scale bar. (b) *Marinobacter vinifirmus* under DAPI filter imaging with 2 µm scale bar. (c) *Marinobacter hydrocarbonoclasticus* under DAPI filter imaging with 2 µm scale bar. 66
- Figure 12 Measured nitrate reduction in bottle 69 enrichment cultures for each transfer over time in days. 2° transfers with sterile ETNP culture and a 95% CH₄-5% CO₂ headspace are plotted with black squares. 3° transfers with sterile ETNP culture and a 95% CH₄/5% CO₂ headspace are plotted with pink upward arrows. 4° transfers with sterile defined MWH media and a 95% CH₄/5% CO₂ headspace are plotted with green downward facing arrows. 67
- Figure 13 Figure 13. Measured nitrate reduction and OD₆₀₀ of anaerobic (left) and aerobic (right) 4° transfers in sterile defined MWH media from bottle 69. Nitrate is plotted in micromolar as open circles. OD₆₀₀ is plotted as open squares. Anaerobic 4° transfers contain a 95% CH₄-5% CO₂ headspace. Aerobic 4° transfers were continuously shaken and given 200 µM lactate. Error bars as shown as SEM. 68
- Figure 14 Unrooted *Marinobacter* genomic tree based on 26 conserved single copy genes. Novel *Marinobacter pacificus* is bolded along with uncultured strains SAT58 and SS8-8 branch highlighted. 69
- Figure 15 Oxygen measured at timepoints in a subset of liquid culture bottles using optode sensors. 70
- Figure 16 Non-metric scaling dimensional analysis of CH₄ and He condition culture bottles. One bottle culture from each condition did not cluster with its respective condition and instead clustered with the other 71

bottle. These bottles were excluded from downstream analysis for n=4 in each condition.

- Figure 17** Unrooted phylogenetic tree of PQQ-dependent alcohol dehydrogenases showing ExaF clade. The phylogeny was constructed *with* related alcohol dehydrogenase proteins (ADH) using *lanthanides and other rare earth elements*, including XoxF and ExaF proteins. ExaF proteins are expanded, and *Marinobacter pacificus* sp. nov. is bolded and listed with *Marinobacter* sp. strain SS8-8 due to 100% identity match (BLASTp metric). Taxonomic names are from GTDB Release 08-RS214. The scale bar represents amino acid substitutions per site. 72
- Figure 18** Figure 18. OD₆₀₀ maximum values for *Marinobacter pacificus* grown in MWH defined minimal media with nitrate, and formate, ethanol, methanol, or lactate as the sole provided carbon source. ANOVA one-way tests against and within each condition are shown where p-value < 0.01 (***) or no significance. Lactate values are shown with diamonds, methanol as triangles, ethanol as squares, and formate as circles. Error bars are shown as SEM. 75
- Figure 19** Figure 19. Gas headspace analysis of oxidized 1-carbon compounds in incubated bottle cultures. 76
- Figure 20** Schema of *Marinobacter pacificus* sp. nov. anaerobic respiration based on proteomic expression and gas headspace analysis. Enzymes are colored by intensity of proteomic expression in the CH₄ condition. Proton gradient is shown for proton movement in denitrification. Formaldehyde and methanol are included as potential carbon sources for ExaF alcohol dehydrogenase based on gas headspace analysis. Schema of hydroxyl radical formation of methanol and formaldehyde from methane oxidation and origin of unknown hydroxyl radicals in the headspace are shown above the extracellular space. Potential photochemical lysis is represented with yellow lines. *Highly upregulated proteins annotated as SoxCD. 78
- Figure 21** Orca Basin redoxcline depth profile. (a) Left: simplified schema of Orca basin water column oxygen and salinity shifts from normosaline, redoxcline, and core brine. (b) Middle: dissolved oxygen (above), nitrate (above), and dissolved Mn²⁺ (below) measured during cruise in 2023, and particulate Mn(IV) (below) and Mn²⁺ (below) (Van Cappellen et al., 1998). (c) Microscopy of samples collected at 2200 meters are shown on the right. Top right: leucoberbelin blue-stained MnO_x particles are visible as dark particles surrounded by blue haloes. Bottom right: simul-staining with leucoberbelin blue and SYBR green stain; MnO_x particles 99

appear black when overlaid with SYBR cell images. Scale bar is 5 microns for simul-staining images and 30 microns for LBB images.

- Figure 22 DIC and SYBR microscopy images of cells from 2200 m and 2300 m samples. Top left, DIC 10x microscopy image of filter sample collected from 2200 m with LBB staining. LBB+ particles are indicated with blue arrows and appear as dark particles with a blue “halo” around them. Iron oxides are indicated with yellow arrows and appear as red-brown particles. Scale bar is 50 microns. Top right, fluorescent 100x microscopy image of filter sample collected from 2200 m simul-stained with LBB and SYBR. Iron oxides are dark particles indicated with yellow arrow. Bottom left, DIC 100x microscopy image of filter sample collected from 2300 m core brine with LBB staining. No blue “halos” were detected but dark particles were frequently noted. Bottom right, microscopy of samples collected from the core brine (2300 m) simul-stained with LBB and SYBR. Dark particles were abundant but none were LBB+ nor were any associated with cells. 101
- Figure 23 XANEs peak data and SEM-EDX images from 2200-meter culture transfer sample 150 $\mu\text{M Mn}^{2+}$. (a) Red, blue, and green lines correspond to representative samples of $\delta\text{-MnO}_2$, $\beta\text{-MnOOH}$, and MnCl_2 , respectively. Bottom black line is the edge maximum position for enrichment sample. Dashed lines indicated edge maxima for each state of Mn. (b) Representative SEM-EDX image of a node-like particle containing manganese. Filamentous material covering node-like particles are presumed to be rod-shaped cells. (c) Representative SEM-EDX image of a stacked particle containing manganese. Rod and cocci-type material is seen within the stacked particle and presumed to be cells. XANES k-edge data and SEM-EDX image correspond to the same enrichment culture bottle (150 $\mu\text{M Mn}^{2+}$ and He headspace). 103
- Figure 24 Quantitative XANEs data of culture transfer sample from 2200-meter culture transfer sample 150 $\mu\text{M Mn}^{2+}$. Energy versus normalized absorbance plotted from XANEs data collected from representative of 2200-meter enrichment cultures (black line). Pure sample of $\delta\text{-MnO}_2$ plotted as energy versus normalized absorbance is plotted alongside our sample in red. Fit of these two lines is 91.7%. 104
- Figure 25 NO_3^- reduction and MnO_x production rates in suboxic enrichment cultures containing inoculant from Orca Basin 2200 meters water samples. Duplicate bottles were taken for each concentration of NO_3^- and Mn^{2+} and are shown with standard error. Nitrate drawdown is represented with green symbols and MnO_x production is represented with black symbols. The rates of drawdown and production for the 100 $\mu\text{M NO}_3^-$ and 50 $\mu\text{M Mn}^{2+}$ condition is shown with circles, the 106

200 $\mu\text{M NO}_3^-$ and 100 $\mu\text{M Mn}^{2+}$ condition is shown with squares, and 300 $\mu\text{M NO}_3^-$ and 150 $\mu\text{M Mn}^{2+}$ condition is shown with triangles. All enrichment cultures plotted contain $\text{CH}_4\text{-CO}_2$ headspaces. Some sample points do not contain error bars which indicate values that fell within standard error from each other.

- Figure 26 MnO_x production in suboxic enrichment cultures containing inoculant from Orca Basin (2200 meter depth). MnO_x production in the 50 $\mu\text{M Mn}^{2+}$ and 100 $\mu\text{M NO}_3^-$ condition is represented by circular symbols, the 100 $\mu\text{M Mn}^{2+}$ and 200 $\mu\text{M NO}_3^-$ condition by squares, and the 150 $\mu\text{M Mn}^{2+}$ and 300 $\mu\text{M NO}_3^-$ condition by triangles. Helium gas headspaces are open symbols, and 95% $\text{CH}_4\text{-5% CO}_2$ gas headspaces are filled in black symbols. Values are shown with standard error (SEM). 107
- Figure 27 16S rRNA phylogenetic trees constructed of enrichment cultures across both gas headspaces (95% $\text{CH}_4\text{/5% CO}_2$ versus 100% He) and all Mn^{2+} addition concentrations. (a) 95% $\text{CH}_4\text{/5% CO}_2$ gas headspace enrichment cultures show *Marinobacter salarius* is the dominate microorganism. (b) 100% helium gas headspace enrichment cultures show *Marinobacter salarius* is a dominant microorganism across all Mn^{2+} concentrations, as well as an uncultured species, *Marinobacter* sp. NP-4. The top twenty most abundant species are shown for each gas headspace condition (a;b). 109
- Figure 28 Relative abundance of Nitrospirota; Ca. Manganirothaceae in Orca Basin. 16S rRNA relative abundance of species detected in Orca Basin depth. Data compiled from station P5 in Orca Basin. 112

LIST OF SYMBOLS AND ABBREVIATIONS

ANI	Average nucleotide identity
CARD-FISH	Catalyzed reporter deposition-fluorescent in situ hybridization
CH ₄	Methane
CO ₂	Carbon dioxide
DAPI	Blue 4',6-diamidino-2-phenylindole fluorescent dye
DHAB	Deep hypersaline anoxic basin
DIA	Data independent analysis
DIC	Differential interference contrast
ETNP	Eastern Tropical North Pacific
ETSP	Eastern Tropical South Pacific
ExaF	Lanthanide-dependent pyrroloquinoline quinone alcohol dehydrogenase
Fdh	Formate dehydrogenase
FL	Free-living
Ftr	Formylmethanofuran-tetrahydromethanopterin N-formyltransferase
Fwd/Fmd	Formylmethanofuran dehydrogenase
He	Helium
LBB	Leucoberbelin blue
MAG	Metagenome assembled genome
Mn(IV)/MnO ₂ /δ-MnO _x	Manganese oxide in the 4+ cation state and delta-manganese oxide with oxygen vacancies
Mn ²⁺	Soluble manganese in the 2+ cation state
MnxG	Putative manganese multicopper oxidase

N ₂	Dinitrogen gas
N ₂ O	Nitrous oxide
NarGHI and NapAB	Nitrate reductases
NirK and NirS	Nitrite reductases
NO	Nitric oxide
NO ₃ ⁻	Nitrate
Nod	Nitric oxide dismutase
NorBC and NorZ	Nitric oxide reductases
NosZ	Nitrous oxide reductase
NuoL	NADH ubiquinone oxidoreductase subunit L
OD ₆₀₀	Optical density at 600 nanometers
ODZ	Oxygen deficient zone
OTU	Operational taxonomic unit
PCC-1	Porin-cytochrome c complex
PF	Particle fraction
pMMO/sMMO	Particulate and soluble methane monooxygenase
Ptd	Multiheme cytochrome
RPKM	Reads per kilobase per million mapped reads
SEM-EDX	Energy dispersive x-ray spectroscopy
STOX	Specialized ultralow oxygen sensors
SYBR	Green fluorescent dye
XANES	X-ray absorption near edge spectroscopy

SUMMARY

Anoxic marine systems are key regions of nitrogen loss mediated by anaerobic microbial communities and contribute ~50% of global loss of bioavailable nitrogen to the atmosphere. This dissertation used culture-dependent and culture-independent methods to explore nitrogen loss metabolisms in novel microbial species in two anoxic marine systems: the Eastern Tropical North Pacific oxygen deficient zone and the Orca Basin deep hypersaline anoxic basin in the Gulf of Mexico. Using metagenomics and metatranscriptomics, I found that the most abundantly transcribed nitric oxide dismutase genes in the Eastern Tropical North Pacific oxygen deficient zone belong to a novel order (UBA11136) of Alphaproteobacteria that couple oxidation of one-carbon compounds with aerobic respiration, possibly using oxygen from nitric oxide dismutation. I then isolated and characterized a novel bacterial species, *Marinobacter pacificus* from the Eastern Tropical North Pacific oxygen deficient zone and characterized the bacterium with epifluorescent microscopy and proteomics. When grown on methane and nitrate, *Marinobacter pacificus* autofluoresces and highly expresses genes for methanol/ethanol oxidation and denitrification, a metabolism not previously reported in *Marinobacter* species. I then enriched bacterial cultures with methane, manganese, and nitrate as substrates from ~2200 meters at Orca Basin brine-seawater interface. *Marinobacter* species were dominant, and consumed nitrate while producing manganese oxides. I found previously described chemolithoautotrophic manganese oxidizing bacteria were present and transcriptionally active for manganese oxidation at ~2200 meters as well. Understanding the full breadth of potential electron acceptors and interactions with

denitrification in anoxic marine systems is essential to constrain nitrogen loss under climate change.

CHAPTER 1. ANOXIC MARINE SYSTEMS AND THEIR BIOGEOCHEMISTRY: ZONES OF INTENSE NITROGEN LOSS

1.1 Abstract

Anoxic marine systems are global “hotspots” for microbial greenhouse gas cycling and marine bioavailable nitrogen loss. Typical microbial denitrification is coupled to organic carbon oxidation and dominates nitrogen transformation to “lost” gaseous forms. However, most anoxic marine systems are organic carbon limited. Elucidating metabolic niches utilizing nontypical denitrification in anoxic marine systems is essential to constrain global marine nitrogen loss. Further, anoxic marine systems are expanding as global oxygen solubility is decreasing with increased oceanic warming and salinity from climate change. Understanding microbial utilization of nitrogen, oxygen, and diverse electron donors is likely critical to understand the greenhouse gas feedback loop in anoxic marine systems. In this chapter, I discuss the physical oceanography causing formation of anoxic marine systems, biogeochemistry of electron acceptors (oxygen and nitrogen) and electron donors (methane and manganese) in anoxic marine systems, and the potential for concurrent nitrate reduction with methane and manganese oxidation.

1.2 Physical oceanography of anoxic marine systems

Oxygen deficient zones (ODZs) and deep hypersaline anoxic basins (DHABs) are anoxic marine systems that persist for thousands of years. ODZs comprise only one percent of the ocean volume, but are key players in global biogeochemical cycles (Thamdrup et al., 2012). ODZs occur at intermediate depths (~100-1,000 meters), typically along eastern

boundary upwelling systems (Espinoza-Morriberon et al., 2018). DHABs form due to dissolution of evaporative salts exposed by tectonic activity on the seafloor (Merino et al., 2019; Varrella et al., 2020). Fjords also experience bottom-water anoxia, typically seasonally (Schinke and Matthäus, 1998; Torres-Beltrán et al., 2017; Canfield and Kraft, 2022; Anstett et al., 2023). While their formation mechanisms differ, ODZs and DHABs share similar biogeochemistry and microbial communities (Jürgens and Taylor, 2018; Merlino et al., 2018).

1.2.1 Intermediate water anoxic marine systems: oxygen deficient zones

Winds along eastern boundary upwelling systems bring nutrient-rich deep waters to the surface, stimulating primary production. The organic matter sinks and stimulates bacterial aerobic respiration, leading to oxygen depletion at intermediate water depths (Wyrski, 1962; Chavez and Messié, 2009; Ulloa et al., 2012; Robinson, 2019; Narvekar et al., 2021). Below the mixed layer (>50 meters), dissolved oxygen drops from ~200 μM to nanomolar levels, before rising again at depths >1000 meters (Revsbech et al., 2009; Thamdrup et al., 2012; Bristow et al., 2016). ODZs are maintained by low ventilation from sluggish and/or low-oxygen circulation (Canfield and Kraft, 2022; Anstett et al., 2023). Physical ventilation supplies low dissolved oxygen to intermediate water depths because of strong stratification (Cheng et al., 2018; Eddebbar et al., 2021; Kwiecinski and Babbin, 2021; Eddebbar et al., 2024; Font et al., 2024).

The four largest ODZs are the Eastern Tropical North and South Pacific (ETNP and ETSP), the Arabian Sea, and the Bay of Bengal (Reid, 1965; Luyten et al., 1983; Karstensen et al., 2008; Kwiecinski and Babbin, 2021; Bourbonnais et al., 2023). The

ETNP, ETSP, and Arabian Sea are eastern boundary upwelling systems, whereas the Bay of Bengal is constrained by land (D'Asaro et al., 2020). The largest ODZ by volume is the ETNP, and the thickest are the Arabian Sea and the ETNP (Kwiecinski and Babbin, 2021; Liu et al., 2024).

The ETNP and ETSP ODZs are in “shadow zones” of subtropical gyres, and therefore do not receive basin scale wind-driven circulation and have sluggish circulation (Luyten et al., 1983; Kessler, 2006). Most oxygen deficient waters in the ETNP and ETSP lie within the 13°C water mass and are distributed by subsurface mesoscale processes (Evans et al., 2020). Both ETNP and ETSP ODZs are stable on the scale of thousands of years but undergo interannual and decadal variability in oxygen content (Ito and Deutsch, 2013). Poor bottom ventilation in the ETNP and ETSP ODZs stabilizes year-round anoxic cores, and bottom water circulation by Pacific Deep Water is oxygen-poor ($<5 \mu\text{M}$) (Duteil et al., 2021; Kawasaki et al., 2022). The ETNP ODZ is periodically oxygenated by eddy-like secondary oxygen maxima, tropical jets, and seasonal upwelling (Margolskee et al., 2019).

Both the Arabian Sea and Bay of Bengal ODZs receive oxygenated, hypersaline water from the Persian Gulf outflow, which ventilates the entire Arabian Sea, including the ODZ (Sheehan et al., 2020; Font et al., 2024). The ventilated waters that reach the western Arabian Sea then continue into the Bay of Bengal ODZ via equatorial currents (Sheehan et al., 2020). The northeastern basin of the Arabian Sea is oxygen depleted due to poor ventilation and/or eastern boundary upwelling (Naqvi, 1991; Gaye et al., 2013; Liu et al., 2024). The Bay of Bengal is a much smaller ODZ, with year-round anoxia from 100-400

meters (Sarma, 2002). A highly productive top layer prevents oxygen from reaching the intermediate waters by vertical or horizontal mixing (Sarma and Udaya Bhaskar, 2018).

Global warming is predicted to enlarge ODZs (Kwiecinski and Babbin, 2021). Oxygen solubility decreases with increasing ocean temperatures, and water column stratification increases because warmer waters prevent deep-water mixing (Keeling et al., 2010; Helm et al., 2011). Pacific Ocean ODZs are currently expanding (Deutsch et al., 2011; Evans et al., 2023b), likely in part from climate change (Stramma et al., 2008; Schmidtko et al., 2017). The predicted future growth of ODZs may expand hypoxic zones and may shrink the anoxic core (Busecke et al., 2022).

1.2.2 Deep water anoxic marine systems: deep hypersaline anoxic basins

Unlike ODZs, which are formed by surface biological and mesoscale physical oceanography, DHABs are formed by dissolution of underlying salt deposits (Cita, 2006). Tectonic activity exposes evaporitic deposits, which dissolve to form brine pools with salinities up to ten times that of seawater (Merlino et al., 2018; Varrella et al., 2020). Because oxygen solubility decreases with increasing salinity, DHABs are anoxic (Green and Carritt, 1967). The high salinity prevents mixing of oxygenated waters from above. A halocline forms directly above the brine pool, where salinity increases over <100 meters to approximately ten times that of seawater (Varrella et al., 2020). Haloclines, also known as chemoclines, or brine-seawater interfaces, are zones of redox stratification and particle trapping of sinking debris (Merlino et al., 2018). Periodic turbidity from currents and submarine landslides disrupt density-stratified brines, in some cases leading to expulsion

of salt masses and creation of new brine pools (Rimoldi et al., 1996; Botz et al., 2007; Sawyer et al., 2019).

Along the Texas-Louisiana continental slope, the Orca DHAB (26°56'N, 91°19'W) has a strong salinity-density gradient that prevents advective mixing and maintains anoxia (Shokes et al., 1977; Pilcher and Blumstein, 2007). Orca Basin was first discovered in 1977 and has remained highly stable without mixing events or current intrusions (Shokes et al., 1977). The Orca Basin DHAB contains a North and South basin separated by a ridge (Addy and Behrens, 1980). The DHAB, which begins at ~2150 meters, is fed by a seafloor-outcropping Jurassic-aged salt diapir on the eastern edge of the basin exposed during a submarine landslide ~8,000 years ago (Pilcher and Blumstein, 2007; Jackson and Hudec, 2017; Merlino et al., 2018; Sawyer et al., 2019). The seafloor below the North and South brine pools contains methane seeps (Joye et al., 2009). Recent USGS piston coring in the south basin exposed evaporites and released hydrocarbons (Lorenson et al., 2002).

Other DHABs are found in the Mediterranean Sea and the Red Sea. The Mediterranean Sea contains the largest number of DHABs discovered to date (Varrella et al., 2020). The deepest DHABs (Bannock, Tyro, Urania, L'Atalante, and Discovery basins; ~3,200-3,500 meters) occur in the Eastern basin of the Mediterranean Sea and are <2,000 years old (Wallmann et al., 1997; Stan-Lotter and Fendrihan, 2012). These DHABs are fed by dissolution of the hydrated magnesium chloride salt bischofite formed during tectonic collisions of African, Eurasian, and Anatolian plates (Hsu, 1973; Stan-Lotter and Fendrihan, 2012). The Red Sea contains several DHABs between ~1,200-1,500 meters depth (Backer and Schoell, 1972; Pautot et al., 1984; Schmidt et al., 2015). Volcanic and seismic activity creates hot brines and hydrothermal sediments (Miller et al., 1965).

1.3 Biogeochemistry of electron acceptors in two anoxic marine systems

Anaerobic microbial metabolisms dominate in DHABs and ODZs. After O₂, nitrate is the highest energy-yielding electron acceptor. DHABs and ODZs are global hotspots of denitrification, the modular reduction of nitrate to dinitrogen gas by microbial enzymes. Denitrification rates are stimulated by particulate organic matter in ODZs (Ward et al., 2008; Kalvelage et al., 2013; Ward, 2013; Babbin et al., 2014). Organic matter stoichiometry of carbon to nitrogen controls rates of denitrification (Babbin et al., 2014). Denitrification has been measured at <5 μM O₂, but enzymatic inhibition of the last two steps has also been measured occurring at <300 nM O₂ in ODZs (Cline and Richards, 1972; Van Cappellen et al., 1998; Lenton and Watson, 2000b, a; Borin et al., 2013; Dalsgaard et al., 2014; Canfield and Kraft, 2022; Evans et al., 2023a). Below, I discuss the cycling of electron acceptors (oxygen and nitrate) in the ETNP ODZ and Orca Basin DHAB.

1.3.1 Oxygen

Oxygen is the highest energy yielding electron acceptor in respiration. Oxyclines in ODZs and DHABs are zones where oxygen is depleted rapidly due to aerobic respiration of organic matter without reoxygenation. High salinity at the brine-seawater interface in DHABs also reduces oxygen solubility (Green and Carritt, 1967; Merlino et al., 2018). However, nanomolar oxygen concentrations (~5 nM) in the anoxic core of ODZs can support aerobic processes, such as nitrite oxidation (Bristow et al., 2016). The persistence of aerobic respiration in anoxic cores of ODZs is also supported by abundant transcription of cytochrome *c* oxidase, which catalyzes the final step of aerobic respiration (Canfield and Kraft, 2022). Oxygenation via physical intrusions, biological production and chemical

reactions in ODZs (see Section 1.1) could support aerobic processes and a cryptic oxygen cycle (Berg et al., 2022). However, the full extent and mechanisms of aerobic respiration in ODZs remains an open question. To date, there is no evidence for aerobic respiration in DHAB brine pools (Merlino et al., 2018).

Secondary chlorophyll *a* maxima in ODZs occur due to oxygenic photosynthesis by the low-light adapted cyanobacterium *Prochlorococcus* performing .(Goericke et al., 2000; Lavin et al., 2010; Ulloa et al., 2021; Wong et al., 2023). Oxygen produced by *Prochlorococcus* fuels a cryptic oxygen cycle in the anoxic core wherein the oxygen that is produced is almost immediately consumed (Cepeda-Morales et al., 2009; Garcia-Robledo et al., 2017). Aerobic metabolisms, like nitrite oxidation and methane oxidation, may be supported by cryptic oxygen cycling (Garcia-Robledo et al., 2017).

Microbes may also produce intracellular oxygen via nitric oxide dismutation for thermodynamically difficult reactions including methane and ammonia oxidation (Ettwig et al., 2010; Ettwig et al., 2012; Kraft et al., 2022). The putative gene, nitric oxide dismutase (Nod), is proposed to catalyze this reaction via oxidation of nitric oxide to N₂ and oxygen gas (Wu et al., 2011). This enzyme has yet to be purified and characterized. Putative Nod was originally found in the strictly anaerobic methane-oxidizing bacterial group NC10, *Methylomirabilota* (Ettwig et al., 2012; Luesken et al., 2012). Since its discovery, Nod has been found in diverse microbes that likely utilize Nod for oxygenic denitrification (Zhu et al., 2020) and nitric oxide detoxification (Zhu et al., 2017; Hu et al., 2019; Elbon et al., 2024; Ruff et al., 2024).

1.3.2 Nitrogen

Anoxic marine systems are zones of intense nitrogen loss. ODZs contribute 30-50% of the ocean's nitrogen loss; with ~70% from denitrification and the remainder from anaerobic ammonium oxidation (anammox) (Cline and Richards, 1972; Thamdrup, 2012; Wright et al., 2012; DeVries et al., 2013; Ward, 2013). The contribution of DHABs to global nitrogen loss is yet to be determined (Merlino et al., 2018). Anammox bacteria are active in both Mediterranean Sea and Red Sea DHABs (Borin et al., 2013; Speth et al., 2017; Merlino et al., 2018). Rates of nitrogen loss from Orca Basin are unconstrained (Merlino et al., 2018), but Mediterranean Sea DHABs have a higher denitrification-to-anammox ratio compared to ODZs, with 85% of nitrogen loss from denitrification at salinities up to 9.2‰ (Borin et al., 2013). Denitrification is also responsible for most organic carbon remineralization within anoxic marine systems, which tightly couples these two processes (Babbin et al., 2014). Viral phage lysis of *Prochlorococcus* in the ETNP ODZ produces organic matter which stimulates denitrification in the anoxic core (Fuchsman et al., 2019).

Denitrification is a modular process. “Single-step” denitrifiers of distinct taxonomies are the main catalysts of nitrogen loss in anoxic marine systems (Zhang et al., 2023). The modular nature of denitrification and the interplay of diverse microbial species makes constraining rates of denitrification in systems challenging. The first module is nitrate reduction to nitrite, driven by the protein complexes NarGHI and NapAB. Nitrate reduction is the least oxygen-sensitive step (Hernandez and Rowe, 1987; Bonin and Raymond, 1990). Across ODZs, variable oxygen levels (0.5 - 25 μM) will inhibit nitrate reduction (Lipschultz et al., 1990; Kalvelage et al., 2011; Bristow et al., 2016). The ETNP ODZ contains a secondary nitrite maximum ($\sim 4 \mu\text{M NO}_2^-$) at the top of the anoxic core,

where nitrite from dissimilatory nitrate reduction accumulates and aerobic processes consuming nitrite are arrested (Cline and Richards, 1972; Lenton and Watson, 2000a; Ulloa et al., 2012; Anstett et al., 2023). Nitrate reductase (*narG*) genes are widely distributed amongst ODZ microbes and are the most abundant denitrification gene by two-fold (Fuchsman et al., 2017; Zhang et al., 2023). SAR11 bacteria are the most abundant in *narG* transcriptional activity (Tsementzi et al., 2016). The Orca Basin DHAB contains a major geochemical shift at the brine-seawater interface (Van Cappellen et al., 1998), below which nitrate is depleted from $\sim 22 \mu\text{M}$ in pelagic seawater to $\sim 3 \mu\text{M}$. There is evidence for dissimilatory nitrate reduction to ammonium at the brine-seawater interface in the Orca Basin DHAB (Stüeken et al., 2024). However, there is no definitive evidence for water column nitrate reduction to nitrite in the Orca Basin DHAB. Nitrate reductases are actively transcribed in the upper and lower interface of a Mediterranean Sea DHAB, but activity sharply decreases with increasing salinity (Pachiadaki et al., 2014).

The second module of denitrification is nitrite reduction to nitric oxide, driven by nitrite reductases (NirK or NirS). Oxygen is more inhibitory to nitrite reduction than nitrate reduction; nitrite reduction is inhibited above $\sim 11 \mu\text{M O}_2$ (Sacks and Barker, 1949; Bonin and Raymond, 1990). However, nanomolar oxygen catalyzes nitrite oxidation back to nitrate in ODZs (Bristow et al., 2016; Bristow et al., 2017; Sun et al., 2021). SAR11 bacteria are suggested to contain nitrite reductase (*nirK*) in the ETNP ODZ (Fuchsman et al., 2017). Picocyanobacteria also contribute to nitrite loss within the anoxic core of the ETNP ODZ (Fuchsman et al., 2019; Aldunate et al., 2020). NAD(P)H-nitrite reductases are highly transcribed in the lower interface of a Mediterranean Sea DHAB (Pachiadaki et al., 2014).

The third module of denitrification is nitric oxide reduction to nitrous oxide. Nitric oxide reduction is catalyzed by nitric oxide reductases that belong to the heme-copper oxidoreductase superfamily (Sousa et al., 2012). NorBC (cytochrome nitric oxide reductase, cNor) and NorZ (quinol nitric oxide reductase, qNor) are the most characterized nitric oxide reductases. NorZ is the “fused” version of NorBC genes, with a quinol binding site in place of a cytochrome binding site (Cramm et al., 1999; Zumft, 2005). Oxygen can also be reduced by nitric oxide reductases at lower efficiencies than cytochrome *c* oxidases, a likely remnant of their shared evolutionary history (Fujiwara and Fukumori, 1996; Forte et al., 2001; Salomonsson et al., 2012; Glass et al., 2023). The lack of O₂ in ODZs makes them marine hotspots for microbial anaerobic greenhouse gas cycling, including production and consumption of nitrous oxide (Bertagnolli and Stewart, 2018). Even though ODZs comprise ~1-3% of marine water volume, the microbial community generates half of global marine nitrous oxide emissions (Ji et al., 2015; Ji et al., 2018). The primary source of nitrous oxide is thought to be nitric oxide (NO) reduction during denitrification (Babbin et al., 2015; Kwiecinski and Babbin, 2021; Bourbonnais et al., 2023). In the ETNP ODZ, a non-canonical version of nitric oxide reductase most related to NorZ dominates abundance and activity (Fuchsman et al., 2017; Zhang et al., 2023). Nitric oxide reductases are transcribed along the interface of a Mediterranean Sea DHAB (Pachiadaki et al., 2014).

Nitric oxide may also be converted to N₂ and oxygen via putative nitric oxide dismutase (Ettwig et al., 2012). Previous studies reported that the dominant NO-transforming protein was Nod related to *Methylomirabilota* (Padilla et al., 2016; Fuchsman et al., 2017; Thamdrup et al., 2019). We re-annotated metatranscriptomes and metagenomes, and found that the most transcribed *nod* genes in the Eastern Tropical North

Pacific ODZ actually belong to a new order of Alphaproteobacteria, UBA11136, not *Methylomirabilota* (Elbon et al., 2024); see Chapter 2.

The fourth module of denitrification is nitrous oxide reduction to dinitrogen gas (N_2), which is catalyzed by two forms of NosZ, type I and type II. Type I NosZ, which was discovered first, is highly sensitive to oxygen (Zumft, 1997). Type II, found originally in single-step denitrifiers in soils, is less sensitive to oxygen and has a higher binding affinity for nitrous oxide (Sanford et al., 2012). NosZ type II from single-step denitrifiers dominates across anoxic marine systems (Bertagnolli et al., 2020). However, low concentrations of oxygen (~ 205 nM) inhibit N_2O reduction (Bertagnolli et al., 2020). Most ODZ nitrous oxide production occurs at the boundaries where low O_2 conditions proliferate (Bourbonnais et al., 2023). Nitrous oxide reductases are transcribed at the upper interface of a Mediterranean Sea DHAB (Pachiadaki et al., 2014). To our knowledge, no data on denitrification and the specific microbes carrying out these processes exist for the Orca Basin DHAB.

1.4 Biogeochemistry of electron donors in two anoxic marine systems

Organic carbon is the most energy-yielding electron donor for denitrification. Heterotrophic remineralization of organic carbon is prevalent in anoxic marine systems due to high productivity and, in DHABs, the particle trap above brine pools (Loginova et al., 2016; Merlino et al., 2018; Fuchsman et al., 2019). Sinking organic carbon-rich particles (marine snow) reach a maximum at the brine-seawater interface (chemocline), and are dissolved into the brine basin, making the Orca Basin DHAB a considerable carbon reservoir (Sackett et al., 1979; Merlino et al., 2018; Diercks et al., 2019). Marine snow

constitutes a “hodge-podge” of organic matter from viral lysis of plankton and bacteria, dead microbial matter, waste matter from zooplankton, and dead zooplankton (Lampitt, 2001). Marine snow is estimated to sink ~100s meters per day in ODZS, and deposits organic matter covered in distinct microbial communities to the seafloor (Lampitt, 2001; Mestre et al., 2018). However, "alternative" electron donors that are less energy-yielding are postulated to be used after organic matter is depleted. Anoxic marine systems contain elevated concentrations of “alternative” electron donors, including methane and manganese. While microbial sulfur and iron cycles are also active in anoxic marine systems, they are not further considered here. Below, I discuss the cycling of potential electron donors (methane and manganese) in the ETNP ODZ and Orca Basin DHAB.

1.4.1 Methane

Anoxic marine systems contain significant reservoirs of methane. The ETNP ODZ is estimated to be the largest seawater reservoir of methane (Sansone et al., 2001). Methane can reach up to ~100 nM in the ETNP anoxic core and ~15 nM in the oxycline (Sansone et al., 2001; Pack et al., 2015; Chronopoulou et al., 2017; Thamdrup et al., 2019). The Orca Basin DHAB contains ~1,000 times more methane than the ETNP ODZ (Thamdrup et al., 2019; Nigro et al., 2020). In the Orca Basin DHAB, ~750 mM methane is produced by biotic methylotrophic methanogenesis and methane seeps (Sackett et al., 1979; Wiesenburg et al., 1985; Whelan et al., 1986; Joye et al., 2009; Zhuang et al., 2016; Nigro et al., 2020). The significant amount of methane in Orca Basin is due to a long residence time in the brine, not high productivity (Wiesenburg et al., 1985). Significant hydrocarbons are stored in the sediments of the Gulf of Mexico (Lorenson et al., 2002; Valentine et al., 2014). Methane from these reservoirs escapes into subsurface plumes, water column and surface,

as well as surrounding marine deep-sea sediments (Kostka et al., 2011; Valentine et al., 2014; Joye, 2015; Bracco et al., 2020).

The minimal methane emissions from ODZs, despite elevated concentrations in the anoxic core, has previously been attributed to denitrification coupled to anaerobic methane oxidation (Padilla et al., 2016; Chronopoulou et al., 2017). In this case, O₂ for methane activation is proposed to be supplied intracellularly by Nod during dismutation of NO to N₂ and O₂ (Murrell et al., 2000; Lieberman and Rosenzweig, 2005; Ross and Rosenzweig, 2017; Zhu et al., 2019). Bacterial methane oxidation is driven by the methane monooxygenase genes which exists in two forms: particulate and soluble (pMMO/sMMO) (Koo and Rosenzweig, 2021). Despite previous evidence that *nod* genes are related to *Methylomirabilota* bacteria, methane oxidation does not correlate with *nod* transcription in ODZs, nor do the *mmo* genes in ODZs belong to *Methylomirabilota* (Padilla et al., 2016; Thamdrup et al., 2019). Instead, most *nod* transcription in the ETNP ODZ can be attributed to a new order of Alphaproteobacteria, UBA11136, which is a potential methanol-oxidizing bacteria that does not contain any methane monooxygenase genes but does have several cytochrome *c* oxidases supporting aerobic respiration (Elbon et al., 2024). Further, almost all transcription of methane oxidation genes across ODZs and seasonally anoxic basins belongs to an obligately aerobic gammaproteobacterial methanotroph, *Methylococcales* (Padilla et al., 2017; Thamdrup et al., 2019; Steinsdóttir et al., 2022b; Schorn et al., 2024). *Methylococcales* are present and even the dominant methanotrophs transcribing denitrification genes in most ODZs (Padilla et al., 2017; Thamdrup et al., 2019).

Despite considerable methane fluxes, there is currently no evidence supporting methane oxidation in the Orca Basin anoxic brine nor in a nearby mud volcano (Joye et al., 2009; Zhuang et al., 2016; Nigro et al., 2020). However, anaerobic methanotrophic archaea dominate the brine-seawater interface in Mediterranean Sea DHABs (Pachiadaki et al., 2014) and were found in a Red Sea DHAB (Merlino et al., 2018). Gammaproteobacteria related to those capable of alkane and aromatic chain oxidation have been detected in the anoxic brine of Orca Basin (Nigro et al., 2020). Further, *Marinobacter*, a genus within Gammaproteobacteria, dominated the Gulf of Mexico open ocean, sediments, and beach sands contaminated with anthropogenic hydrocarbons following the Deepwater Horizon blowout (Kostka et al., 2011; Yang et al., 2016; Karthikeyan et al., 2020b). Overall, the fate of methane in Orca Basin and other DHABs remains unknown. Chapter 3 was motivated by outstanding questions about microbial methane transformation in the ETNP ODZ.

1.4.2 Manganese

Many anoxic marine systems contain large peaks of particulate manganese oxides (MnO_x) in the anoxic core (Saager et al., 1989; Johnson et al., 1996; Van Cappellen et al., 1998). The Arabian Sea and ETNP ODZs contain elevated concentrations of manganese, but the ETSP has lower levels of Mn than in typical intermediate water masses (Vedamati et al., 2014). Manganese sources for the ETNP ODZ likely originate from the Rio Balsas via sediment accumulation and release, or mixing above the continental shelf (Bolster et al., 2022). The Orca Basin DHAB begins to accumulate Mn in the suboxic zone and has two distinct peaks of particulate Mn(IV) (~400 nM) and soluble Mn^{2+} (>400 μM) at the base of the brine-saltwater interface and anoxic core, respectively (Van Cappellen et al.,

1998). Manganese sources to Orca Basin are continental dust and discharge from the Mississippi River delta (Trefry and Presley, 1982; Trefry et al., 1984).

Microbial manganese (Mn^{2+}) oxidation is ubiquitous in marine systems (Hansel, 2017). Two step electron transfers oxidize soluble Mn^{2+} to particulate Mn(IV) oxides (Tebo et al., 2004). Mn oxides can be formed biotically, abiotically, or by a combination of both. For example, ligand binding of Mn(III) occurs after biotic Mn^{2+} oxidation (Oldham et al., 2015; Oldham et al., 2017). Putative enzymes are proposed to support manganese oxidation including a multicopper oxidase (Tebo et al., 2005; Hansel, 2017; Yu and Leadbetter, 2020; Huang et al., 2022). However, enzymatic pathways for Mn^{2+} oxidation continue to be elusive, and the identity and mechanism of Mn^{2+} -oxidizing microbes in anoxic marine systems are largely unknown. In the Black Sea, Mn^{2+} oxidation is a strictly aerobic process that can operate down to $\sim 5 \mu\text{M O}_2$ (Tebo, 1991; Clement et al., 2009).

Many heterotrophic Mn^{2+} -oxidizing bacteria are physically associated with ferromanganese crusts and nodules via biofilm matrices (Stein et al., 2001; Templeton et al., 2005; Yli-Hemminki et al., 2014; Yu and Leadbetter, 2020). It is unknown if Mn^{2+} -oxidation by heterotrophs, including *Marinobacter* and *Idiomarina* species, is an energy-gaining process or a toxicity response driven by metal-transforming enzymes (Tebo et al., 2005; Templeton et al., 2005; Hansel, 2017). Mn^{2+} -oxidizing bacteria are proposed to be responsible for manganese nodule formations (Tebo et al., 2005). Cells isolated from nodules are thus thought to be Mn^{2+} -oxidizers (Templeton et al., 2005). Whether Mn^{2+} -oxidation provides any energy gain for a cell is overall unknown (Canfield et al., 2005; Hansel, 2017). Manganese can be toxic and cellular activity for Mn^{2+} is predominantly stress response (Martin and Waters, 2022). Chapter 4 focuses on identification and

characterization of microbes at the manganese oxide peak above the anoxic brine of the Orca Basin.

1.5 Potential for denitrification concurrent with methane and manganese oxidation

Oxygen is the highest energy yielding electron acceptor for oxidizing methane and manganese, and may be thermodynamically required (Tebo et al., 2004; Ettwig et al., 2010; Ettwig et al., 2012; Yu and Leadbetter, 2020; Huang et al., 2022; Steinsdóttir et al., 2022a; Cai et al., 2023). However, there are several hypotheses regarding connections between the oxygen and nitrogen cycle in anoxic marine systems. Denitrification coupled to methane and manganese oxidation have been postulated to require interactions with a cryptic oxygen cycle (Canfield et al., 2005; Raghoebarsing et al., 2006; Padilla et al., 2016; Garcia-Robledo et al., 2017; Padilla et al., 2017; Lappan et al., 2023). Below, I discuss interactions between oxygen, nitrogen, methane, and manganese measured in lab cultures and *in-situ*.

1.5.1 Nitrate/nitrite reduction coupled to methane oxidation

Methane monooxygenase remains the only characterized enzyme found in methane oxidizing bacteria. Under methane monooxygenase-catalyzed methane oxidation, oxygen is required to activate methane (Peng et al., 2021). However, methane oxidation can occur under extremely low concentrations of oxygen, even concurrently with anaerobic respiration and fermentation. Lab cultures of aerobic methanotrophic Gammaproteobacteria oxidize methane while simultaneously denitrifying (Kits et al., 2015a). *Methylomonas denitrificans* (sp. nov. type strain FJG1), will perform denitrification, producing nitrous oxide as the final product, and continue to oxidize methane under hypoxia (Kits et al., 2015a). Several electron donors including methane

were also used by *Methylobacterium album* strain BG8 for nitrite reduction to nitrous oxide under hypoxia (Kits et al., 2015b). Further, methanotrophic Gammaproteobacteria can use fermentation-based methanotrophy under oxygen limitation and upregulate bacteriohemerythrin to shuttle oxygen directly to *mmo* to catalyze methane oxidation (Chen et al., 2012; Kalyuzhnaya et al., 2013). These mechanisms are predicted to lower overall oxygen demand for the cell while maintaining energy conservation and respiration.

Similar to anoxic marine systems, freshwater anoxic lakes also contain *Methylococcales* as the dominant methane oxidizer in the anoxic core, alongside NC10 bacteria (Steinsdóttir et al., 2022a; Reis et al., 2024; Schorn et al., 2024). *Methylococcales* in lakes employ mixotrophic lifestyles that confer significant advantages to sporadic O₂ mixing into anoxic waters by combining strictly aerobic methane oxidation with denitrification, fermentation, and additional alternative electron acceptors (Fe, Mn, etc.) for energy conservation (Reis et al., 2024; Schorn et al., 2024). Therefore, an alternative hypothesis can be proposed for anoxic marine systems: trace oxygen supply is shunted/conserved to support activation and oxidation of methane, while denitrification and fermentation are used for energy conservation and respiration in *Methylococcales*.

1.5.2 Nitrate reduction coupled to manganese oxidation

Despite the apparent requirement for O₂ in Mn²⁺ oxidation, coupling denitrification to Mn²⁺ oxidation is thermodynamically feasible (LaRowe et al., 2021). However, the predicted ΔG value ($-14.9 \text{ kJ (mol e}^{-})^{-1}$) are below the theorized minimum for energy conservation (Müller and Hess, 2017). Chemolithoautotrophic Mn²⁺-oxidizing bacteria use nitrate as the sole nitrogen source, and O₂ for Mn²⁺ oxidation (Yu and Leadbetter, 2020).

There remains a lack of understanding of a mechanism in lab cultures for a cell or cell consortium performing Mn^{2+} -oxidation concurrently with nitrate reduction under anaerobic conditions. However, dark oxygen production in deep-sea systems fueled by nitrate-reduction and supporting manganese oxidation by *Deferribacterota*, and other deep-sea microbes, is a recently postulated mechanism that warrants future investigation (Zheng et al., 2025).

1.6 Research scopes and objectives

In this dissertation, I studied denitrifying microbial communities in enrichment cultures from two anoxic marine systems: (1) the Eastern Tropical North Pacific oxygen deficient zone (ETNP ODZ), and (2) the Gulf of Mexico deep hypersaline anoxic basin, North basin (Orca Basin). I sought to understand the contributions of marine nitrogen loss by microbes that use diverse electron donors in respiration and metabolism by characterizing microbial processes of nitrogen loss where O_2 is not playing a significant role in metabolism nor other biogeochemical processes. In Chapter 2, I propose that a novel Alphaproteobacteria is responsible for the most transcribed nitric oxide reductase (Nod) in the ETNP ODZ. In Chapter 3, I report a new *Marinobacter* species isolated from long-term ETNP ODZ cultures and an anaerobic one-carbon metabolism for the *Marinobacter* genus. In Chapter 4, I identify potential nitrate-reducing bacteria concurrently oxidizing Mn^{2+} at the manganese oxide peak in the Orca Basin. In Chapter 5, I conclude this thesis and discuss future work.

CHAPTER 2. NOVEL ALPHAPROTEOBACTERIA TRANSCRIBE GENES FOR NITRIC OXIDE TRANSFORMATION AT HIGH LEVELS IN A MARINE OXYGEN DEFICIENT ZONE

This work was published in ASM Journals, Applied and Environmental Microbiology, Vol. 90, No. 4, 2024 under the same title, Novel Alphaproteobacteria transcribe genes for nitric oxide transformation at high levels in a marine oxygen-deficient zone, by Claire E. Elbon, Frank J. Stewart, and Jennifer B. Glass.

2.1 Abstract

Marine oxygen deficient zones (ODZs) are portions of the ocean where intense nitrogen loss occurs primarily via denitrification and anammox. Despite many decades of study, the identity of the microbes that catalyze nitrogen loss in ODZs are still being elucidated. Intriguingly, high transcription of genes in the same family as the nitric oxide dismutase (*nod*) gene from *Methylomirabilota* has been reported in the anoxic core of ODZs. Here, we show that the most abundantly transcribed *nod* genes in the Eastern Tropical North Pacific ODZ belong to a new order (UBA11136) of Alphaproteobacteria, rather than *Methylomirabilota* as previously assumed. Gammaproteobacteria and Planctomycetia also transcribe *nod*, but at lower relative abundance than UBA11136 in the upper ODZ. The *nod*-transcribing Alphaproteobacteria likely use formaldehyde and formate as a source of electrons for aerobic respiration, with additional electrons possibly from sulfide oxidation. They also transcribe multiheme cytochrome (here named *ptd*) genes for a putative porin-cytochrome protein complex of unknown function, potentially involved in extracellular electron transfer. Molecular oxygen for aerobic respiration may

originate from nitric oxide dismutation via cryptic oxygen cycling. Our results implicate Alphaproteobacteria order UBA11136 as a significant player in marine nitrogen loss and highlight their potential in one-carbon, nitrogen, and sulfur metabolism in ODZs.

2.2 Introduction

Marine oxygen deficient zones (ODZs) contribute up to half of the ocean's nitrogen loss (DeVries et al., 2013) and are a major source of marine emissions of the potent greenhouse gas nitrous oxide (N₂O) (Yang et al., 2020). The primary source of the N₂O at the oxic-anoxic interface and in anoxic waters in ODZs is denitrification (Babbin et al., 2015; Frey et al., 2020). The microbial enzyme responsible for N₂O production during denitrification is nitric oxide reductase (Nor), which uses electrons from cytochrome *c* (cNor) or quinol (qNor), to reduce nitric oxide (NO) to N₂O (Wasser et al., 2002; Zumft, 2005; Kraft et al., 2011). In the qNor family, there are *bona fide* qNor enzymes and NO dismutase (NOD). NOD proteins lack the quinol-binding site, seemingly preventing the enzyme from taking up external electrons; instead, NOD is theorized to disproportionate NO into dinitrogen and O₂ in methane-oxidizing *Methylomirabilota* bacteria (Ettwig et al., 2010; Ettwig et al., 2012) and in the alkane-oxidizing gammaproteobacterium HdN1 (Zedelius et al., 2011).

The Eastern Tropical North and South Pacific (ETNP and ETSP) ODZs are the world's largest and second largest ODZs, and the subjects of extensive microbial ecology studies. Abundant NO reductase-like genes and transcripts in the ETNP and ETSP ODZ cluster in the same enzyme subfamily as NOD (Dalsgaard et al., 2014; Ganesh et al., 2014; Padilla et al., 2016; Fuchsman et al., 2017). Due to the similarity of ODZ Nod proteins to

those of *Methylomirabilota* (NC10), it was initially presumed that ODZ bacteria also used Nod proteins to disproportionate NO into N₂ and O₂ for use in intra-aerobic methane oxidation (Dalsgaard et al., 2014; Padilla et al., 2016; Thamdrup et al., 2019). However, (Fuchsman et al., 2017) found that the peak of *nod* gene abundance in the ETNP ODZ correlates with a peak of modeled N₂O production (Babbin et al., 2015) and does not correlate with abundance of methane monooxygenase genes, suggesting that Nod proteins in the ETNP ODZ are potentially an important source of N₂O, and are unlikely to be involved in methane oxidation. The plausibility that Nod proteins can reduce NO to N₂O is supported by a study of a novel eukaryotic denitrification pathway in foraminifera (*Globobulimina* spp.) that produces N₂O while expressing Nod (Woehle et al., 2018). Yet, the phylogenetic identity and metabolic context of marine Nod proteins, which are a key biological source of either N₂O or O₂+N₂ in marine ODZs, remain unresolved.

In this study, we sought to determine the identity, predicted metabolism, and environmental niche of the ODZ organism responsible for the highly transcribed *nod* genes first discovered in (Padilla et al., 2016). We found that the most abundantly transcribed *nod* genes in the ETNP ODZ belong to Alphaproteobacteria in the novel order UBA11136. Significant transcription of *nod* genes was limited to waters with <1 μM O₂. These *nod*-transcribing alphaproteobacteria also transcribe genes involved in aerobic respiration, which was unexpected given that they inhabit anoxic waters, as well as genes involved in oxidation of formaldehyde, likely indicating methylotrophy. Genes encoding multi-heme cytochrome proteins potentially implicated in nitrogen or iron cycling were also transcribed.

2.3 Methods

2.3.1 *Nod phylogeny and gene neighborhood*

Amino acid sequences of highly transcribed nod genes “ETNP 2014 Stn10 150m” and “ETNP 2013 Stn6 300m” were acquired from the authors of (Padilla et al., 2016). These sequences were used for BLASTP searches of ODZ metagenomes in the IMG-JGI database and the non-redundant protein (nr) database in NCBI. Sequences (n=53, 731 gap-free sites) were aligned using the MAFFT online server with the L-INS-i method (Katoh et al., 2019). A phylogeny was generated with 1000 bootstraps using model LG+I+G4 using W-IQ-Tree (Trifinopoulos et al., 2016). The phylogeny was visualized using FigTree v.1.4.4, and the fasta file (Nod_alignment) is available as a supplemental dataset. Gene neighborhoods were generated using the EFI Gene Neighborhood Tool (Zallot et al., 2019) with single sequence BLAST of the UniProt database using the amino acid sequence Ga0066848_100037855 (JGI IMG) as the Nod query with an e-value cutoff of 10^{-5} and with 10 genes upstream and downstream the gene of interest.

2.3.2 *Transcription of nod genes in ETNP ODZ depth profiles*

Magic Basic Local Alignment Search Tool (Boratyn et al., 2019) was used to search ETNP ODZ metatranscriptomes (PRJNA727903; Mattes et al. (2022)) using representative nucleotide sequences for Planctomycetia-like (Ga0066826_100064333 (JGI IMG)), Gamma-like (PBRC01000062.1:19833-22205 (NCBI)), and Alpha-like (Ga0066848_100037855 (JGI IMG)) *nod* genes. Default parameters were used except for the score threshold (18). Read hits were normalized to reads per kilobase million (RPKM).

2.3.3 *Metagenomic binning*

Binning of metagenome-assembled genomes (MAGs) was performed using the KBase platform (Arkin et al., 2018). ETNP ODZ metagenomes were collected in 2013 and sequenced by Joint Genome Institute (JGI) using an Illumina HiSeq 2500 as described in Ruiz-Perez et al. (2021). Assemblies for the ETNP ODZ metagenomes (Ruiz-Perez et al., 2021) containing Alpha-type *nod* genes (ETNP201310SV72 (GOLD Analysis Project ID Ga0066848; stn10 300m) and ETNP201306SV43 (GOLD Analysis Project ID Ga0066829; stn6 300m) were imported from JGI IMG into KBase. Metagenomic assemblies were binned into MAGs using MaxBin2 v2.2.4 (Wu et al., 2016). The two MAGs containing *nod* genes (MAG ETNP2013_S10_300m_22 from ETNP201310SV72 and ETNP2013_S06_300m_15 from ETNP201306SV43) were selected for further analysis. Average nucleotide identity was calculated using FastANI (Jain et al., 2018). MAG taxonomy and genome quality was evaluated by GTDB-Tk v2.3.2 (Chaumeil et al., 2022). MAGs were annotated with RASTtk v1.073 (Brettin et al., 2015). Metagenomic reads were mapped to MAGs using Bowtie2 (Langmead and Salzberg, 2012).

2.3.4 *Alphaproteobacterial NuoL phylogeny*

Alphaproteobacterial NADH ubiquinone oxidoreductase subunit L (NuoL) and mitochondrial ND5 marker proteins (n=320) were aligned as in Cevallos and Degli Esposti (2022) with additional representation of UBA11136. A maximum likelihood phylogeny with 1000 bootstraps was constructed using IQ-tree (Nguyen et al., 2015) using the LG+F model with ultrafast bootstrap (Hoang et al., 2017). Taxonomic names and clades are from Cevallos and Esposti (2022) and GTDB Release 08-RS214. Alphaproteobacteria MAGs containing *nod* genes were classified as belonging to order UBA11136 using GTDB-Tk v2.3.2 (Chaumeil et al., 2022).

2.3.5 *Mapping transcripts to metagenomic bins*

Metatranscriptomic mapping to MAGs was performed using the KBase platform (Arkin et al., 2018). RNA-seq data (Mattes et al., 2022) were imported from the depth with highest *nod* transcription, the secondary nitrite maximum (126 meters, NCBI run SRR14460584) and aligned to MAGs using the Bowtie2 (Langmead and Salzberg, 2012) app in KBase. The Cufflinks v2.2.1 (Trapnell et al., 2012) app in KBase was then used to assemble the aligned RNA-seq data into a set of transcripts and to calculate the relative abundances of the transcripts expressed in fragments per kilobase of exon per million fragments mapped (FPKM).

2.3.6 *Cellular localization and heme numbers*

Cellular locations of Ptd proteins were predicted using PSORTb v3.0.3 analysis (Yu et al., 2010). Numbers of heme-binding motifs per protein were identified by counting CXXCH sequences. Ptd gene neighborhoods was generated using the EFI Gene Neighborhood Tool (Zallot et al., 2019) with single sequence BLAST of the UniProt database using the amino acid sequence Ga0066848_100031354 (JGI IMG) as the PtdA query, with an e-value cutoff of 10^{-5} and with 10 genes upstream and downstream the gene of interest.

2.4 **Data availability**

The KBase bioinformatic pipeline and MAGs are at <https://narrative.kbase.us/narrative/106999>. Original metagenomic reads are available at BioProject PRJNA375524 (ETNP201306SV43, SAMN06344130) and BioProject PRJNA375542 (ETNP201310SV72, SAMN06344148). MAG Alphaproteobacteria

bacterium ETNP2013_S06_300m_15 was deposited into BioProject PRJNA375524 (BioSample SAMN38229257, WGS Accession JAZDBU000000000) and Alphaproteobacteria bacterium ETNP2013_S10_300m_22 was deposited into BioProject PRJNA375542 (BioSample SAMN38228782, WGS Accession JAZDCE000000000).

2.5 Results

2.5.1 *Transcribed nod sequences in the ETNP ODZ belong to Alphaproteobacteria, Gammaproteobacteria, and Planctomycetia*

Our reanalysis of highly transcribed *nod* genes in the ETNP ODZ (Padilla et al., 2016) shows that these genes belong to Alphaproteobacteria rather than a member of *Methylomirabilota* as previously assumed. Querying the Nod amino acid sequences from (Padilla et al., 2016) against ETNP ODZ metagenomes in the IMG-JGI database returned multiple 100% identity matches, including a *nod* gene (Ga0066848_100037855) on a scaffold with hypothetical genes with 100% identity to Alphaproteobacteria metagenome-assembled genomes (MAGs) from the ETNP ODZ (Uzun et al., 2020). We binned previously sequenced ETNP ODZ metagenomes Ga0066848 (ETNP201310SV72) and Ga0066829 (ETNP201306SV43) (Ruiz-Perez et al., 2021) into MAGs. Contigs with the most highly transcribed *nod* genes were present in two Alphaproteobacteria MAGs (GTDB taxonomy: UBA11136 sp002686135; species representative: Rhodospirillaceae bacterium isolate ARS27) with 97% average nucleotide identity. Querying the Nod amino acid sequences from (Padilla et al., 2016) against NCBI's non-redundant protein database returned matches to other MAGs assigned to Alphaproteobacteria order UBA11136 from low-oxygen marine settings (ETNP, Saanich Inlet, and the Black Sea; 78-80% identity),

the marine magnetotactic alphaproteobacterium *Magnetovibrio blakemorei* MV-1 (75% identity), Gammaproteobacterium HdN1 (66% identity), and *Methylomirabilota* spp. (66% identity).

To glean additional insights into evolutionary relationships, we updated a previous Nod phylogeny (Hu et al., 2019) with additional amino acid sequences from marine MAGs (Tully et al., 2018; Cabello-Yeves et al., 2021; Lin et al., 2021) and ETNP ODZ metagenomes (Ruiz-Perez et al., 2021), subdivided in free-living cells (0.2-1.6 micron) and cells from the particle fraction (>1.6 micron; **Figure 1A**). The Nod topology was generally consistent with a previous phylogeny from (Fuchsman et al., 2017), with additional taxonomic data from MAGs in the TARA oceans dataset further constraining Nod placement (Tully et al., 2018). As expected based on the binning and BLAST results, the Nod sequence from (Padilla et al., 2016) (Ga0066848_100037855) clustered phylogenetically with marine Alphaproteobacteria (hereafter “Alpha-type Nod”); this clade contained three unique sequences, all of which were present in multiple metagenomes and all from the free-living fraction, and one of which was identical to that of Rhodospirillaceae NP1106 (MBV28360). Four unique ODZ Nod sequences clustered with marine Gammaproteobacteria (OTU II in (Fuchsman et al., 2017), hereafter “Gamma-type Nod”); these sequences were monophyletic with a cluster of Gammaproteobacteria Nod cluster sequences from sewage sludge, including Gammaproteobacterium HdN1 (Ehrenreich et al., 2000) and other wastewater Gammaproteobacteria. Multiple ETNP ODZ metagenomes contained Gamma-type Nod sequences identical to those of Gammaproteobacteria NP964 (MBP20251). Gamma-type Nod had ~70% identity to Alpha-type Nod. Several ODZ Nod sequences, all from the particle fraction (“PF”)

clustered with marine Deltaproteobacteria in a clade of monophyletic *nod* genes from groundwater *Methylomirabilis*, Deltaproteobacteria, and Acidobacteria MAGs (~65% identity to Alpha-type Nod). Six unique Nod ODZ protein sequences (two of which were present in multiple metagenomes) clustered with Planctomycetia (OTU I in (Fuchsman et al., 2017), hereafter “Planctomycetia-type Nod”), and were primarily found in free-living cells (“FL”) and had ~40% identity to Alpha-type Nod. Intriguingly, two ODZ sequences clustered in the eukaryotic *Globobulimina* genus (~50% identity to Alpha-type Nod). Viral Nod sequences from Saanich Inlet (~55% identity to Alpha-Nod) clustered with the viral Nod sequence previously reported by (Gazitúa et al., 2021) from the Eastern Tropical South Pacific ODZ (St16 OMZ 317E).

We investigated gene neighborhoods surrounding ODZ *nod* genes in the three main phylogenetic clusters of ODZ sequences: Planctomycetia-type Nod, Gamma-type Nod, and Alpha-type Nod. Whereas “unknown Nor-related” marine Bacteroidota sequences were located on an operon with other *nor* genes, there was no consistent gene neighborhood for *nod* sequences (**Figure 1B**). Planctomycetia-type *nod* genes were not located in the vicinity of any genes with recognizable related function. Gamma-type *nod* gene neighborhoods contained ferredoxins and cytochrome *b₅₆₁* genes for electron transport. Upstream of the Alpha-type *nod* in *Rhodospirillaceae* NP1106 is a cluster of formylmethanofuran dehydrogenase genes (*fmd/fwd*) used in C1 metabolism via tetrahydromethanopterin/methanofuran-linked reactions.

Immediately upstream or downstream of *nod* genes, helix-turn-helix transcriptional regulators were common (**Figure 1B**). Neighboring Gamma-type and *Methylomirabilis nod* genes, LuxR-type regulators were common; these regulators have diverse functions

and their potential connection to Nod remains unclear. Neighboring Alpha-type and Bacteroidota (e.g. *Cecembia calidifontis*) *nod* genes, Rrf2-type regulators were present. The protein NsrR in the Rrf2 family regulates global cellular response to NO toxification by directly sensing NO with an iron-sulfur cluster (Bodenmiller and Spiro, 2006; Tucker et al., 2010). The presence of this NsrR-like regulator suggests that Nod in marine Alphaproteobacteria and Bacteroidota may be involved in nitrosative stress response and NO detoxification.

2.5.2 *Alphaproteobacterial nod is highly transcribed in anoxic waters.*

We assessed transcription of Alpha, Gamma-, and Planctomycetia-type *nod* genes from the oxycline to upper ODZ (secondary nitrite maximum) using ETNP ODZ metatranscriptomes from an onshore station with a shallower oxycline (P1; **Figure 1C**) and an offshore station with a deeper oxycline (P2; **Figure 1D**) (Mattes et al., 2022). In both oxyclines, transcription was low (4-10 reads per kilobase per million mapped reads (RPKM), n=8) for all three *nod* types (**Figure 1C, D**). Below the oxyclines, *nod* transcripts began to rise and were highest at the secondary nitrite maxima, with Alpha-type (184-274 RPKM, n=4) > Gamma-type (55-95 RPKM, n=4) > Planctomycetia-type (13-19 RPKM, n=4).

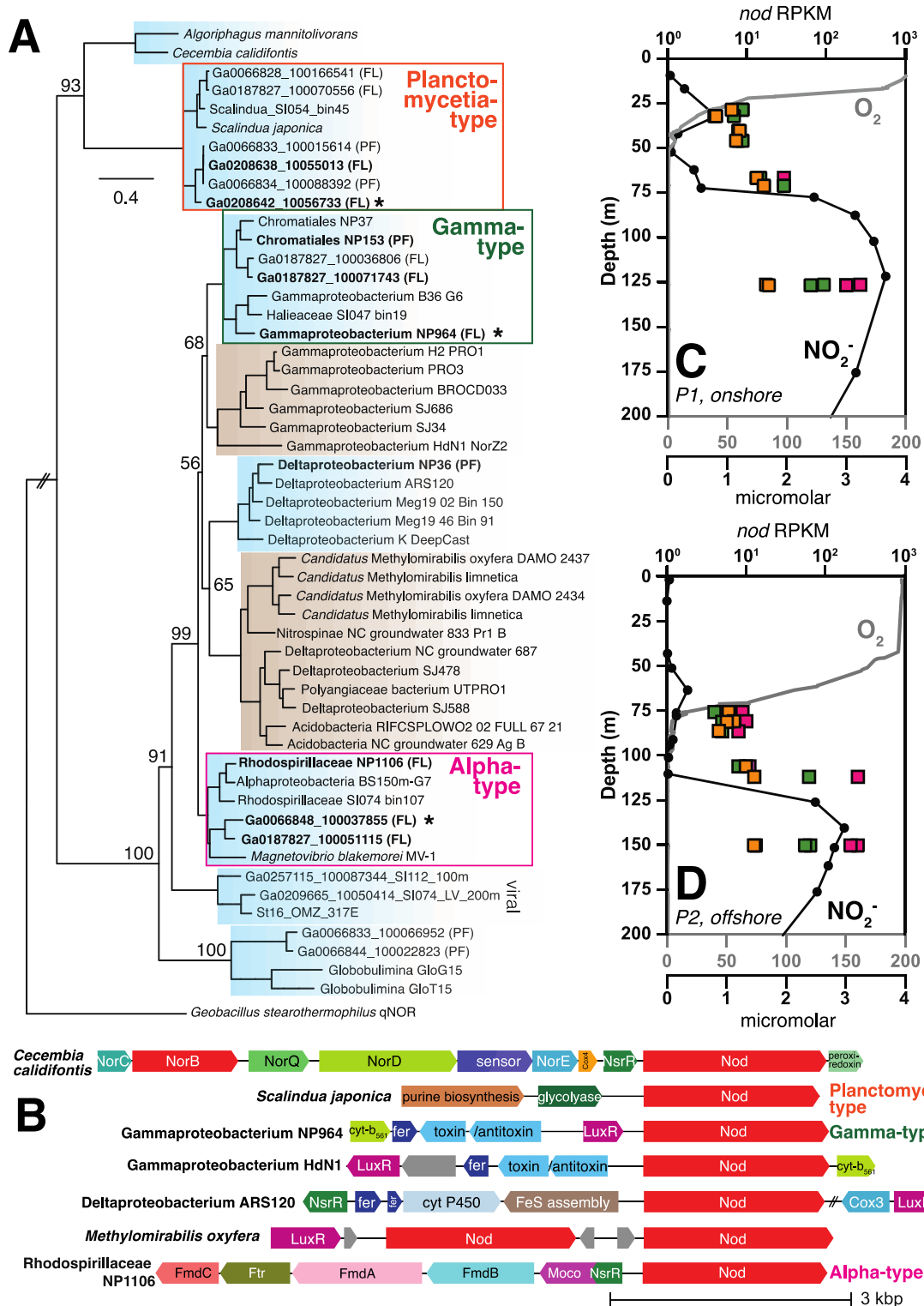


Figure 1. Marine Nod clades, gene neighborhoods, and depth profiles of transcription. (A) Maximum likelihood phylogeny of nitric oxide dismutase (Nod) amino acid sequences in marine (blue) and select terrestrial (brown) taxa, primarily from marine

MAGs (Tully et al., 2018; Cabello-Yeves et al., 2021; Lin et al., 2021) and ETNP ODZ metagenomes (Ruiz-Perez et al., 2021). Branch support was evaluated using 1000 rapid bootstrap replicates, with bootstrap values shown for deep branches. The tree is drawn to scale, with branch lengths in number of substitutions per site. Bold sequences represent those present in multiple ETNP ODZ metagenomes. “PF” indicates genes from the particle fraction (>1.6 µm fraction) of filters. “FL” indicates genes from the free-living fraction (0.2-1.6 micron) collected on Sterivex filters. The most highly transcribed ETNP ODZ sequence is indicated with an asterisk. The qNor sequence *Geobacillus stearothermophilus* was used as the outgroup. (B) Gene neighborhoods surrounding *nod* genes in select taxa. GenBank contigs: *Cecembia calfontis* SGXG01000001, *Scalindua japonica* BAOS01000045, Gammaproteobacteria NP964 PBRC01000062, Gammaproteobacterium HdN1 FP929140, Deltaproteobacteria NZCL01000067, *Candidatus Methyloirabilis oxyfera* FP565575, and *Rhodospirillaceae* NP1106 PCBZ01000014. Unlabeled gray genes are hypothetical. (C, D) Oxygen and nitrite concentrations (circles), and *nod* transcripts (squares, as reads per kilobase per million mapped reads (RKPM)) with depth in ETNP ODZ P1 (onshore) and P2 (offshore) sites.

2.5.3 *MAGs with highly transcribed nod gene represent a new order of Alphaproteobacteria.*

In order to assess the phylogeny of the *nod*-containing Alphaproteobacteria MAGs, we constructed an alphaproteobacterial phylogeny using the conserved protein NADH ubiquinone oxidoreductase subunit L (NuoL) as in Cevallos and Degli Esposti (2022), with additional representation of order UBA11136 including our MAG ETNP2013_S10_300m_22 (**Figure 2**). MAG ETNP2013_S06_300m_15 was not included in the phylogeny because its *nuoL* gene was truncated. UBA11136 is situated in the phylogeny near other orders found in ODZs.

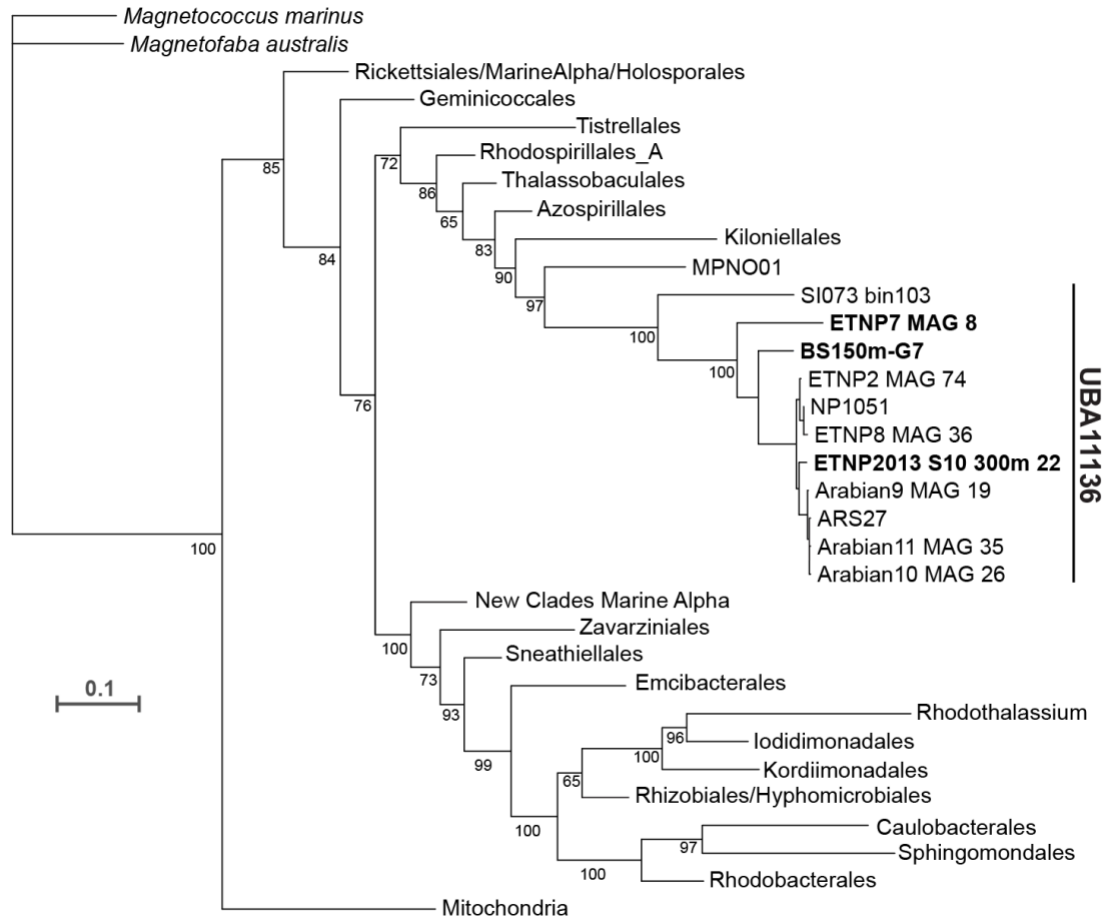


Figure 2. Phylogeny of Alphaproteobacteria showing order UBA11136, with *nod*-containing MAGs. The phylogeny was constructed using the Alphaproteobacterial phylogenetic marker NADH ubiquinone oxidoreductase subunit L as in Cevallos and Esposti (2022). Order UBA11136 is expanded, and *nod*-containing MAGs are bolded. Taxonomic names are from Cevallos and Esposti (2022) and GTDB Release 08-RS214. The scale bar represents amino acid substitutions per site.

2.5.4 Alphaproteobacteria transcribe genes for formate metabolism, aerobic respiration, and a multiheme cytochrome complex

To glean insight into potential roles for Nod in cellular context, we sought to reconstruct the electron transport chain of the Alphaproteobacteria with the most highly transcribed *nod* genes (Alphaproteobacterium MAG ETNP2013_S10_300m_22 and

Alphaproteobacterium MAG ETNP2013_S06_300m_15, 73% and 69% estimated completeness, respectively) at the secondary nitrite maximum. Of total metagenomic reads, 0.38% map to ETNP2013_S10_300m_22 and 0.39% map to ETNP2013_S06_300m_15. In both MAGs, *nod* was in the top three most transcribed genes in the ETNP ODZ (~44,000 FPKM), after a bacterial nucleoid DNA-binding protein and a potassium gated channel protein. In addition to *nod*, we found that genes for formaldehyde oxidation via tetrahydromethanopterin/methanofuran-linked reactions, including formylmethanofuran dehydrogenase (*fwd/fmd*) and formylmethanofuran-tetrahydromethanopterin N-formyltransferase (*ftr*), were transcribed in both MAGs. Both MAGs also transcribed NAD-dependent formate dehydrogenase. Thus, the alphaproteobacterium appears to be capable of conversion of formaldehyde to formate and use of formate as a source of electrons for NADH:ubiquinone oxidoreductase (Complex I; **Figure 3**). The source of formaldehyde is likely methanol oxidation, as pyrroloquinoline quinone (PQQ)-dependent ethanol/methanol dehydrogenases were found in Alphaproteobacteria MAGs from low-oxygen marine settings. Methane monooxygenase genes were not found in the partial Alphaproteobacteria MAGs, precluding our ability to rule out the possibility of these genes in the missing portions of the genomes. The Alphaproteobacteria PQQ-dependent dehydrogenase genes contained the motif DYDG, which is characteristic of the lanthanide-containing form of the enzymes rather than calcium form (Keltjens et al., 2014).

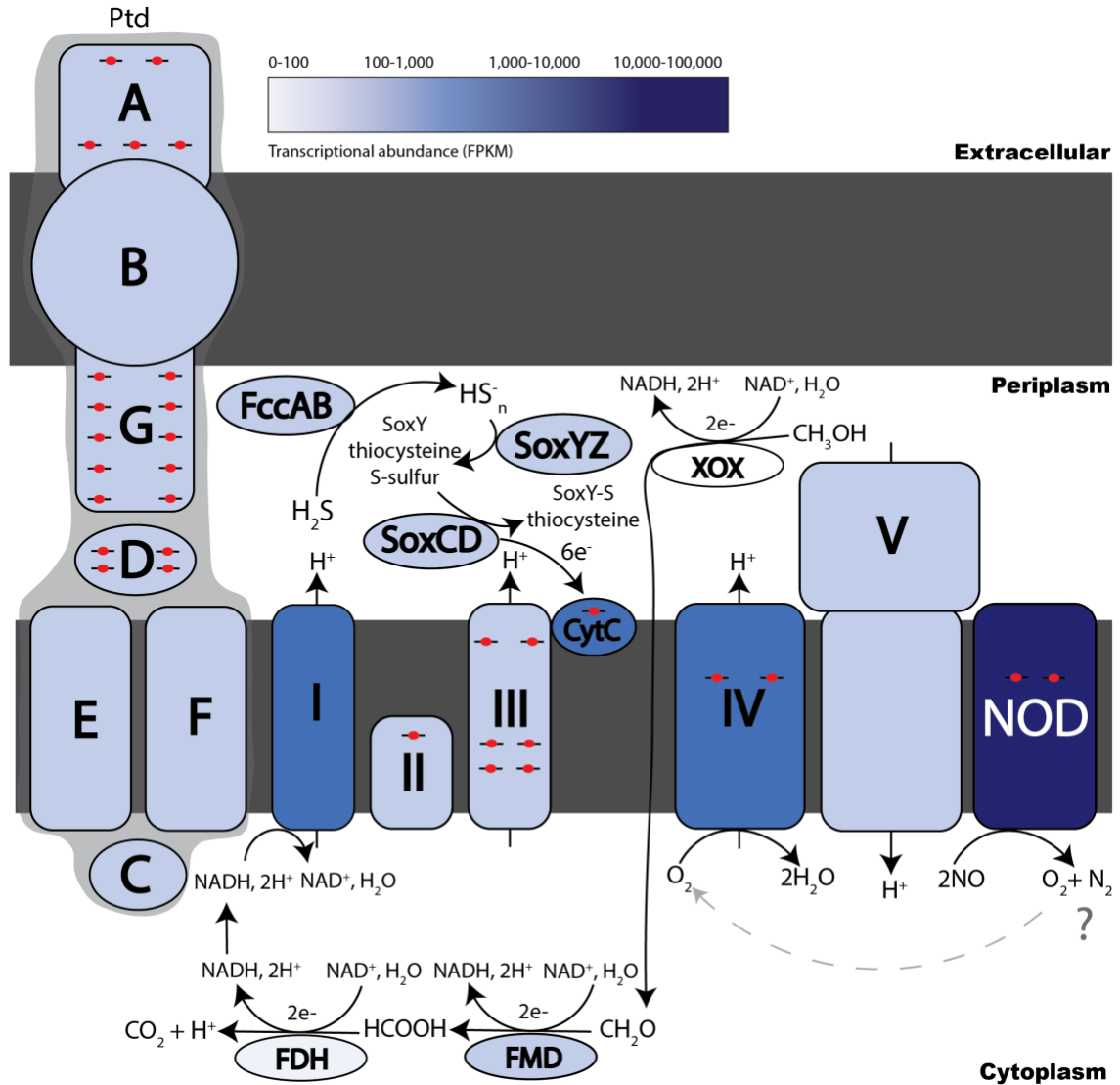


Figure 3. Schematic of the electron transport chain in *nod*-containing ODZ Alphaproteobacteria. Enzymes were included based on presence and transcriptional activity of metagenome-assembled genomes (MAGs) assigned to Alphaproteobacteria (GTDB taxonomy: UBA11136 sp002686135; see text). The color of each protein is chosen according to transcriptional activity and represented from 0-100, 100-1,000, 1,000-10,000, and 10,000-100,000 FPKM in gradient from lighter to darker blue. Heme proteins are indicated by red circular hemes with the cartoon number corresponding to the number of actual hemes present on each protein. Hypothetical Ptd proteins are labelled A, B, C, D, E, F, and G, and location within the cell is determined using Psort bacterial localization prediction tool. ETC complexes I-V found in Alphaproteobacteria MAGs are labelled with proposed interactions between formate oxidation and complex I NADH electron transfer. Highly transcribed NOD protein and predicted O₂ generation is shown as feeding into A1 type CCO complex IV reduction. Additional electrons for CytC and the ETC are proposed to come from

sulfur oxidation carried out by the flavocytochrome *c* sulfide dehydrogenase (FccAB, FCC), and sulfane-sulfur dehydrogenase (SoxCD) with the multi-enzyme carrier complex (SoxYZ).

A full aerobic electron transport chain (Complex I, II, III, and IV) and F0F1-type ATP synthase were transcribed in both bins (**Figure 3**). Complex IV (cytochrome *c* oxidase) was type A1 according to the (Sousa et al., 2012) classification, and the *cox* operon in the GTDB species representative Rhodospirillaceae ARS27 was subtype b (COX2-COX1-CtaB-CtaG_Cox11-COX3-DUF983-SURF1-CtaA1-M32-Tsy-M16B) according to the Geiger et al. (2023) classification. Sulfur oxidation genes, including flavocytochrome *c* sulfide dehydrogenase (FccAB), sulfane hydrogenase (SoxCD), and carrier protein SoxYZ, were also transcribed, as were numerous transposes (**Figure 3**).

Genes for a multiheme cytochrome complex were transcribed in both bins. To our knowledge, this putative operon has not previously been described. Hereafter, we designate it the *ptdABCDEFG* operon for its sequence of penta/tetra/deca-heme proteins, interspersed with other conserved proteins. *ptdAB* genes are highly transcribed in our Alphaproteobacteria MAGs, but it is unclear if the rest of the operon is also highly transcribed, because it was truncated in our MAGs' scaffolds. The *ptd* gene cluster consists of a penta-heme protein with a C-terminal beta-sandwich (PtdA), a porin (PtdB), a FAD/NAD(P)-binding oxidoreductase (PtdC), a periplasmic tetra-heme protein (PtdD), a cyclic nucleotide-binding domain protein with two 4Fe-4S clusters (PtdE), a cytoplasmic transmembrane ferric reductase-like protein (PtdF), and a periplasmic deca-heme protein (PtdG; **Figure 3**). The function of this complex is unknown, but the presence of genes encoding a porin and multiple multiheme proteins resembles porin-cytochrome protein complexes involved in extracellular reduction electron transfer during Fe(III) and Mn(IV)

reduction (Richardson et al., 2012; Shi et al., 2014). PtdA has a homolog to a penta-heme cytochrome *c*₅₅₂ protein of unknown function in a thermophilic purple sulfur gammaproteobacterium (Chen et al., 2019) and is in the same COG family (COG3303) as formate-dependent nitrite reductase, NrfA. *ptdABCDEFG* genes were prevalent in Alphaproteobacteria, Gammaproteobacteria, Nitrospirales, and Planctomycetes MAGs from marine or high salinity environments (**Figure 4**).



Figure 4. Gene neighborhoods of pentaheme-tetraheme-decaheme genes from select organisms. Depicted heme spacing is approximate. All organisms are from saline environments (seawater, marine sediment, or saline spring).

2.6 Discussion

This study predicts the previously ambiguous identity of the microorganisms that make the dominant nitric oxide-transforming protein (Nod) in the world's largest ODZ, the Eastern Tropical North Pacific. Extensive horizontal gene transfer of *nod* genes between microbial genomes is evident from the lack of conservation of gene neighborhood and patchy phylogeny (Fuchsman et al., 2017), which may be mediated by viral infection (Gazitúa et al., 2021). We found that the most transcriptionally active *nod* genes in the ETNP upper ODZ belong to the novel Alphaproteobacteria order UBA11136. Alpha-type

nod transcript abundances (~200 RPKM) are similar to those of dissimilatory nitrate reductase (*narG*) in the ODZ (Tsementzi et al., 2016). The *nod*-transcribing Alphaproteobacteria are also transcribing genes for formaldehyde oxidation, likely as a source of electrons to the respiratory chain via NAD reduction by formate dehydrogenase. Sulfide may be used as a supplemental electron donor and/or may be concomitantly oxidized for detoxification (Callbeck et al., 2021; Schmitz et al., 2023).

Our discovery of a putative porin-cytochrome complex (*ptd* operon) in marine bacteria was unexpected. Porin-cytochrome complexes have been best studied for their role in extracellular electron transport, particularly for respiratory metal reduction and oxidation (Richardson et al., 2012; Shi et al., 2014). It is conceivable that the Ptd complex is involved in iron reduction in ODZs; there is iron reduction at the secondary nitrite maximum and it is hypothesized to be bacterially mediated, but the microbes involved have yet to be determined (Moffett et al., 2007; Glass et al., 2015). Alternatively, the presence of *ptdABCDEFG* genes in numerous nitrite-oxidizing bacteria (Nitrospirales) could imply the involvement of these genes in nitrogen cycling; PtdA was in the same COG family as formate-dependent nitrite reductase (Simon et al., 2000) and PtdC is similar to a flavohemoprotein with predicted nitric oxide dioxygenase activity, also annotated as hydroxylamine oxidoreductase-linked cytochrome. The function of PtdABCDEFG remains completely unknown and requires future biochemical characterization.

On the other end of the electron transport chain, high transcription of a heme/copper terminal oxidase suggests that O₂ is being used as the terminal electron acceptor in *nod*-transcribing Alphaproteobacteria MAGs. The transcribed heme/copper oxidase is A1-type (low O₂ affinity), also present in mitochondria, and adapted for high O₂ concentrations.

Low O₂ affinity A1-type heme/copper oxidases are transcribed in other anoxic environments (Berg et al., 2022). Because ODZs have extremely low concentrations of molecular oxygen below the oxycline, O₂ for aerobic respiration may be generated *in situ* and rapidly consumed. Given that the function of Nod is proposed to be dismutation of two NO molecules into N₂ and O₂ (Ettwig et al., 2010), it is possible that the O₂ source for aerobic respiration in the UBA11136 MAGs is NO dismutation, although other sources of O₂ (e.g. *in situ* photosynthesis, mixing) in anoxic waters are also conceivable (Garcia-Robledo et al., 2017). The physiological uses of Gamma-type and Planctomycetia-type Nod may be different from Alpha-type Nod, although this remains to be investigated.

The source of NO, the presumed substrate for Nod, may be generated in the same organism using Nod, or generated by a different organism (or chemical pathway). Nitric oxide was positively correlated with nitrite in the Eastern Tropical South Pacific ODZ, and was only detectable when O₂ was <1-2 μM (Lutterbeck et al., 2018). In the Eastern Tropical North Pacific, NO concentration and turnover rates were elevated at O₂ <100 mM (Ward and Zafiriou, 1988). Both studies suggest that the NO in ODZs likely originates from nitrification or nitrifier denitrification, while genomic analyses indicate that the copper-containing nitrite reductase (*nirK*) in SAR11 bacteria (presumably performing denitrification) may be a key source of NO (Fuchsman et al., 2017). Because most ODZ denitrifiers specialize in only one of the three steps (NO₂⁻ reduction, NO reduction, and N₂O reduction) (Zhang et al., 2023), and known nitrite reductases were not identified in our MAGs, existing data indicate that the NO that is used as a substrate for alphaproteobacterial Nod is not generated *in vivo*. (Only 4 out of 32 *nod*-containing MAGs contained a nitrite reductase gene: two Gammaproteobacteria MAGs contained *nirK*, one

Myxococcota MAG contained *nirS*, and one Scalindua MAG contained *nirS*). It is also possible that another uncharacterized enzyme produces NO.

This study suggests that marine Alphaproteobacteria from order UBA11136 are actively reducing NO under anoxia, as implied by their abundant transcription of *nod* genes. While there is strong evidence that the substrate for Nod in ODZs is NO based on its abundance, the products of this enzyme (N₂O vs. N₂+O₂) remain uncertain. Nod is theorized to disproportionate NO into N₂ and O₂ in methane-oxidizing *Methylomirabilota* bacteria (Ettwig et al., 2010; Ettwig et al., 2012), but no biochemical characterizations of Nod have been published to date, and foraminifera expressing Nod produce N₂O (Woehle et al., 2018). The apparent lack of other denitrification genes in *nod*-transcribing Alphaproteobacteria is consistent with the observation that denitrification in ODZs is largely divided into distinct microbial taxa (Dalsgaard et al., 2014; Fuchsman et al., 2017; Zhang et al., 2023). For example, although nitrate reductase (*narG*) genes are widely distributed amongst ODZ microbes (Zhang et al., 2023), SAR11 bacteria appear to dominate in *narG* transcriptional activity (Tsementzi et al., 2016). Our finding that the transcription of *nod* is catalyzed primarily by marine Alphaproteobacteria implies that this taxon contributes significantly to marine nitrogen loss.

2.7 Conclusion

We sought to identify the microbe(s) responsible for the abundant transcription of nitric oxide dismutase (*nod*) in the ETNP ODZ. We found that the most abundantly transcribed *nod* genes in the Eastern Tropical North Pacific ODZ belong to a new order (UBA11136) of Alphaproteobacteria, and that Gammaproteobacteria and Planctomycetia

transcribe *nod* at lower relative abundance in the upper ODZ. We infer from metagenomics and transcriptomics that UBA11136 is an aerobic bacteria using formaldehyde and formate as a source of electrons, with additional electrons possibly from sulfide oxidation. Molecular oxygen for aerobic respiration may originate from nitric oxide dismutation via cryptic oxygen cycling. We further identified transcription of multiheme cytochrome (here named *ptd*) genes for a putative porin-cytochrome protein complex of unknown function and propose its involvement in extracellular electron transfer by UBA11136. The lack of cultured representatives of this novel Alphaproteobacterial clade prevents us from comparing our results to known biochemical functions or metabolisms, however. Intriguingly, UBA11136 constitutes a deep branching clade of Alphaproteobacteria that has recently been implicated in a new model for eukaryogenesis (Esposti, 2023). It is now hypothesized that eukaryogenesis originated in the primordial ocean with a marine Alphaproteobacteria whose lineage is remanent in modern-day oxyclines (Cevallos and Degli Esposti, 2022; Geiger et al., 2023). Future work in isolating and characterizing UBA11136 will shed light on its function in the modern-day ETNP ODZ, including potential oxygen generation with *nod*, as well as provide a model extant organism to understand the bacterial player in eukaryogenesis.

**CHAPTER 3. DENITRIFYING *MARINOBACTER PACIFICUS* SP. NOV. FROM
AN OXYGEN DEFICIENT ZONE GROWS UNDER A METHANE
HEADSPACE AND OXIDIZES ETHANOL, METHANOL, AND FORMATE**

A portion of this work will be published in a manuscript in preparation authored by Claire E. Elbon, Héctor Gabriel Torres- De Jesús, Helen M. Tran, Emma A. Aycock, Nidhi Desai, Ashley S. Kleinman, Christopher E. Mason, Jennifer Kaiser, Brook L. Nunn, Frank J. Stewart, and Jennifer B. Glass.

3.1 Abstract

Methane oxidation is highly active in the anoxic core of the Eastern Tropical North Pacific oxygen deficient zone (ETNP ODZ). Extensive study of the anoxic core links methane oxidation activity to obligate aerobic methanotrophs transcribing methane monooxygenase and nitrate reduction genes. Overall, anaerobic 1-carbon oxidation coupled to nitrate reduction remains understudied in the ETNP ODZ. I sought to study potential metabolisms of 1-carbon oxidation coupled to nitrate reduction by enriching for bacteria in long-term concentrated cell enrichment cultures from the ETNP ODZ. I isolated a novel *Marinobacter* species, here named *M. pacificus*, that forms a clade with two other uncultured strains. In anaerobic cultures, *M. pacificus* conserves energy for growth under a 95% methane headspace with 100 μ M nitrate and is autofluorescent at \sim 465 nm. Proteins catalyzing methanol/ethanol/formaldehyde oxidation (ExaF), formate oxidation (Fdh), the full suite of denitrification, and cellular growth and replication (FtsH and ATP synthase subunits) were significantly abundant under a 95% methane headspace. *M. pacificus* grows aerobically with with formate, methanol, ethanol, and lactate. The 95% methane gas

headspace of bottles with actively denitrifying cultures contains formaldehyde and methanol, which *M. pacificus* oxidizes to formate and CO₂. I postulate that *Marinobacter pacificus* conserves energy for growth from nitrate reduction coupled to 1-carbon oxidation of methanol and formaldehyde. Methane oxidation in the gas headspace is catalyzed by abiotic hydroxyl radicals from photochemistry or an unknown N-oxide interaction. To my knowledge, this is the first study of anaerobic oxidation of one-carbon compounds by a denitrifying *Marinobacter* species.

3.2 Introduction

Oxygen deficient zones (ODZs) comprise only ~1% of the ocean but are key players in global biogeochemical cycles (Thamdrup et al., 2012). High rates of aerobic respiration rapidly deplete O₂ in the oxycline; below the oxycline, a secondary nitrite peak indicates a metabolic switch to anaerobic nitrate reduction (Ulloa et al., 2012). The largest ODZ by volume is the Eastern Tropical North Pacific oxygen deficient zone (ETNP ODZ) (Kwiecinski and Babbin, 2021). Methane oxidation in the anoxic core of the ETNP ODZ has been linked to denitrification (Padilla et al., 2016; Thamdrup et al., 2019). Obligately aerobic methanotrophs comprise the majority of transcriptional activity for methane oxidation and nitrate reduction in the anoxic core (Thamdrup et al., 2019). Far less studied is additional carbon metabolisms, including 1-carbon compounds methanol, ethanol, formaldehyde, and formate in the ETNP ODZ (Henríquez-Castillo et al., 2022).

Several one-carbon electron sources can support denitrification in obligate methanotrophic bacteria under hypoxia, including methane, methanol, formaldehyde, and formate (Kits et al., 2015b). While methane is oxidized by methane monooxygenase

(MMO), methanol, ethanol, and formaldehyde can be directly oxidized to formate by recently characterized lanthanide-dependent pyrroloquinoline quinone alcohol dehydrogenase, ExaF (Good et al., 2016; Good et al., 2019; Yanpirat et al., 2020). Methanol is supplied to marine systems in significant quantities from phytoplankton (Mincer and Aicher, 2016). Indeed, several abundant marine bacteria oxidize methanol for growth using lanthanide-dependent pyrroloquinoline quinone alcohol dehydrogenases, including *Roseobacter* and OM43 (Ramachandran and Walsh, 2015; Howat et al., 2018). Ethanol may be supplied in the anoxic core via excretions from fish travelling within the oxycline experiencing hypoxia (Torres et al., 2012).

An understudied source of oxidized 1-carbon compounds are particles sinking through the anoxic core, as referred to as marine snow. Marine snow constitutes a “hodge-podge” of organic matter from viral lysis of plankton and bacteria, dead microbial matter, waste matter from zooplankton, and dead zooplankton (Lampitt, 2001). In an oligotrophic water column, a particle is an abundance of organic material in an otherwise devoid system that is quickly utilized (Hach et al., 2020). Particles can serve as microniches of heterogenous microbial communities within a highly homogenous water column (Flintrop et al., 2018) and as anoxic hotspots supporting anaerobic microbes within a water column (Bianchi et al., 2018). Indeed, detected microbial communities, their activity, and their genomic traits are markedly different between free-living and particle-associated samples in a water column (Ganesh et al., 2015; Rieck et al., 2015; Taylor et al., 2018; Leu et al., 2022).

Alteromonas have been found at high abundances in the ETNP ODZ particulate fraction (>1.6 microns) co-occurring with another heterotroph, *Marinobacter*, and primary

producers *Prochlorococcus* (Henríquez-Castillo et al., 2022). *Marinobacter* and *Alteromonas* are considered essential “helper” heterotrophs for growing *Prochlorococcus* in lab settings in part by their “carbon for iron” symbiosis in marine environments (Morris et al., 2008; Amin et al., 2012). Interactions with methane and additional 1-carbon compounds coupled to nitrate reduction may occur by *Marinobacter* and other heterotrophic “helpers” in the ETNP ODZ but are understudied and a mechanism is unknown.

I sought to understand potential bacteria using methane oxidation coupled to denitrification in the ETNP ODZ from long term enrichments of concentrated cells. I isolated a novel *Marinobacter* species, here named *Marinobacter pacificus*, grown under methane headspace with nitrate. Since this novel species came from cultures under methane and nitrate conditions, I hypothesized that *Marinobacter pacificus* can perform methane oxidation coupled to denitrification conserving energy for growth. I performed culture transfers, tracked cell growth under several carbon sources and anaerobic conditions, analyzed the methane gas headspace in cultures and performed proteomics to elucidate the metabolism occurring under anaerobic conditions with methane headspace and nitrate as the sole carbon and nitrogen sources. I found that *M. pacificus* is autofluorescent at ~465 nm under anaerobic growth and performs complete denitrification under a 95% methane 5% CO₂ headspace. Further, *M. pacificus* expresses lanthanide- and PQQ-dependent alcohol dehydrogenase protein, ExaF, formate dehydrogenase, Fdh, and the full suite of denitrification genes, as well as ATP synthase subunits and FtsH enzyme supporting growth and replication. Last, we detected formaldehyde and methanol in the methane gas headspace of bottle cultures, supporting methane oxidation to oxidized 1-carbon species

used by expressed ExaF protein in *M. pacificus*. *Marinobacter pacificus* conserves energy for growth from nitrate reduction coupled to methanol and formaldehyde oxidation. I propose that abiotic methane oxidation driven by hydroxyl radicals provides methanol and formaldehyde used by *M. pacificus*.

3.3 Methods

3.3.1 Culture enrichment and transfers

3.3.1.1 Establishment of primary enrichments

On R/V *Oceanus* cruise OC1705A (May 2017), bottle enrichments were inoculated with seawater from the secondary nitrite maximum (130 m) at station 6 (18°54' N, 104°54' W) of the ETNP ODZ, where ambient NO₂⁻ was 3 μM and dissolved O₂ was <1 μM. For each bottle, 100 mL of seawater was sampled from a Niskin bottle into a 160 mL serum bottle, which was then purged of O₂ by bubbling for at least 5 min with ultra-high purity N₂ gas and capped with a red stopper. 2 L of seawater was filtered onto 0.2 μm GTTP filters to concentrate cells. Bottles were then reopened and one filter was added to each bottle. Each bottle was then re-sparged with ultra-high purity N₂ gas for 1 min and recapped. A subset of bottles was then amended with 6 mL ultra-high purity CH₄ into 60 mL headspace and overpressured to 25 psi with ultra-high purity N₂ (hereafter 90% N₂/10% CH₄), and either 100 mM NO₃⁻ or 100 mM NO₂⁻ (**Table 1**). Bottles were transported back to Georgia Institute of Technology and stored in the dark at 25°C for approximately four years.

Table 1. Bottle IDs for primary enrichments from May 2017.

Bottle ID	Headspace	NO_x⁻ addition
62, 63, 64	100% N ₂	100 mM NO ₃ ⁻
65, 66, 67	100% N ₂	100 mM NO ₂ ⁻
68, 69, 70	90% N ₂ /10% CH ₄	100 mM NO ₃ ⁻
71, 72, 73	90% N ₂ /10% CH ₄	100 mM NO ₂ ⁻

3.3.1.2 *ETNP ODZ seawater medium*

In January 2021, seawater from the ETNP ODZ (17°04.771' N, 107°44.366' W) was collected from a combination of depths from the oxycline and deeper, filtered (0.22- μ m), and stored at 25°C in the dark. Before transfers, the ETNP ODZ seawater was filtered 2x through 0.22- μ m filters to remove residual cells. 2x0.22 filtered sterile controls showed no change in nitrite, confirming the biological activity in subsequent transfers came from the inoculum. 5 mL of filter-sterilized 10 mM NaNO₃ or 10 mM NaNO₂ in artificial seawater was added to 2x filtered ETNP ODZ water (500 mL) to yield a final concentration of 100 μ M NO₃⁻ or NO₂⁻. The prepared 500 mL bottles of ETNPODZ+100 μ M NO_x growth media were then sparged with sterile He gas to remove O₂ for anaerobic transfers.

3.3.1.3 *Secondary and tertiary transfers*

In March 2021, secondary (2°) transfers were established by 1:10 dilutions of inoculum from primary cultures (**Table 1**) into sterile 160 mL serum bottles. 500 mL bottles of ETNPODZ+100 μ M NO_x and original bottle cultures 69 and 71 were transported

into an anoxic (97% N₂/3% H₂) chamber. 9 mL inoculum was transferred with a sterile 26-gauge needle and 3 mL syringe into sterile 160 mL serum bottles containing 91 µL of ETNPODZ+100µM NO_x media. The new transfers were then sealed in the chamber with sterile, He-sparged, red rubber bottle tops and sealed with aluminum crimp tops. The headspace of every bottle was then exchanged outside of the chamber to overpressure using two sterile 27-gauge needles attached to gas lines with 0.22-µm filters. The gas headspace for the methane condition of 2° transfers for the 69 and 71 bottle cultures were changed to a 95% CH₄/5% CO₂ gas mixture to promote growth, and 100% helium was used as an inert gas control. The above 1:10 dilution methods were then repeated to start 3° transfers of bottle 69 with inoculum from the 2° transfer of bottle 69 after ~40 days of incubation.

3.3.1.4 *MWH defined minimal media*

Defined minimal seawater media and agar plates were created for targeted enrichment and isolation of novel *Marinobacter* species using informed genomics. MWH media (Henson et al., 2020) was used as the basal artificial seawater minimal media, with modifications. Amino acid, misc., fatty acid, and inorganic nitrogen mixes were not added here because *Marinobacter* spp. can synthesize all amino acids and assimilate nitrate as the sole nitrogen source. We added 50 nM of vanadium chloride, 50 nM of sodium selenate, and 100 nM of sodium tungstate dihydrate to the vitamin mix. 500 mL bottles of MWH minimal+nitrate were prepared for anoxic transfers in the same way as the ETNPODZ+100 µM NO_x growth media.

3.3.1.5 *Marinobacter isolation and growth in minimal seawater media*

Isolation was performed in June 2024 using our modified MWH minimal+nitrate media (Henson et al., 2020) with nitrate as sole electron acceptor. Lactate was added in addition to the methane headspace for initial isolation steps to support growth of *M. pacificus*. Isolation experiments were performed by addition of 0.5 mL of 3° inoculum (**Table 1**) onto sterile MWH minimal+nitrate agar plates with 200 μ M lactate and grown both aerobically in a dark cabinet and anaerobically in a covered dark Anaerobic jar (Millipore; 1136810001) sparged to overpressure with a 95% CH₄/5% CO₂ gas mixture. After growth was observed as colonies for both conditions over ~7 days, streak inoculations were performed into 15 mL aerobic tubes and Balch tubes for anaerobic growth containing 10 mL of MWH minimal+nitrate plus 200 μ M lactate in aerobic and helium-sparged bottles, respectively. Aerobic 15 mL tubes were grown in 25°C shaking, light conditions and anaerobic 15 mL tubes were grown in a dark cabinet with tube inversions performed every 12 hours. Growth was tracked using optical density 600 nm (OD₆₀₀). MWH media supported growth of our novel species while maintaining the phylogenetic characteristics observed with growth in sterile ETNP media. After 7 days, 160 mL bottles containing 91 mL of He-sparged MWH minimal+nitrate growth media were prepared in 5 replicates in the anaerobic chamber for 1:10 inoculations into liquid culture bottles from the 15 mL tubes. The headspace of the new transfers in 160 mL bottles was then exchanged with 95% CH₄/5% CO₂ gas mixture or 100% He gas to overpressure.

For autofluorescence imaging, *Marinobacter vinifirmus* and *Marinobacter hydrocarbonoclasticus* strains isolated from the Gulf of Mexico sands (provided by the Joel Kostka lab, Georgia Institute of Technology) were grown aerobically in modified MWH minimal medium with 200 μ M lactate and 100 μ M NO₃⁻ with shaking at 25°C.

Growth was measured over 14 days using optical density at 600 nm (OD₆₀₀). Both strains were previously found capable of growth under denitrifying conditions.

3.3.1.6 *M. pacificus* growth on formate, methanol, ethanol, and lactate in MWH media

Shaking well plate growth curves were performed in 2025 with 180 µL modified MWH minimal+nitrate media (Henson et al., 2020) with nitrate as sole electron acceptor and 20 µL of *M. pacificus*. The BioTek Synergy HTX multimode well plate reader was set to a 48 well plate linear continuous read in an interval of every 15 seconds (Agilent; 16022315). 200 µM lactate was added to positive controls for aerobic shaking growth in 48 well plates. Formate, methanol, and ethanol additions ranged from 25 mM to 100 mM concentrations for growth. Aerobic growth was measured using optical density (OD₆₀₀) as a proxy for growth for *Marinobacter pacificus* over 48–72-hour periods at 25°C.

3.3.1.7 *Epifluorescent microscopy*

Each sample (25 mL) was fixed in 1% sterile paraformaldehyde diluted from 20% (Thermo Fisher, 047340-9M) and incubated for 24 hours at 4°C. Samples were then vacuum filtered onto 0.2 µm polycarbonate membrane filters (25 mm, Millipore Sigma, GTTP02500) at ~10 Hg pressure. Each filter was rinsed with 5 mL of 0.2 µm filter-sterilized PBS and 5 mL of 75% ethanol diluted in sterile MilliQ water, following by drying on a Kimwipe in the dark. Each filter sample was cut into eight sections with a sterile razor blade and stained with 5 µL SYBR™ Green I Nucleic Acid Gel Stain (Invitrogen, S7563) as described in Patel et al. (2007). SYBR stained filters were mounted onto glass slides with 10 µL Citiflour AF1 glycerol-PBS solution containing an amine antifadent mounting media (EMS, 17970-25 brand, 50-302-34) and either stored at -20°C or immediately

imaged under DAPI and GFP filters with a Zeiss Z.1 epifluorescent microscope. Cell counts were then enumerated using Fiji cell counting tools (Schindelin et al., 2012).

3.3.1.8 Spectral unmixing and emission spectra

We performed spectral unmixing on a Zeiss 780 confocal structured illumination microscope at the Georgia Institute of Technology microscopy core. Excitation was 405 nm. The resolution of spectral detection was set at 3 nm distance for 415 to 600 nm. Spectra were measured on stained and unstained cells from original and secondary NO₃-CH₄ bottle cultures.

3.3.1.9 Fluorescent in-situ hybridization

We performed fluorescent in-situ hybridization microscopy (FISH) to enumerate *Marinobacter* and *Flavobacteriales* from 1°, 2°, and 3° cultures. The *Marinobacter* (Mrb-0625-a) probe (McKay et al., 2016) binds completely to the 16S rRNA region of our *Marinobacter*. We also used a *Flavobacteriales* probe (CF998) for catalyzed reporter depositional-fluorescent in-situ hybridization (CARD-FISH) on fixed filters. We then performed FISH and CARD-FISH microscopy with probe Mrb-0625-a and CF998. Because *Marinobacter* are gammaproteobacteria, we used the CARD-FISH probe Gam42a to enumerate total Gammaproteobacteria (Manz et al., 1992).

We followed standard FISH and CARD-FISH protocols with probe-specific modifications (Pernthaler et al., 2001; Pernthaler et al., 2002). Fluorescently labelled FISH probe Mrb-0625-a was labelled at the 5'-end with cyanine 3 (CY3). CARD-FISH probes CF998 and Gam42a were labelled with a horseradish peroxidase conjugate at the 5'-end.

After the washing step for CARD-FISH, filters were placed in the amplification buffer with containing tyramide labelled with Cyanine 3. Probes for FISH were purified with PAGE and CARD-FISH probes were purified with HPLC (Biomers). The percent formamide used for Mrb-0625-a FISH probe was 20% based on optimum conditions established previously (McKay et al., 2016). The percent formamide used for Gam42a and CF968 CARD-FISH probes was 35% and 55%, respectively (Manz et al., 1992; Acinas et al., 2015). We used a Zeiss Z.1 microscope for initial cell counts and images of FISH and CARD-FISH filters. Stacked overlay images were taken with SYBR green ds-DNA stain and imaged under DAPI filter for three image overlays compiled in FIJI (Schindelin et al., 2012). A Zeiss 780 confocal structured illumination microscope was also used to image FISH and CARD-FISH filters as well as to take higher quality images of cell morphologies.

3.3.2 *Nutrient detection and quantification*

3.3.2.1 *Nitrate and nitrite*

Liquid cultures were assayed for nitrite and nitrate by Griess assay as in García-Robledo et al. (2014). Inside of an anoxic chamber (97% N₂/3% H₂), 1 mL sample was removed from each serum bottle and filtered (0.22 µm) into a 1.5 mL tube, followed by addition of 100 µL of Griess reagent and reaction in the dark for 15 minutes, then measured on a spectrophotometer at 540 nm. 100 µL of vanadium chloride was then added to samples and reacted for 30 minutes in a 60°C water bath to reduce nitrate to nitrite. Samples were again measured spectrometrically at 540 nm. Standard curves of nitrate and nitrite were made in artificial seawater. Bottles were re-gassed to overpressure after each sampling.

3.3.2.2 Headspace nitrous oxide

Bottle tops were sterilized with 70% ethanol. Samples (1 mL) were removed from each serum bottle by syringe and injected into a gas chromatograph with a HayeSep N column and a ^{63}Ni electron capture detector for N_2O detection (GC-ECD, SRI). A 1-ppm N_2O standard (Scotty) was used for calibration.

3.3.2.3 Oxygen

Oxygen was tracked in bottle culture enrichments for proteomics using contactless self-adhesive sterilized oxygen sensor spots (OXSP5-ADH-STER; PyroScience) attached to the side of 160 mL sterile bottles. Blank optical fiber PICFIB2 cables with a PICO-connector were used to measure oxygen spots in 160 mL serum bottles and was connected to a FireSting- O_2 optical oxygen meter connected to a PC for continuous readouts and timepoint measurements. 100% O_2 saturation and 0% O_2 saturation saltwater calibrations were performed using standard protocols in the PyroScience handbook.

3.3.2.4 PTR sampling of gas headspace of cultured bottles with 95% CH_4 5% CO_2

Detection of the four oxygenated compounds was conducted using Ionicon's Proton Transfer Reaction Time-of-Flight Mass Spectrometer (PTR-ToF-MS) 4000 (Ionicon Analytik GmbH, Innsbruck, Austria). The PTR-ToF-MS operated with a mass range spanning mass-to-charge (m/z) 18–256, while the drift tube was held at a temperature of 70°C , pressure at 2.60 mbar, and $E/N = 120$ Td. Instrument sampling rate was 50 sccm. Data collection in counts per second (cps) and peak separation of 1-second averaged spectra were conducted via Ionicon's PTR-Viewer 3.4.3 software. A 50 sccm overflow of

ultra-high purity nitrogen (N₂) gas standard was used to determine the baseline spectra. Adding 1 sccm of 95% CH₄-5% CO₂ gas standard had no impact on the recorded spectra.

Gas samples from the headspaces of eight vials were extracted using a 1 mL airtight syringe and injected into N₂ stream. These headspaces included: three helium (He), three 95% CH₄-5% CO₂ matrices with bacterial samples, and two 95% CH₄-5% CO₂ matrices with bacterial samples exposed to O₂. The headspaces of all vials containing the bacterial sample showed similar increases in m/z 31, corresponding to formaldehyde (CH₂O), and m/z 33, corresponding to methanol. Acetaldehyde (C₂H₄O) to m/z 45, and ethanol (C₂H₆O) to m/z 47 showed no significant increases across all vials. Figure X shows one injection of each headspace type (He, 95% CH₄-5% CO₂, and O₂-contaminated).

3.3.3 *Microbial identification and activity*

3.3.3.1 16S rRNA Sequencing

We performed 16S rRNA Sanger sequencing on the original bottle enrichment cultures as well as 2° and 3° transfers. DNA was extracted for initial 16S rRNA sequencing using boil purification. Cell biomass was pelleted and heated in 20 µL TE buffer at 95°C for 10 minutes in a PCR machine. 16S rRNA was then amplified using universal primers 8F and 1492R. PCR products were purified, cloned, and ligated into pCR 4-TOPO competent *E. coli* cells (Thermo Fisher; K4575J10). Sanger sequencing was performed at the Georgia Tech Molecular Evolution Core sequencing facility. A near complete 16S rRNA sequence of *Marinobacter pacificus* (~1470 bp) was obtained. Results were analyzed in 4 peaks (nucleobases) and reverse and forward sequences were combined using 4Peaks to create nearly complete 16S rRNA sequences.

3.3.3.2 Metagenomics

Liquid samples were extracted using a modified version of live-filtering and concentration into 1.5 mL sterile tubes using a sterile pipetting of medium over the filter to wash the cells into the tube due to low biomass. DNA was extracted using a QIAamp DNA Mini Kit (Qiagen) with used 3x times more lysozyme (5 μ g) than suggested, incubated them for 5 minutes, then placed them in the freezer for 10 minutes. We then thawed and vortexed the samples, repeating this process until the tubes had significant lysis. Extracted samples were sent to Cornell Weil School of Medicine with ProMethION sequencing. Extracted gDNA barcoded with Native Barcoding Kit 96 v14 (SQK-NBD114.96) and sequenced on a PromethION 96 using flow cells (FLO-PRO114M). The Basecalling Algorithm was Dorado v.0.5.3 with Model: dna_r10.4.1_e8.2_400bps_sup v4.2.0. Eight samples total were run from the ETNP ODZ enrichment cultures. Raw reads and read N50 is summarized in Table 3 for all samples. Produced reads were converted into assembled contigs in KBase (Arkin et al., 2018). We binned the assembled contigs into MAGs using MetaSpades via BV-BRC metagenomic binning service GUI (Nurk et al., 2017) and the RASTtk annotation pipeline (Brettin et al., 2015). We produced several MAGs across enrichment samples that were identical to each other in average nucleotide identity (ANI) analysis at the species level (~99%; (Rodriguez-R and Konstantinidis, 2016)). We performed phylogenetic classification in KBase using V1.2 beta version of GTDB taxonomy with ANI to uncultured strains of *Marinobacter* (Parks et al., 2021).

A MAG of *Marinobacter pacificus* was created using patch scaffolding program RaqTag with our highly abundant MAG across samples >98% identical with ANI and classified as *Marinobacter pacificus* sp. nov. (Alonge et al., 2022). *Marinobacter pacificus*

is comprised of 112 contigs and contains a N50 value of 21,349 for a total of 2,245,055 bp and has a GC content of 58%, estimated contamination of ~6% and ~4,500 predicted genes.

We performed a second round of genomic sequencing after isolation attempts using MWH minimal+nitrate media for growth on aerobic and anaerobic conditions. We used a DNeasy PowerWater kit for this round of genomic DNA isolation (QIAGEN). We followed the method for extraction of liquid samples with the only modification of a 10-minute freeze-thaw cycle before incubation in lysozyme. Extracted samples then sequenced by ProMethION (Cornell Weil School of Medicine). The same methods outline above were followed for this second round of sequencing and metagenomic binning.

3.3.3.3 Proteomics

Protein digestion and desalting. We used the S-Trap™ micro high recovery protocol to solubilize oxidized metal precipitants and precipitate proteins (Tsantilas et al., 2024). Sample homogenization was performed by addition of 0.5 µL 10X HALT protease inhibitors and 0.4 µg MgCl₄ to each cell pellet suspended in ~200 µL milliQ water. Samples were then sonicated 3 times, 15 seconds each at 3 watts alternating in dry ice in ethanol to keep the sample cold. Sonicated samples were then dried down on a Savant™ SpeedVac™ (Thermo Scientific™ DNA130230) for ~2 hours and stored at -80°C. The next day, 100 µL high recovery urea-SDS (5% SDS, 8 M urea, 100 mM glycine) lysis/ solubilization buffer was added to each tube and vortexed and incubated for 10 minutes to solubilize proteins. 100 µL samples suspended in lysis buffer were reduced by adding 4 µL of aqueous TCEP to yield final solution of 120 mM) and incubated at 37°C for 15 min. Alkylation was performed next by adding 4 µL of 500 mM iodoacetamide to each sample

and incubating at room temperature for 15 minutes. Samples were then acidified with the addition of 10 μ L 55% aqueous phosphoric acid to each sample.

The following steps deviate from the typical S-Trap protocol (Protifi; S-Trap™ micro spin column digestion protocol): 660 μ L of S-trap binding buffer was aliquoted into lo-bind S-trap tubes (Protifi; K02-micro-160). The following steps were then performed as quickly as possible. 2 μ g of trypsin/lys-C mix (1:1 trypsin/Lys-C suspended in 25 μ L 50 μ M TEAB) was added into each acidified sample and immediately mixed by pipetting up and down, then the mixture for each sample was immediately transferred into the S-Trap binding buffer held in the micro spin column. Samples were mixed by pipetting up and down. Samples were spun in Eppendorf tube bench-top centrifuge into standard 1.5 mL sterile tube, 165 μ L of mixture at a time at 4,000 g for 1 minute until all solution passed through. Flow through was removed between each 1-minute increment spin. Samples were then washed with 150 μ L S-Trap buffer added to the spin column of each sample and centrifuge 4 times total with flow-through removal between each spin. Protein was maintained between washes. 0.5 μ g of trypsin in 25 μ L of 50 mM TEAB, pH 8 was added to the top of each protein S-trap (Protifi; K02-micro-160) ensuring no bubbles were atop the protein trap. The spin column was loosely capped and incubated in a sterile 1.5 mL tube for 2 hrs at 47°C for trypsin in a water-saturated atmosphere.

The elution steps were as follows: elute peptides with 40 μ L each of 50 mM TEAB added to the trypsin. Centrifuge at 4,000 x g for 1 minute. Elute peptides with 40 μ L 0.2% aqueous formic acid. Centrifuge at 4,000 x g for 1 minute. Elute hydrophobic peptides with 35 μ L 50% acetonitrile, 0.2% formic acid. Centrifuge at 4,000 x g for 1 minute. The peptides were speed vacuum dried in a Savant™ SpeedVac™ (Thermo Scientific™

DNA130230) until no liquid was visible. Each sample was reconstituted in 20 μl 2% acetonitrile + 0.1% formic acid for concentrations of 2 $\mu\text{g } \mu\text{L}^{-1}$. Dried peptides were re-dissolved in 0.5 μL of 500 $\text{fmol } \mu\text{L}^{-1}$ PRTC + 9.5 μl of 0.1% formic acid for a total 19.5 μL of sample for each replicate. 7 μL of each sample was added to the total pooled sample for DIA. 7 μL of sample was used for each individual DIA analysis.

LC-MS/MS. The mass spectrometry analysis was performed on a QExactive at the University of Washington Proteomics Resource (UWPR; Seattle, WA). Peptides were chromatographically separated (precolumn, 2.7-cm by 100- μm internal diameter [ID]; analytical column, SilicaTip, 30-cm by 75- μm ID; packed in-house with resin, 3- μm C18-AQ) with a Thermo EASY-nLC system (3 to 95% acetonitrile and 0.1% vol/vol formic acid; 300 nL min^{-1} for 90 min) directly in line with a Fusion Lumos Orbitrap Tribrid mass spectrometer (Thermo Fisher Scientific) operated in data independent acquisition (DIA) mode. To generate a peptide spectral library, 1 μg of a pooled sample containing equal parts from each peptide digest was analyzed with six gas-phase fractions covering m/z 400 to 1,000 in increments of 100 m/z (4 m/z staggered MS2 windows and 2 m/z overlap). Each bioreplicate was then quantified in single DIA analyses (MS1, m/z 400 to 1,000; 8 m/z staggered MS2 windows and 4 m/z overlap). A quality control was made from 10 μl QC, 2% acetile nitrile, and 30 μL 0.1% formic acid.

Protein identification and data analysis. The protein database used for correlating spectra with protein identifications was generated from the *Marinobacter pacificus* sp. nov. metagenome assembled by the GUI version of PATRIC isolated from the 1° 69 bottle (bv-brc). The MAG-based protein database was combined with 50 common contaminants and quality control peptides (trypsin). Comet parameters included: reverse concatenated

sequence database search, trypsin enzyme specificity, cysteine modification of 57 Da (resulting from the iodoacetamide) and modifications on methionine of 15.999 Da (oxidation). Calculated false discovery rates (FDR) were <0.01.

Spectral libraries for searching the DIA data were generated using Carafe, a tool that generates experiment-specific spectral libraries (Wen et al., 2024). Carafe trains deep learning models using the collected DIA data to generate predicted experiment-specific fragment ion intensity and peptide fragment ion spectra. DIA-NN (Data-Independent Acquisition Neural Network) was used to process and analyze the DIA MS to identify peptides using the sample-specific spectral library generated by Carafe. DIA-NN uses advanced machine learning algorithms, including neural networks, to accurately identify peptides from complex DIA data, relying on matching detected peptide signals with theoretical spectra (Wen et al., 2024). In total, 856 proteins were detected with DIA-NN. NMDS and limma scripts were used in R to identify significant differences and calculate differential abundance between CH₄ and He conditions.

3.4 Results

3.4.1 Methane stimulates bacterial growth in long term enrichments

After five years of incubation of seawater cultures at 25°C, cultures with 10% CH₄ contained significantly more cells than cultures with only N₂ (**Figure 5**). In the presence of 10% CH₄, similar cell abundances were present with 100 mM NO₃⁻ (3.8 (± 1.1) x 10⁵ cells mL⁻¹ (n=3)) or 100 mM NO₂⁻ (1.7 (± 0.6) x 10⁵ cells mL⁻¹ (n=3)) (**Figure 5**). With N₂-only headspace, similar cell abundances were present with 100 mM NO₃⁻ 3.0 (± 2.0) x 10⁴ cells mL⁻¹ N₂ + NO₃⁻ (n=3) or 100 mM NO₂⁻ (1.8 (± 0.4) x 10⁴ cells mL⁻¹ N₂ + NO₂⁻ (n=3))

(Figure 5). Cellular autofluorescence in the DAPI channel (365 nm excitation) was present in all bottles (Figure 5).

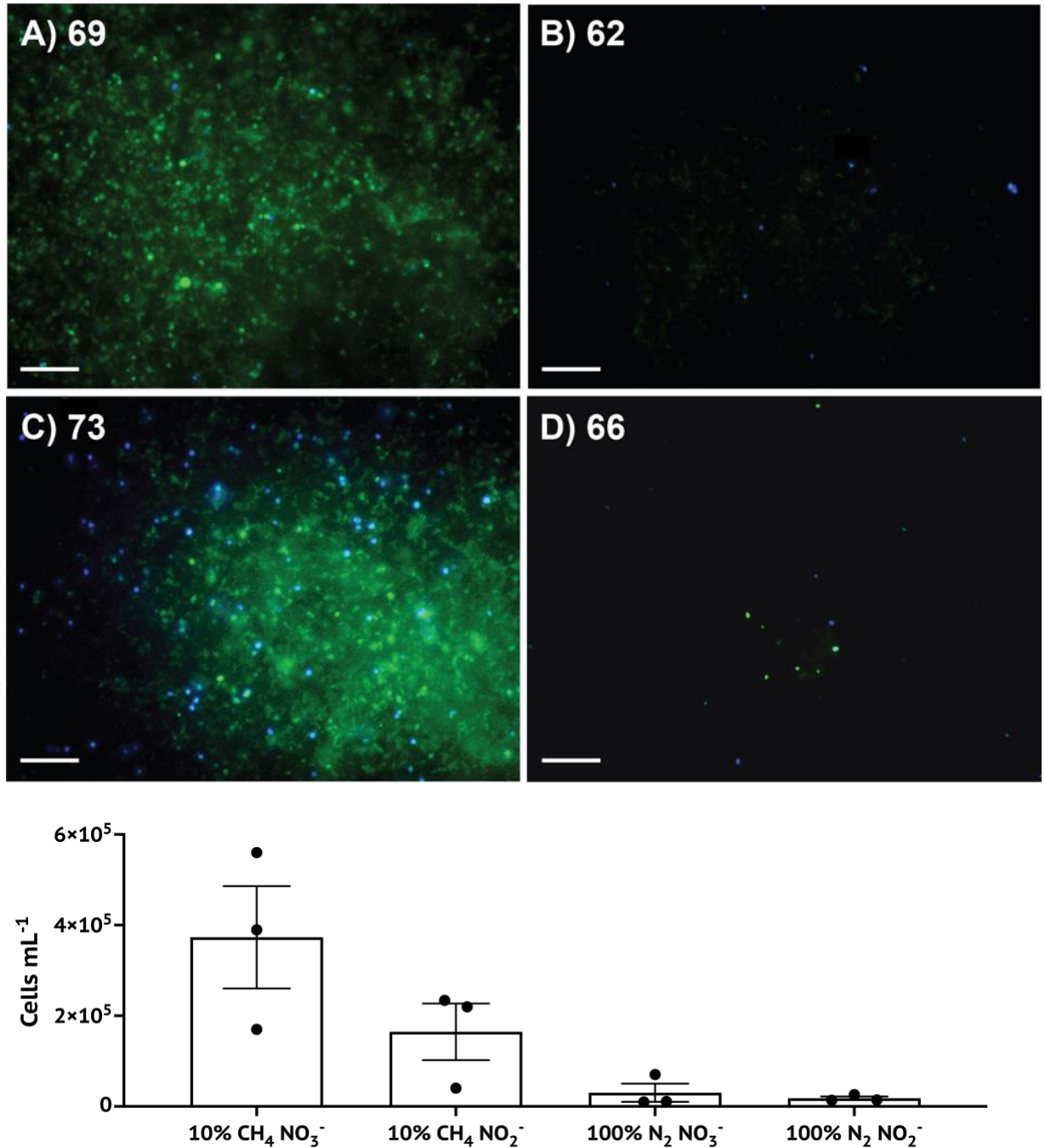


Figure 5. SYBR-stained cell images from enrichment bottles imaged in 2021 and corresponding triplicate cell count values of each condition. No DAPI stain was used. Numbers in panels A-D correspond to Table 1. SYBR-stained cells imaged under GFP filter channel are shown are green. Blue autofluorescence imaged in DAPI filter aligns

with SYBR-stained cells. Scalebar is 10 μm . Cell counts of triplicate bottle cultures are shown with standard error of the mean (SEM).

3.4.2 Secondary transfers of bottle 69 produce nitrous oxide under methane

Bottles 69 and 71 were chosen for 2° transfers due to significantly higher cell counts. Cellular autofluorescence was further observed in 2° transfers and cell morphology shifted from cocci (**Figure 5c**) to rods (**Figure 6a**). The cellular community in 2° transfers from bottle 71 looked like considerable DNA packing for replication was occurring (**Figure 6a**). The cell community in 2° transfers from bottle 69 also seemed to be forming biofilm communities (**Figure 6b**). Additionally, we found that 2° and 3° transfers from bottle 69 produced nitrous oxide only under a nitrate and methane headspace (**Figure 7**). 10% to 40% of nitrogen was converted to intermediate product nitrous oxide from nitrate. However, allowing nitrate to become depleted in bottle cultures led to a peak and decrease in nitrous oxide following nitrate depletion (data not shown). We focused on bottle 69 culture and subsequent transfers to understand metabolic pathways and potential mechanisms producing nitrous oxide, a potent greenhouse gas.

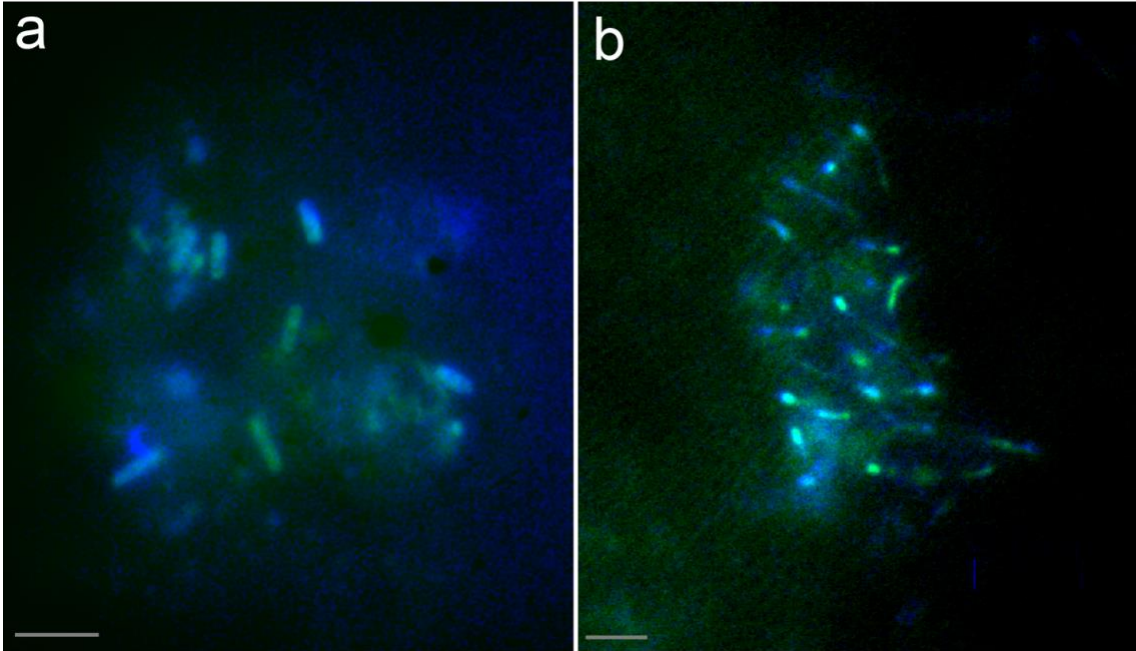


Figure 6. Stacked microscopy images of the same section of a filter stained with SYBR (green) DNA stain and imaged under the DAPI (blue) channel with no DAPI stain from 2° transfers. (a) Microscopy of cell morphology from 71 bottle 2° transfers. (b) 2° overlaid image of SYBR (green) stained cells and DAPI (blue) under 95% CH₄/5% CO₂ headspace. Gray scale bar is 2 microns for both images.

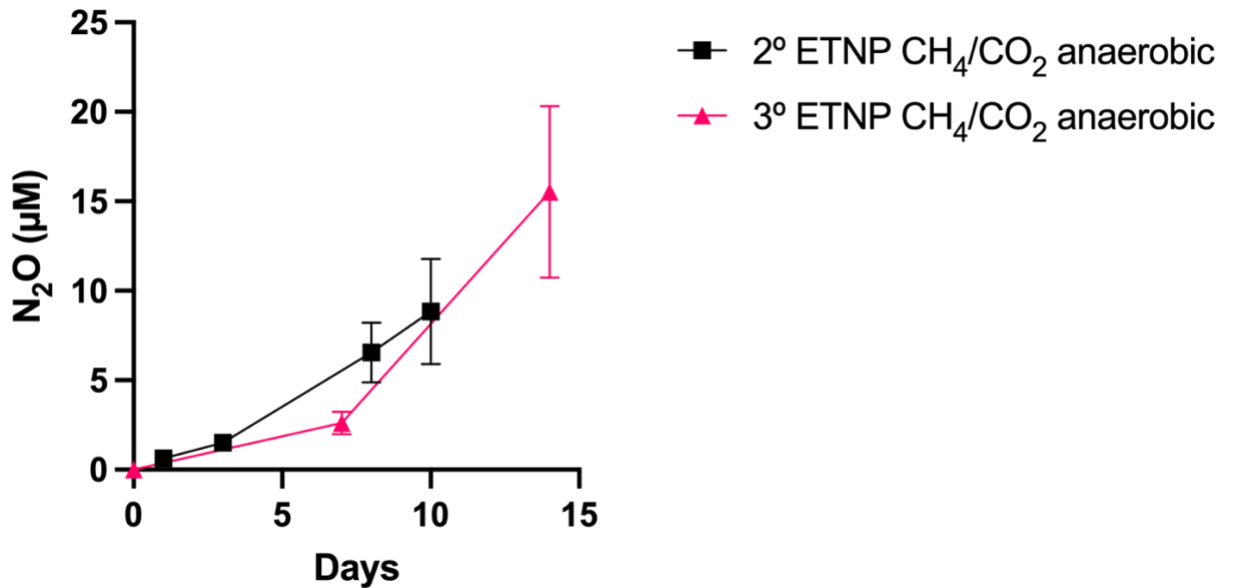


Figure 7. Nitrous oxide production in bottle 69 enrichment cultures for 2° and 3° triplicate transfers over time in days. 2° transfers with sterile ETNP culture and a 95% CH₄/5% CO₂ headspace are plotted with black squares. 3° transfers with sterile

ETNP culture and a 95% CH₄/5% CO₂ headspace are plotted with pink upward arrows. Error bars are shown as SEM.

3.4.3 *Marinobacter* spp. dominate in transfers with nitrate

After transfer to 95% CH₄/5% CO₂ headspace, Gammaproteobacteria (*Marinobacter* spp.) and Bacteroidia (Flavobacteriales) were enriched. Sanger sequencing was used to obtain full length sequences of dominant microbes to select FISH and CARD-FISH probes for quantitative analysis. We found that *Flavobacteriales*, *Marinobacter* spp., and *Alphaproteobacteria* were dominant in most 16S rRNA sequencing runs. Fluorescent in-situ microscopy (FISH) using the Mrb-0625-a probe confirmed the presence of *Marinobacter* across bottle enrichment culture transfers, including the original bottle enrichments (**Figure 8a, 8b, 8c**). We found that Mrb-0625-a probe hybridized cells comprise ~70% of the community in secondary transfers and typically overlap with autofluorescent cells (**Figure 8d, 8e**). Cell morphology changed from cocci to rods across transfers (**Figure 8**). Since *Marinobacter* are Gammaproteobacteria, we also performed CARD-FISH with gammaproteobacterial probe (Gam42a). Gam42a-hybridized cells dominated cell counts (~98%) and ~90% of autofluorescence is associated with the cells that hybridized with Gam42a (**Figure 8f, 8g, 8h**).

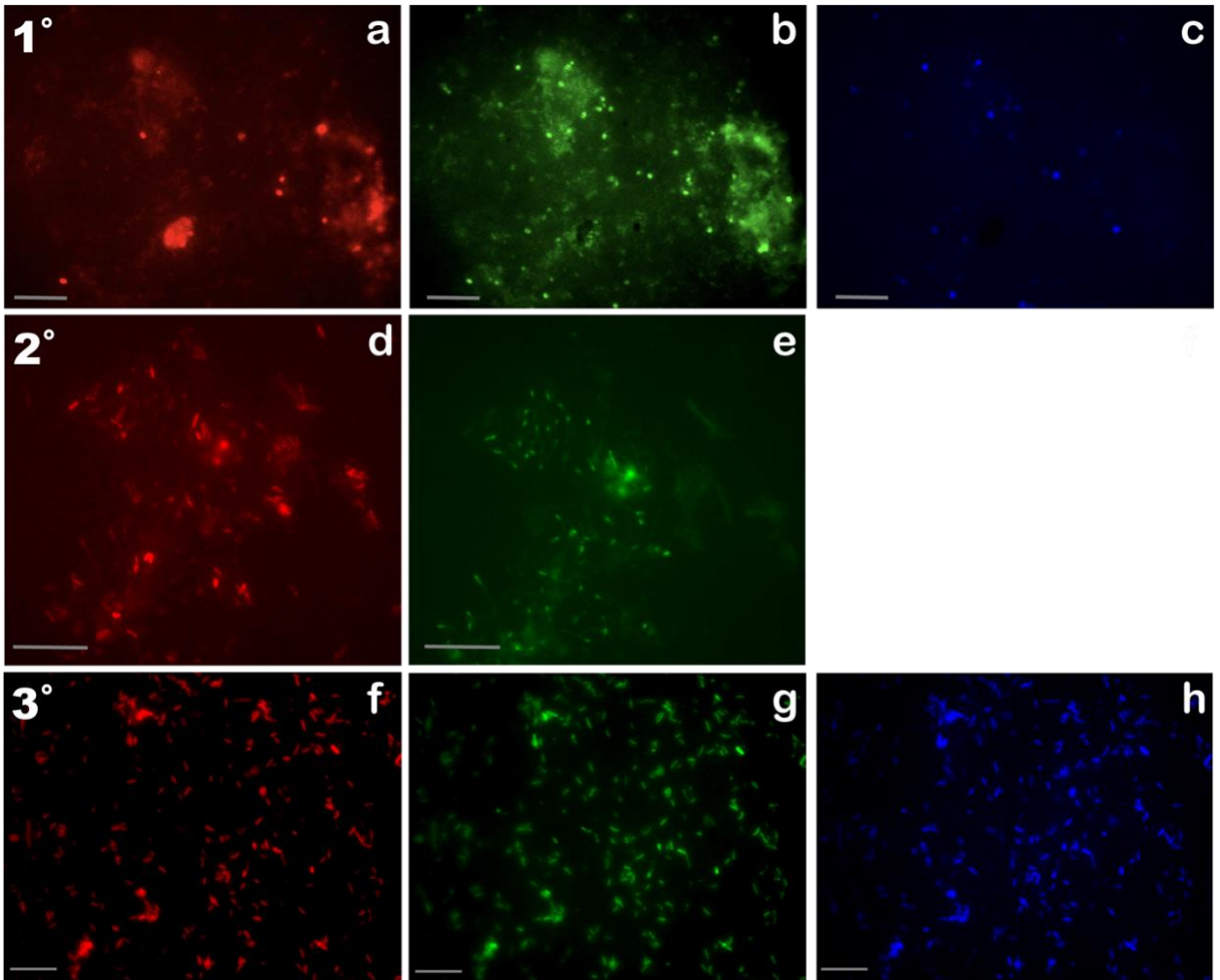


Figure 8. Microscopy of cells hybridized with *Marinobacter* (Mrb-0625-a) probe (red), SYBR (green) DNA stain, and imaged under the DAPI (blue) channel with no DAPI stain from 69 bottle and transfers. (a,b,c) 1° bottle contain a microbial community that hybridize with *Marinobacter* probe ~50%. (d,e) 2° transfer cultures hybridize with *Marinobacter* probe ~70%. (f,g,h) 3° transfers cultures hybridize ~98% with gam42 CARD-FISH probe. Approximately 90% of autofluorescent cells also hybridize with gammaproteobacteria probe in 3° transfers which glow under DAPI wavelength excitation. Gray scale bar is 5 microns for all images.

~20% of cells hybridize with probe CF998 and do not overlap with autofluorescent cells in bottle enrichments (**Figure 9**). *Flavobacteriales* comprise a small portion of the community in 1° and 2° culture bottles and are not detected in 3° transfers and beyond.

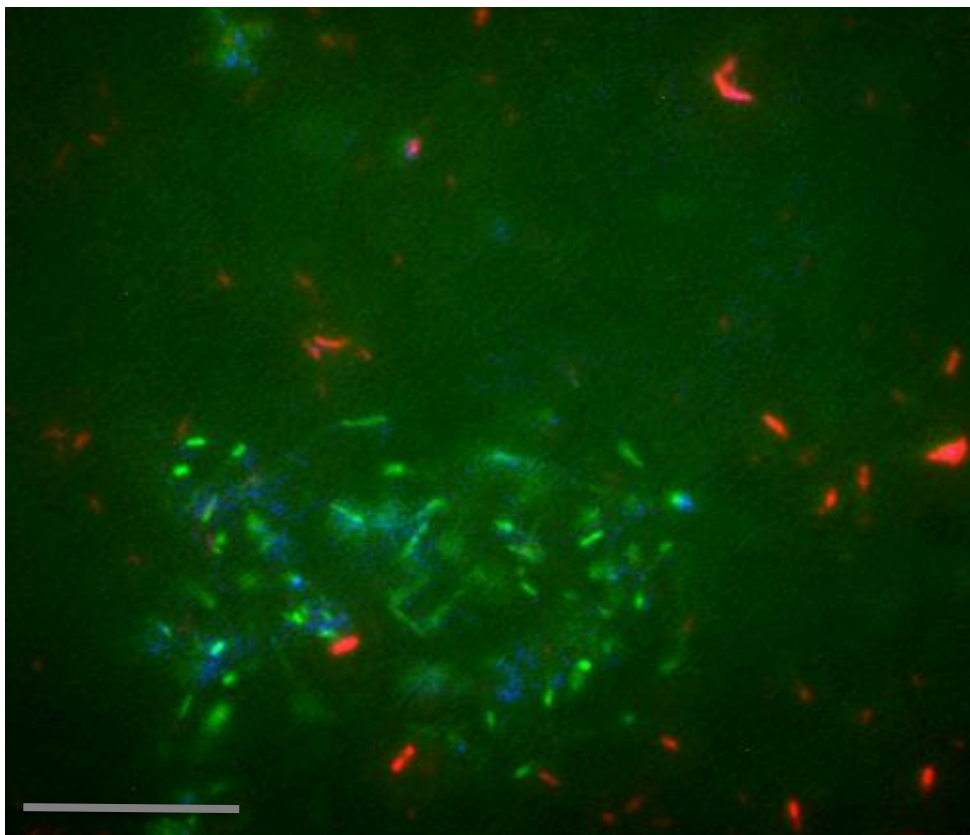


Figure 9. Overlaid image of microscopy of cells hybridized with CARD-FISH Flavobacteriales probe (CF998) probe (red) from 1° 69 bottle culture. SYBR (green) DNA stain image and cellular autofluorescence under DAPI-filter (blue) excitation overlaid with CARD-FISH image. No DAPI stain was used. Gray scale bar is 10 microns.

3.4.4 Cellular autofluorescence emits at 465 nm in unstained cells

During cell counts of bottle cultures using only SYBR green stain, we found cellular autofluorescence in the DAPI blue wavelength channel (365 nm) that was increased under methane headspaces (**Figure 5**). To ensure the blue cellular autofluorescence was not an artifact of the green SYBR staining microscopy, or that any DAPI stain contamination occurred, we performed additional imaging of 1° bottle cultures from each condition listed in Table 1 under the DAPI channel (365 nm) without any stain. We continued to observe bright fluorescence of cells under the DAPI channel in ETNP

ODZ enrichments without any staining (**Figure 10**). We performed emission spectra analysis to identify the range of wavelengths where excitation was occurring from 405-750 nm. This method allows for us to ensure that “crosstalk” is not occurring in fluorescent staining, i.e., SYBR green stain causing blue fluorescence due to overlap in excitation wavelengths/colors. We found distinct wavelength peaks for blue at ~465 nm in unstained filters from original cultures (**Figure 10**). We then performed spectral unmixing to isolate individual emission spectra and further confirm emission spectra from cellular autofluorescence on SYBR-stained filters to. We found the peak maxima again occurring at ~465 nm, with a smaller, secondary peak at ~510 nm. Cellular autofluorescence is brighter in ETNP sterile media than in any defined/complex media used in attempts to culture and isolate cells, including minimal MWH media.

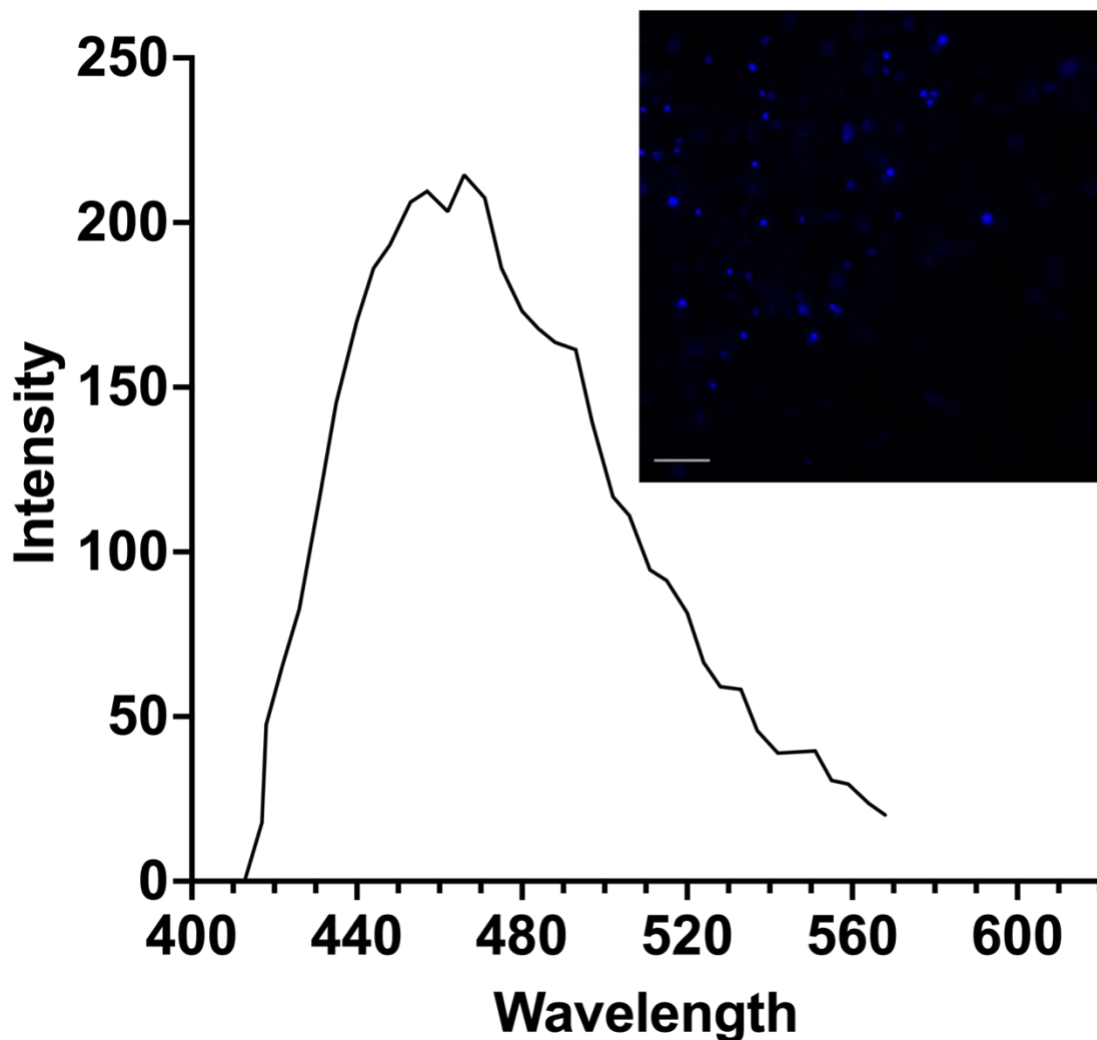


Figure 10. Intensity versus wavelength plotted for emission spectra from 405 nm excitation of unstained cells. Inset image taken from unstained 1° bottle 69 using structured illumination microscopy (SIM) during concurrent spectral analysis. Gray scale bar is 5 microns.

3.4.5 Autofluorescence in related bacteria

To determine whether autofluorescence is present in other hydrocarbon-degrading bacteria, we examined an aerobic methylotrophic bacterium (*Methylorubrum extorquens* AM1) and Gulf of Mexico beach sand strains *Marinobacter hydrocarbonoclasticus* and

Marinobacter vinifirmus (Kostka et al., 2011). We observed autofluorescence occurring in all three species when unstained (**Figure 11a, 11b, 11c**).

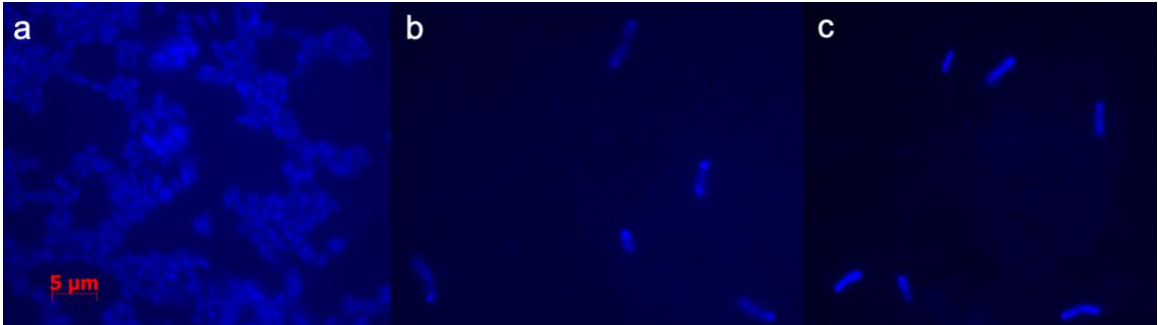


Figure 11. Images of unstained bacteria under DAPI-filter microscopy. (a) *Methylobacterium extorquens* AM1 strain under DAPI filter imaging with 5 µm scale bar. (b) *Marinobacter vinifirmus* under DAPI filter imaging with 2 µm scale bar. (c) *Marinobacter hydrocarbonoclasticus* under DAPI filter imaging with 2 µm scale bar.

3.4.6 Consistent nitrate reduction supports growth both aerobically and anaerobically over enrichment of *Marinobacter*

Over three transfers of bottle 69, nitrate reduction rates remained similar on 95% CH₄/5% CO₂ headspace: twice 0.22 sterile filtered ETNP 2° (1.3 ± 0.8 µM d⁻¹ (n=3)), twice

0.22 sterile filtered ETNP 3° ($3.3 \pm 0.1 \mu\text{M d}^{-1}$ (n=3)), and 4° transfers in defined minimal media (MWH) ($3.4 \pm 0.6 \mu\text{M d}^{-1}$ (n=3)) (**Figure 12**).

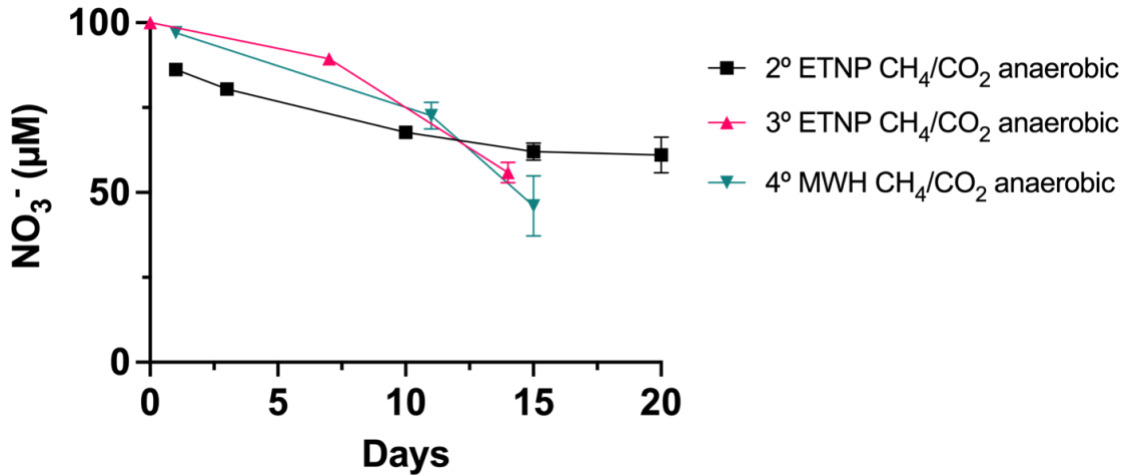


Figure 12. Measured nitrate reduction in bottle 69 enrichment cultures for each transfer over time in days. 2° transfers with sterile ETNP culture and a 95% CH₄-5% CO₂ headspace are plotted with black squares. 3° transfers with sterile ETNP culture and a 95% CH₄/5% CO₂ headspace are plotted with pink upward arrows. 4° transfers with sterile defined MWH media and a 95% CH₄/5% CO₂ headspace are plotted with green downward facing arrows. Errors bars are shown as SEM.

Nitrate reduction and increasing OD₆₀₀ values occurred in both anaerobic and aerobic 4° MWH transfers from bottle 69. Rates of nitrate reduction in 4° transfers are higher in anaerobic ($4.7 \pm 0.2 \mu\text{M h}^{-1}$ (n=6)) versus aerobic ($3.1 \pm 1.2 \mu\text{M h}^{-1}$ (n=6)) growth conditions over hours of incubation (**Figure 13**). Concurrent cell growth measured as OD₆₀₀ was approximately one-fold higher in aerobic tubes (**Figure 13**).

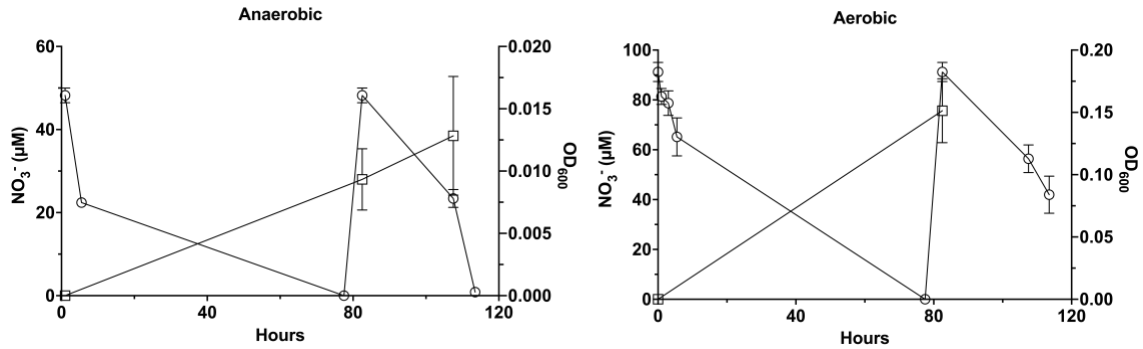


Figure 13. Measured nitrate reduction and OD₆₀₀ of anaerobic (left) and aerobic (right) 4° transfers in sterile defined MWH media from bottle 69. Nitrate is plotted in micromolar as open circles. OD₆₀₀ is plotted as open squares. Anaerobic 4° transfers contain a 95% CH₄-5% CO₂ headspace. Aerobic 4° transfers were continuously shaken and given 200 µM lactate. Error bars as shown as SEM.

3.4.7 *Marinobacter pacificus* sp. nov. forms a clade with two uncultured strains

We assembled several *Marinobacter* metagenome assembled genomes (MAGs) across 69 bottle culture transfers that were identical to each other in average nucleotide identity (ANI) analysis at the species level (~99%). This *Marinobacter* MAG is most closely related to unclassified *Marinobacter* strain SAT58 from the South Pacific (~98%, accession) and SS8-8 from a deep-sea hydrothermal sulfidic vent in the Indian Ocean (98%, accession). Both strains are *Marinobacterium* sp002707215 in the GTDB taxonomy database (Parks et al., 2021). We propose the species name *Marinobacter pacificus* sp. nov. Our novel species forms an unclassified clade with strain SAT58 and strain SS8-8, two additional unclassified and uncultured strains (**Figure 14**).

Oxygen tensions in subset of liquid cultures of *M. pacificus* grown for proteomics remained $< 1 \mu\text{M O}_2$ for each condition throughout (Figure 15). Oxygen tensions were $\sim 600 \text{ nM}$ higher in the CH_4 treatments than the He treatments (Figure 15).

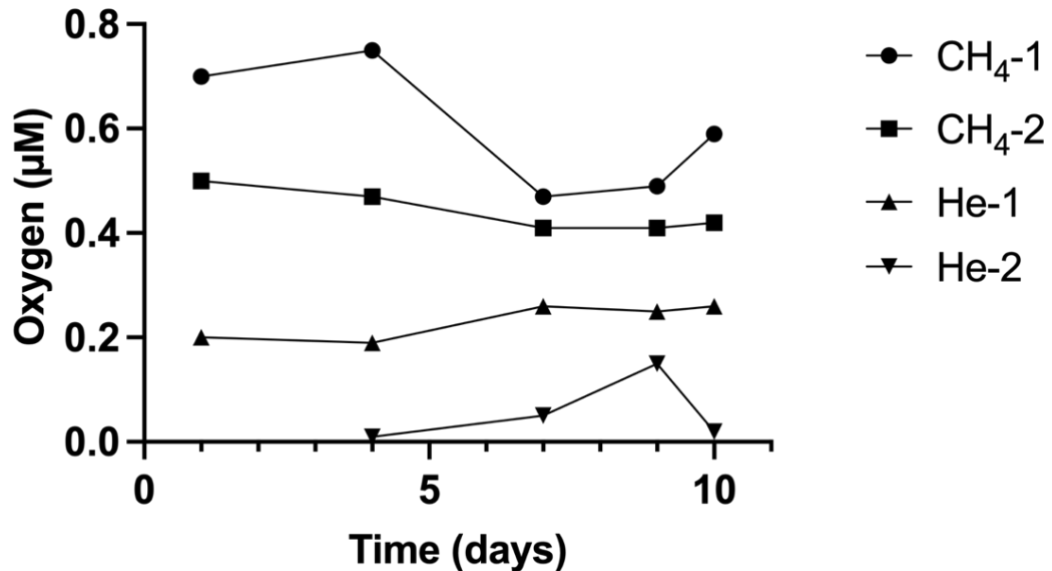


Figure 15. Oxygen measured at timepoints in a subset of liquid culture bottles using optode sensors.

Non-metric dimensional scaling analysis identified four methane and four helium bottle cultures as significantly different from each other (Figure 16). One replicate from each condition was removed after NMDS analysis as these bottles did not cluster within their respective groups and instead clustered with each other and away from all other replicates. Total replicates for further downstream analysis were then changed from $n=5$ to $n=4$.

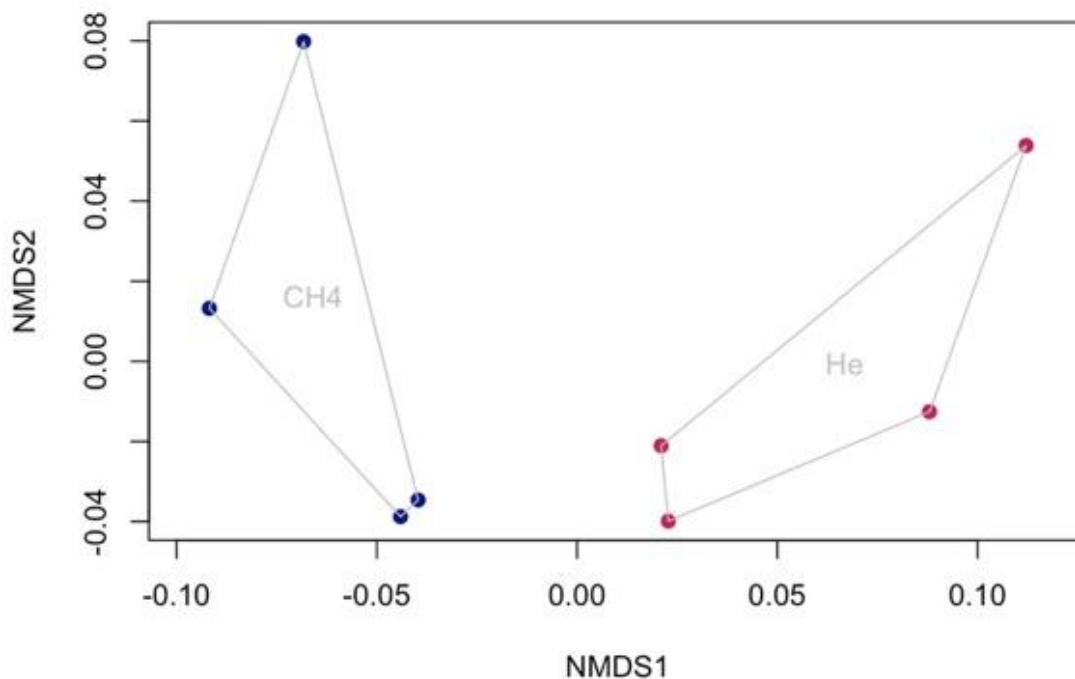


Figure 16. Non-metric scaling dimensional analysis of CH₄ and He condition culture bottles. One bottle culture from each condition did not cluster with its respective condition and instead clustered with the other bottle. These bottles were excluded from downstream analysis for n=4 in each condition.

Most proteins supporting denitrification were highly abundant in both conditions without significant differences in expression (0 log-fold change; **Table 2**). Proteins involved in oxygenic respiration, particularly cytochrome *cbb₃* oxidase were not detected but were present in the genome. Accessory proteins including nitrate/nitrite transporter NarK and nitrite reductase associated c-type cytochrome NirN, were significantly abundant in the He condition (3 and 4 log fold change, respectively; **Table 2**). There was significantly high abundance of a PQQ-dependent Quino(hemo)protein alcohol dehydrogenase in the CH₄ condition (-3 log-fold change; **Table 2**). *M. pacificus* PQQ-dependent alcohol dehydrogenase clusters within the ExaF clade that includes characterized protein in *Methyloburbrum extorquens* and *Dechloromonas occulta* (**Figure**

17). The CH₄ headspace expressed PQQ-dependent ExaF protein in *Marinobacter pacificus* shares 100% sequence identity to ExaF in uncultured *Marinobacter* sp. SS8-8, one of the closest relative strains to *M. pacificus* sp. nov. (**Figure 17**). There was significantly increased expression of formate dehydrogenase (Fdh3A) and accessory proteins in the CH₄ condition (-4 log-fold change; **Table 2**).

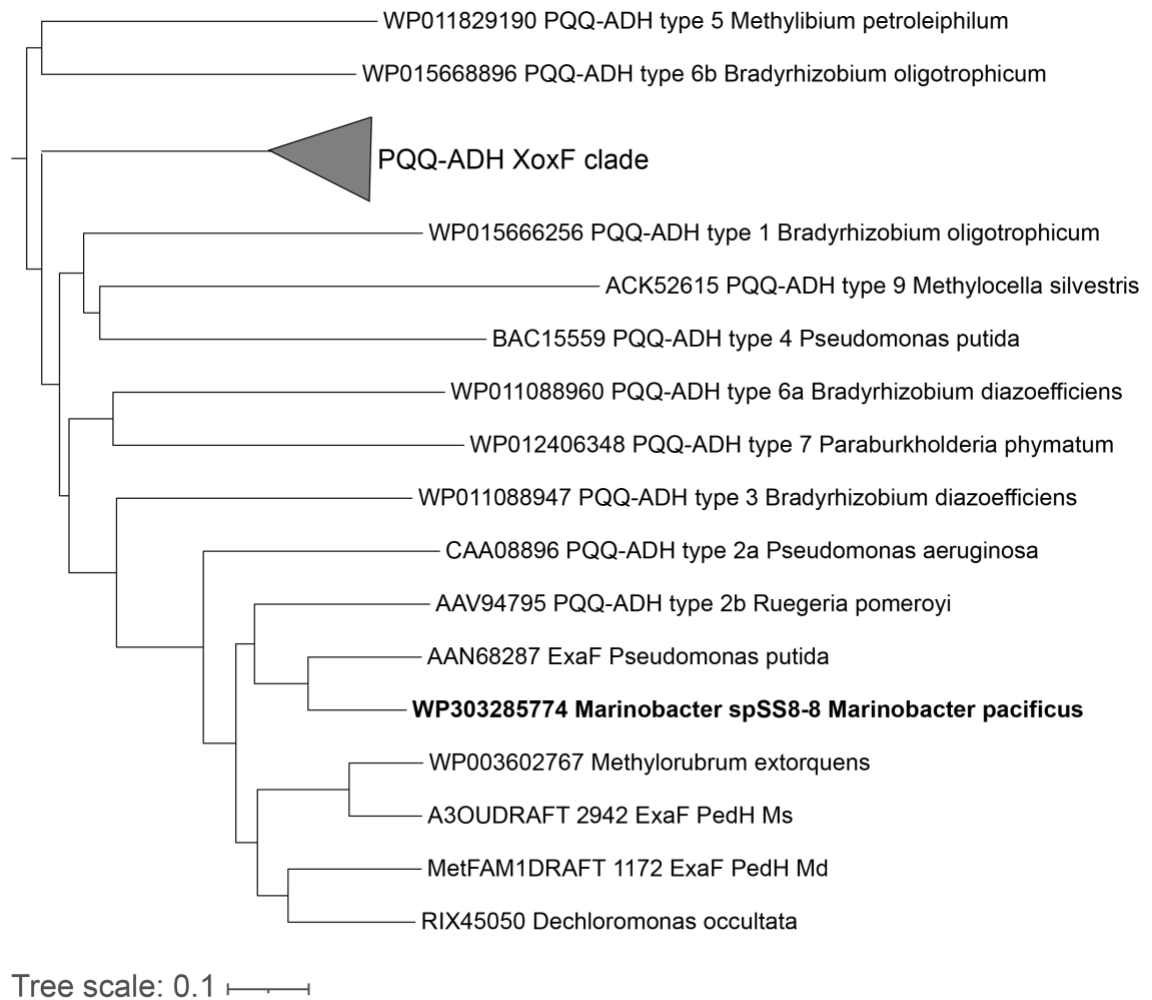


Figure 17. Unrooted phylogenetic tree of PQQ-dependent alcohol dehydrogenases showing ExaF clade. The phylogeny was constructed with related alcohol dehydrogenase proteins (ADH) using lanthanides and other rare earth elements, including XoxF and ExaF proteins. ExaF proteins are expanded, and *Marinobacter pacificus* sp. nov. is bolded and listed with *Marinobacter* sp. strain SS8-8 due to 100% identity match (BLASTp metric). Taxonomic names are from GTDB Release 08-RS214. The scale bar represents amino acid substitutions per site.

Proteins supporting cell replication, including ATP synthase subunits, were abundantly expressed in both headspace conditions (**Table 2**). FtsH, an essential zinc metalloprotein for cell growth and division, was +1 log fold-change more abundant under the helium condition (**Table 2**). However, 1 log fold-change is below our threshold for significant differential abundance, and there was relatively high expression of FtsH for CH₄ as well. There was a significant increase in abundance of cytochrome *c* proteins in the CH₄ condition (-2 to -8 log fold change; **Table 2**).

Table 2. Respiration and growth proteins that are highly abundant in both methane and helium headspaces. Significantly different abundance is reported as log fold change (logFC), log-transformed change in proteomic abundance between the two conditions (methane versus helium) where negative LogFC is significant expression under methane and positive logFC is significant expression under helium. Average expression log fold change (Ave Expr Log) is the log transformed average protein expression across both conditions and all duplicates. T-test numbers (t) represent significant differences between methane and helium conditions. *Values non-log transformed since abundance is not differentially significant between conditions.

Protein annotation	logFC	Ave Expr Log	t	P value
NAD(P)H dehydrogenase (quinone), Type IV (EC 1.6.5.2)	-3	13	-3	0.01
Quino(hemo)protein alcohol dehydrogenase, PQQ-dependent (EC 1.1.2.8)	-3	17	-8.8	0.0
Cytochrome C550 (Soluble cytochrome C)	-8	12	-3	0
Hypothetical protein (PQQ-dependent catabolism-associated beta-propeller protein; TIGR03866)	-11	9	-3	0

Table #2 continued.

Formate dehydrogenase-O, major subunit (EC 1.2.1.2)	-4	17	-6.0	0.000
Periplasmic sulfane dehydrogenase, molybdopterin-containing subunit SoxC	-3	13.3	-5.3	0.0004
Periplasmic sulfane dehydrogenase, diheme c-type cytochrome subunit SoxD	-8	11.6	-2.5	0.04
Cell division-associated, ATP-dependent zinc metalloprotease FtsH	+1	14.8332166	3	0.016
ATP synthase epsilon chain (EC 3.6.3.14)	N/A	8E+06*	N/A	N/A
FKBP-type peptidyl-prolyl cis-trans isomerase FklB (EC 5.2.1.8)	N/A	7E+07*	N/A	N/A
ATP synthase alpha chain (EC 3.6.3.14)	N/A	1E+08*	N/A	N/A
ATP synthase F0 sector subunit b (EC 3.6.3.14)	N/A	3E+07*	N/A	N/A

3.4.9 *Marinobacter pacificus* sp. nov grows on formate, ethanol, and methanol as the sole carbon source

Aerobic incubations with formate, ethanol, methanol, and lactate were tracked using OD₆₀₀ and showed growth under all conditions (**Figure 18**). Lactate was supplied as a positive control for growth against all other carbon sources. 25 mM formate led to the

overall maximum OD₆₀₀ values. There were significant differences in OD₆₀₀ max within formate conditions (**Figure 18**). Between formate and methanol, and ethanol and methanol, there were also significant differences in OD₆₀₀ max (**Figure 18**). No significant differences between ethanol and methanol concentrations were found (**Figure 18**).

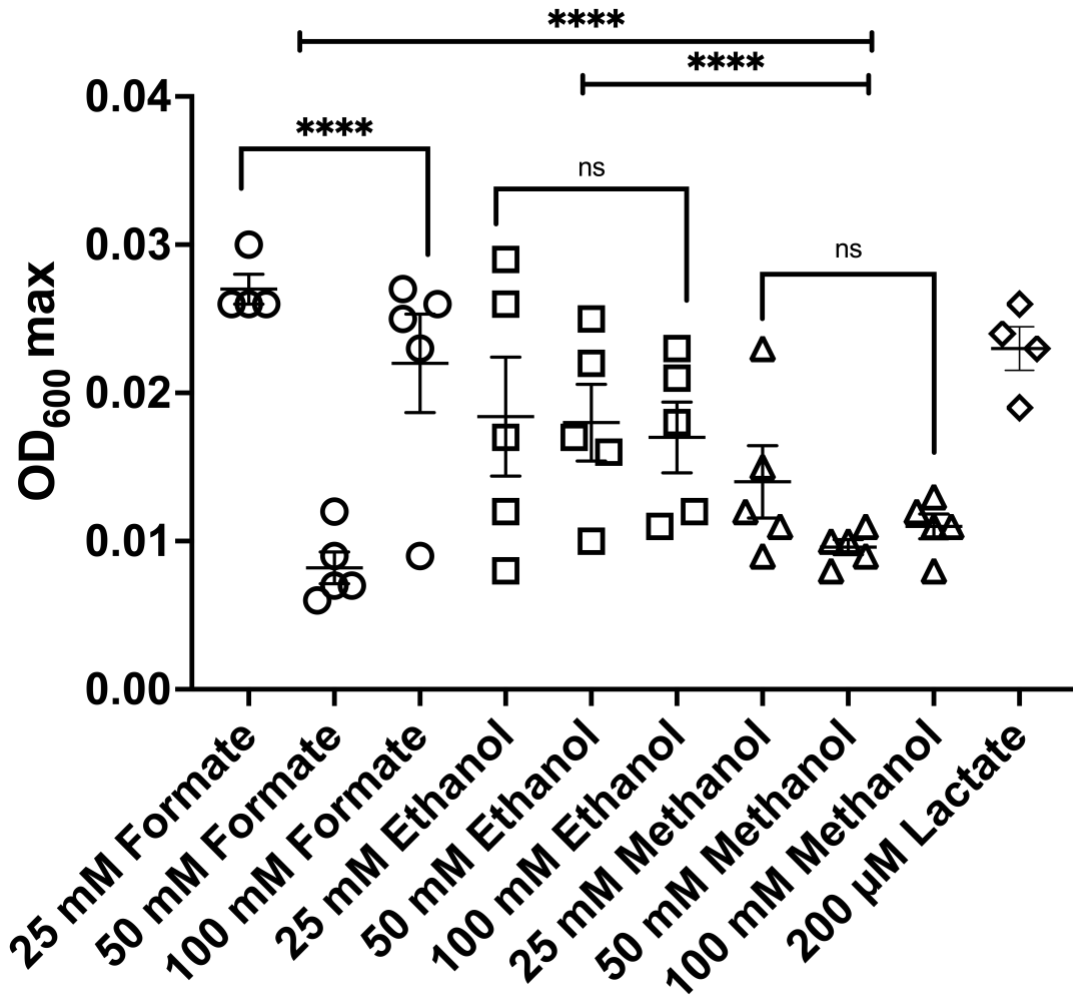


Figure 18. OD₆₀₀ maximum values for *Marinobacter pacificus* grown in MWH defined minimal media with nitrate, and formate, ethanol, methanol, or lactate as the sole provided carbon source. ANOVA one-way tests against and within each condition are shown where p-value < 0.01 (****) or no significance. Lactate values are shown with diamonds, methanol as triangles, ethanol as squares, and formate as circles. Error bars are shown as SEM.

3.4.10 95% methane bottle cultures contain methanol and formaldehyde in the headspace

Analysis of direct flow from the 95% CH₄ – 5% CO₂ gas tank did not detect any oxidized 1-carbon species, including methanol and formaldehyde (**Figure 19**). However, bottle cultures incubated with *M. pacificus* and filled to overpressure with the 95% CH₄ – 5% CO₂ gas contained significant quantities of methanol and formaldehyde (**Figure 19**). *M. pacificus* bottle cultures with 100% helium as the headspace also did not contain any oxidized 1-carbon species, nor did we detect any methane contamination (**Figure 19**). Further, 95% CH₄ – 5% CO₂ gas bottle cultures that were opened to extract sample, which are oxygen contaminated, had decreased quantities of oxidized 1-carbon species methanol and formaldehyde (**Figure 19**). Overall, methanol is the most abundant oxidized 1-carbon compound present in 95% CH₄ – 5% CO₂ gas bottle cultures.

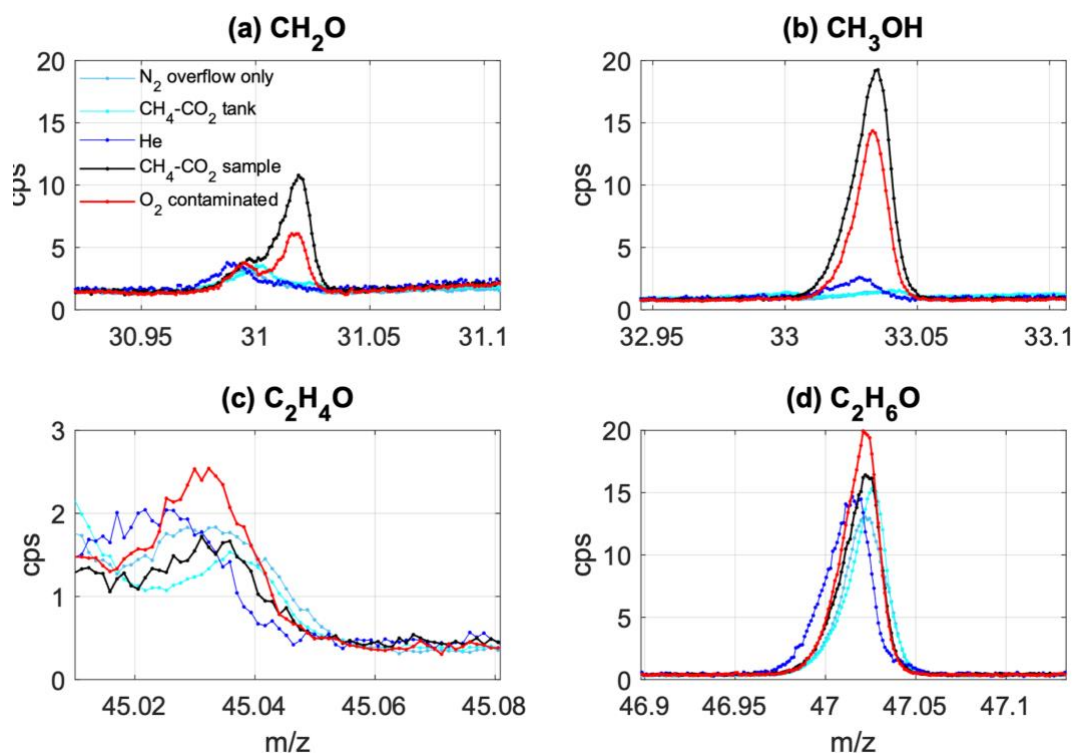


Figure 19. Gas headspace analysis of oxidized 1-carbon compounds in incubated bottle cultures. 1 s averaged spectra of only N₂ overflow (light blue), direct sampling of the 95% CH₄-5% CO₂ gas standard (cyan), He sample (dark blue), CH₄-CO₂

sample (black), and O₂-contaminated CH₄-CO₂ sample (red) from the PTR-ToF-MS for the following attributed species: (a) formaldehyde (CH₂O), (b) methanol (CH₃OH), (c) acetaldehyde (C₂H₄O), and (d) ethanol (C₂H₆O).

3.5 Discussion

In this study, I isolated a novel *Marinobacter* species through anaerobic iterative transfers from long-term enrichment cultures taken with concentrated water from the secondary nitrite maximum of the ETNP ODZ. I propose the name *Marinobacter pacificus* for this novel species, which forms a clade with two uncultured *Marinobacter* strains. *Marinobacter pacificus* was isolated from anaerobic enrichments given nitrate and a methane headspace, is autofluorescent at ~465 nm, reduces nitrate to nitrous oxide and presumably N₂ gas and expresses the proteins PQQ-dependent alcohol dehydrogenase, formate dehydrogenase, and the full suite for denitrification under a 95% methane headspace. Gas headspace dynamics indicate that methane in the headspace is being oxidized abiotically. I postulate that it may be through photochemical lysis and/or hydroxyl radicals formed from N-oxide species interactions in the headspace (**Figure 19; 20**). A mechanism of anaerobic metabolism has not yet described for the genus *Marinobacter* despite long standing knowledge of their facultatively anaerobic lifestyle (Handley and Lloyd, 2013).

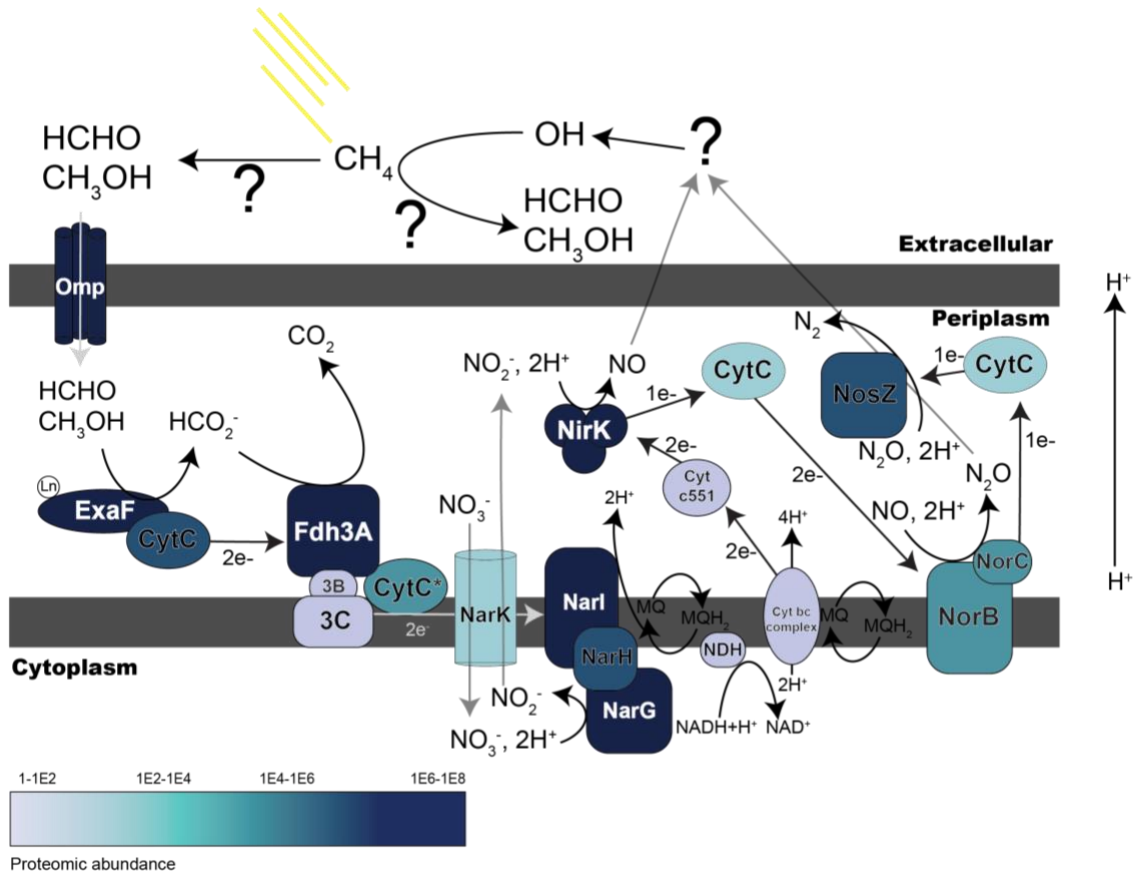


Figure 20. Schema of *Marinobacter pacificus* sp. nov. anaerobic respiration based on proteomic expression and gas headspace analysis. Enzymes are colored by intensity of proteomic expression in the CH₄ condition. Proton gradient is shown for proton movement in denitrification. Formaldehyde and methanol are included as potential carbon sources for ExaF alcohol dehydrogenase based on gas headspace analysis. Schema of hydroxyl radical formation of methanol and formaldehyde from methane oxidation and origin of unknown hydroxyl radicals in the headspace are shown above the extracellular space. Potential photochemical lysis is represented with yellow lines. *Highly upregulated proteins annotated as SoxCD.

Rates of nitrate reduction were consistent over 2° to 4° anaerobic transfers that enriched for *Marinobacter pacificus*. Production of nitrous oxide stopped occurring after 3° transfers. Reduced oxygen contamination into bottle cultures may have stopped nitrous oxide production (Bertagnolli et al., 2020). Cellular growth, tracked by optical density at 600 nm, increased in both anaerobic cultures with a 95% methane headspace and aerobic cultures given 200 μM lactate. However, optical density was 1-fold higher in aerobic

cultures versus anaerobic (**Figure 13**). Nitrate reduction was $\sim 1 \mu\text{M h}^{-1}$ faster in anaerobic cultures, but aerobic nitrate reduction occurred at similar rates to earlier anaerobic transfers. *Marinobacter* are capable of aerobic denitrification without production of nitrous oxide (Liu et al., 2016).

Neither proteins or genes supporting methane oxidation were detected for *Marinobacter pacificus*. However, PQQ-dependent alcohol dehydrogenase (ExaF) and formate dehydrogenase (Fdh) are significantly upregulated for denitrifying *M. pacificus* under a 95% methane headspace (**Table 2**). The significantly upregulated PQQ-dependent alcohol dehydrogenase falls within the clade of PQQ-dependent ethanol dehydrogenase (ExaF) in *Methylobacterium extorquens* AM1 and *Dechloromonas occulta* (Good et al., 2016; Szeinbaum et al., 2020). *M. extorquens* ExaF protein has been characterized as the first non-XoxF-type alcohol dehydrogenase that uses lanthanides as a cofactor, and can utilize methanol, ethanol, and formaldehyde as substrates (Good et al., 2016; Good et al., 2019). Consistent with the high protein abundance of ExaF alcohol dehydrogenase, *M. pacificus* can grow aerobically with ethanol, methanol, and formate as the carbon source (**Figure 18**). Carbon substrates other than a 95% methane – 5% CO₂ gas headspace mix were not added to our bottle cultures, but proteomic expression of ExaF protein in *D. occulta* has been reported under methane headspace without additional carbon substrates (Szeinbaum et al., 2020). The high protein abundance of ExaF suggests that methane is being converted to methanol, ethanol, and/or formaldehyde in the headspace by some mechanism (Good et al., 2016; Good et al., 2019). To my knowledge, utilization of ExaF protein to produce formate under denitrifying conditions has not yet been described (Good et al., 2016; Good et al., 2019; Szeinbaum et al., 2020).

Formate, produced from ExaF oxidation of presumed methanol, ethanol, or formaldehyde, can then be oxidized by formate dehydrogenase (Fdh), which was also significantly abundant under a 95% methane headspace. *M. pacificus* likely has the same type of respiratory formate dehydrogenase (Fdh) as *Roseobacter* species (Howat et al., 2018). Concurrent expression of the full suite of denitrification with formate dehydrogenase may support the full respiration pathway of anaerobic nitrate reduction with formate as studied in *E. coli* (Yamamoto and Ishimoto, 1977); **Figure 20**). No nitrous oxide production was detected across all culture bottles for proteomics corresponds with high protein abundance of NosZ (**Figure 20**). High expression of cytochrome *c* in the CH₄ condition supports the electron shuttling needed for denitrification and alcohol oxidation (**Figure 20; Table 2**). Periplasmic sulfane dehydrogenase, molybdopterin-containing subunit SoxC and periplasmic sulfane dehydrogenase, diheme c-type cytochrome subunit SoxD likely are misannotated and instead are molybdopterin transferring and cytochrome *c* accessory enzymes for Fdh3 formate dehydrogenase (Niks and Hille, 2019).

Formaldehyde and methanol are created in the 95% methane 5% CO₂ headspace of 160 mL serum bottles (**Figure 19 and 20**). I propose that this reaction is occurring abiotically via photochemical lysis or hydroxyl radical interactions from N-oxides (Gómez Alvarez et al., 2013; Bhattarai et al., 2021; Polat et al., 2021). Due to the significant amount of methane provided to the bottles, low amounts of abiotic methane oxidation could support cells with the required methanol and formaldehyde. Future investigations with isotopic tracers are needed to understand interactions between the headspace and bacteria.

The monophyletic genus *Marinobacter* falls within Gammaproteobacteria and are considered biogeochemical “opportunitrophs” found in most marine habitats and redox

gradients due to their halotolerance and large genome (Handley and Lloyd, 2013). Despite their marine ubiquity, the biogeochemical role of *Marinobacter* remains largely unexplored in natural ocean systems. Carbon assimilation genes for *Marinobacter* support the ribulose monophosphate (RuMP) pathway associated with gammaproteobacterial type I methanotrophs (Khmelenina et al., 2018). Hydrocarbon degradation of diverse compounds has been described aerobically in most species of *Marinobacter*, including one-carbon compounds formate and ethanol, but not methane or methanol (Handley and Lloyd, 2013). However, hypersaline *Marinobacter* species are found in high arctic, hypersaline methane seeps despite no known methane oxidation mechanism or associated genes such as methane monooxygenase (Niederberger et al., 2010; Lay et al., 2012). Several strains are also found in methane-associated systems including hydrothermal vents, seafloor, and deep-sea environments (Kaye et al., 2011). In oxygen deficient zones, *Marinobacter litoris* is a distinct strain to the ETSP ODZ and *Marinobacter hydrocarbonoclasticus* has been found in the particulate fraction of the ETNP ODZ alongside *Prochlorococcus* and *Alteromonas* cycling carbon (Henríquez-Castillo et al., 2022; Anstett et al., 2023). It is conceivable that *Marinobacter* species could utilize methanol, ethanol, and formate produced from fish undergoing hypoxia and phytoplankton detritus in the particulate fraction under anoxia (Mincer and Aicher, 2016).

3.6 Conclusion

Here, I identified a novel *Marinobacter* species: *M. pacificus* and propose a potential 1-carbon anaerobic metabolism for the *Marinobacter* genus. *M. pacificus* was isolated from long-term enrichment cultures taken at the Eastern tropical north Pacific oxygen deficient zone given nitrate and methane headspaces. All species of *Marinobacter* are described as

facultative anaerobes capable of nitrate reduction. This characterization of 1-carbon oxidation under denitrifying conditions is the first to my knowledge for the genus *Marinobacter*. I found that *M. pacificus* is autofluorescent at ~465 nm and expresses a lanthanide-dependent pyrroloquinoline quinone alcohol dehydrogenase, ExaF, and formate dehydrogenase, Fdh, as well as the full suite of proteins for denitrification. *Marinobacter* species are well-known for their hydrocarbon-degrading metabolisms and ability to use nitrate under denitrifying conditions. However, there are few studies on the mechanism of anaerobic hydrocarbon degradation, particularly 1-carbon compounds. I postulate from proteomic results that *M. pacificus* oxidizes methanol or ethanol, formed in the methane headspace by hydroxyl radical oxidation provided by N-oxide species, to formate and using the electrons to catalyze denitrification. Further work should be completed to understand the complete abiotic oxidation and interactions occurring in the headspace. Additionally, the role of *Marinobacter* in the ETNP ODZ particulate fraction warrants additional study in non-culture enrichment experiments.

**CHAPTER 4. IDENTIFICATION AND CHARACTERIZATION OF
MANGANESE-OXIDE ASSOCIATED MICROBES ABOVE A DEEP
HYPERHALINE ANOXIC BASIN**

A portion of this work will be published by Claire E. Elbon, Jordan M. McKaig, Helen M. Tran. Tran, Rui Cai, Emma A. Aycock, Danielle Goudeau, Carley Ross, Miguel Desmarais, Benjamin Klempay, Emilie J. Skoog, Yuanzhi Tang, Ellery D. Ingall, Rex R. Malmstrom, Jeffery S. Bowman, Britney E. Schmidt, and Jennifer B. Glass, and the Oceans Across Space and Time Team.

4.1 Abstract

Manganese cycling bacteria have previously been detected above and below an Mn(IV) oxide peak (~2200 meters) in the Orca basin DHAB along the Texas-Louisiana continental slope. However, biotic MnO_x occurs at O₂ < 1 μM (presumed anoxia), and nitrate depletion (~22 μM to ~3 μM), which led us to explore potential anaerobic manganese oxidation occurring with nitrate reduction by performing enrichment, detection, and activity sampling targeting ~2200 meters. We employed leucoberbelin blue (LBB) MnO_x staining for microscopic detection of cell associations and spectrometric quantification and overall found that microbial cells at the Mn(IV) peak (~2200 meters) consume nitrate and produce what is likely δ-MnO_x covered in biofilms. *Marinobacter* became a dominant species over ~40 days of dark enrichment in transfer cultures from ~2200 meters of Orca Basin. We additionally assembled a transcriptionally active MAG of novel chemolithotroph Mn²⁺-oxidizer, *Ca. Manganitrophaceae* at ~2200 meters. Several

species of anaerobic, nitrate-utilizing bacteria are actively contributing to manganese oxidation at ~2200 meters in Orca Basin.

4.2 Introduction

Microbial manganese (Mn^{2+}) oxidation is ubiquitous in marine systems (Tebo et al., 2005; Cho et al., 2018). Mn^{2+} -oxidizing bacteria are physically associated with ferromanganese crusts and oxides via biofilm matrices (Stein et al., 2001; Templeton et al., 2005; Yli-Hemminki et al., 2014; Yu and Leadbetter, 2020). Microbial cells isolated directly from oxides are indeed predominantly Mn^{2+} -oxidizers, and Mn(IV)-reducers, contributing to particle formation and creating a closed Mn-cycle (Templeton et al., 2005; Blöthe et al., 2015). However, whether Mn^{2+} -oxidation provides any energy gain for the cell is largely unknown; the majority of Mn^{2+} -oxidizing bacteria currently known are heterotrophic and employ a mixotrophic lifestyle (Canfield et al., 2005; Templeton et al., 2005; Hansel, 2017). Further, Mn^{2+} is a highly toxic metal and most cellular activity for Mn^{2+} are stress responses (Martin and Waters, 2022).

Two step electron transfers oxidize soluble Mn^{2+} to particulate Mn(IV) oxides (Tebo et al., 2004). Mn oxides (MnO_x) can be formed biotically, abiotically, or by a combination of both. For example, ligand binding of Mn(III) occurs after biotic Mn^{2+} oxidation (Oldham et al., 2015; Oldham et al., 2017). Putative enzymes are proposed to support manganese oxidation including a multicopper oxidase (Tebo et al., 2005; Hansel, 2017; Yu and Leadbetter, 2020; Huang et al., 2022). However, exact enzymatic pathways for Mn oxidation continue to be elusive, and the identity and mechanism of Mn^{2+} -oxidizing microbes in anoxic marine systems are largely unknown.

The Orca Deep DHAB along the Texas-Louisiana continental slope (26°56'N, 91°19'W) has a strong salinity-density gradient that prevents advective mixing and maintains anoxia (Shokes et al., 1977; Pilcher and Blumstein, 2007). Salinity begins to increase at 2150 meters below sea level, fed by a seafloor salt dome on the eastern flank (Merlino et al., 2018; Sawyer et al., 2019). Manganese oxidizing and reducing bacteria have previously been detected directly above and below (respectively) a particulate Mn(IV) oxide peak in Orca Basin where both Mn²⁺ and Mn(IV) is significantly higher than overlying seawater (Van Cappellen et al., 1998). However, Mn(IV) oxides occur at O₂ < 1 μM (presumed anoxia) and nitrate depletion (~22 to ~3 μM), which led us to explore potential anaerobic manganese oxidation occurring with nitrate reduction.

Stratified marine anoxic basins contain a redoxcline, which is a transition zone from oxygen depletion to total anoxia caused by H₂S or high salinity, the latter is the case in Orca basin (Shokes et al., 1977; Van Cappellen et al., 1998; Dellwig et al., 2012). The redoxcline is an area of intense microbial redox cycling of “alternative” electron acceptors and donors, including nitrate and typically trace metals such as manganese (Trefry et al., 1984; Tebo and Emerson, 1986) (**Figure 18b**). Orca Basin contains sharp transition zones in the redox ladder due to salinity stratification preventing lateral movement in the water column (Shokes et al., 1977). The redoxcline has cryptic manganese cycling, with measurable accumulation of Mn²⁺ and Mn(IV) (Trefry et al., 1984; Van Cappellen et al., 1998) (**Figure 18b**). Accumulation of Mn(IV) particles by of Mn²⁺-oxidizing bacteria has been found in several pelagic marine anoxic basins, including the Black Sea, the Baltic Sea, and Orca Basin (Tebo and Emerson, 1986; Tebo, 1991; Neretin et al., 2003; Dellwig et al., 2012; Varrella et al., 2020). Oxygen below the limits of detection where Mn²⁺-

oxidizing bacteria are active, and Mn oxides accumulate, supports the hypothesis for an anaerobic process in stratified marine anoxic basins (Canfield et al., 2005).

In the Black Sea, Mn²⁺-oxidation has been determined to be a strictly aerobic process that can operate at oxygen levels as low as ~5 μM (Tebo, 1991; Clement et al., 2009). Yet, despite the apparent requirement for oxygen in Mn²⁺-oxidation, coupling this process to denitrification is thermodynamically feasible with $\Delta G_r = -14.9 \text{ kJ (mol e}^{-})^{-1}$ (Eq. 1) (LaRowe et al., 2021).



Chemolithoautotrophic Mn²⁺-oxidizing bacteria, *Candidatus* Manganitrophaceae of the Nitrospirota phylum, use nitrate as the sole nitrogen source, but still require oxygen for oxidation of manganese (Yu and Leadbetter, 2020). It remains unknown if a cell or cell consortium can catalyze anaerobic Mn²⁺-oxidation coupled to nitrate reduction for cell growth. We hypothesized that active Mn²⁺-oxidizing microbes are using anaerobic nitrate reduction at the Mn(IV) particulate peak in Orca Basin, and that produced MnO_x contains physically associated Mn²⁺-oxidizing cells. We sought to identify the Mn²⁺-oxidizing bacteria associated with MnO_x particles within Orca Basin and determine if these microbes can produce MnO_x under enrichment cultures. We found that microbial cells at the Mn(IV) oxide peak consume nitrate and produce what is likely δ-MnO_x.

4.3 Methods

4.3.1 Field geochemical sampling

All samples were collected on R/V *Point Sur* (Pt_Sur_26_23) during June-July 2023. Filter samples were taken directly from the CTD rosette throughout the water column from normosaline seawater to the anoxic core brine, with discrete sampling at and around the Mn(IV) peak at 2200 meters. Here, we refer to ~2200 m as the Mn(IV) peak. Anoxic water sampling for enrichment cultures were focused on the Mn(IV) peak. All samples discussed here were collected from station P1 and P5 (N'27°00.968' W'91°16.447'; N'27°00.274 W'91°25.107, respectively).

All geochemical samples were filtered through a 0.45-micron polypropylene filter. Fe(III) and Mn²⁺ samples were acidified immediately after filtration to a pH of ~1. All samples were analyzed manually on board using a spectrophotometer within a few days of sample collection. Methods of analysis were adapted from "Methods of Seawater Analysis" (Hansen and Koroleff, 1999; Kremling, 1999). Briefly, Nitrate was measured with a cadmium column method without dilutions. Manganese (2⁺) was measured by reacting with formaldoxime and concentrated ammonium hydroxide mixed reagent. A variation of the Winkler Titration method was performed on water samples for dissolved oxygen. The Winkler Titration method begins with fixing the dissolved oxygen as soon as it has been collected. On the deck, immediately beside where the CTD Rosette was stationed, 0.9mL 2.021M solution of MnCl₂ tetrahydrate and 0.9 mL alkaline-iodide-azide solution was added to a full scintillation vial to displaced 1.8 mL of the sample water. The sample was capped with a scintillation cone cap. Any dissolved oxygen present was fixed into a white cloudy precipitate of Mn(OH)₂. The sample with the precipitate was left to settle for about 2 hours so that no precipitate is displaced during the next step. Once all precipitate was settled to the bottom of the vial, 1 mL of phosphoric acid was pipetted in to dissolve the

precipitate back into solution and the sample was inverted a few times to increase efficiency of the dissolution reaction. After all precipitate was dissolved, the titration began. Variable volumes of the sample were added to 10 mL beakers. Sodium thiosulfate was added to the sample on a stir plate until the color shifted to pale yellow. Then, one drop of starch indicator was added. Sodium thiosulfate was added by decreasing increments until the sample turned clear. This was done at least three times for each sample with different sample volumes to ensure an accurate average could be calculated. The amount of sodium thiosulfate added was used to calculate the dissolved oxygen in mg/L.

4.3.2 Field anoxic water sampling for cultures and filter sampling

Anoxic water samples were taken immediately from Niskin bottles once the CTD was back onboard using an anoxic overflow capping method into 160 mL sterile serum bottles with red rubber tops kept under helium gas for 6-months prior and crimped with aluminum tops. The bottles were immediately taken to a 5°C cold van onboard and sparged with N₂ gas replacing 10 ml of liquid. 100 µM of N₂-sparged anoxic sodium nitrate (NO₃⁻) dissolved in artificial seawater to 10 mM concentrations (Sigma-Aldrich; 221341) was added to each 160 mL bottle and then stored in the dark at 5°C for the duration of the cruise and in the lab once back on land. 50 and 20-mL samples for filtering were taken at the same depths/identical Niskin bottles as anoxic enrichment bottles after those samples were collected with sterile 50 mL Falcon® Centrifuge Tubes (CLS352070), immediately fixed with 20% formaldehyde diluted to a final concentration of 1% (47608; Sigma-Aldrich), incubated for 24 hours, and then filtered onto GTTP Isopore membrane 0.2 µm pore size, hydrophilic polycarbonate membrane, 25 mm diameter filters (Millipore Sigma,

GTTP02500) with a 1225 Sampling Manifold (Millipore Sigma; xx2702550) at ~10 Hg pressure and stored at -20°C until downstream analysis.

A subset of bottle samples was collected at sea using the same anoxic overflow method targeting the Mn(IV) peak for BioOrthogonal Non-Canonical Amino acid Tagging (BONCAT) incubations and laser-microdissection (LMD) metagenomic sequencing that target the microbial community physically attached to MnO_x particles. Bottle culture incubations were run for 3 days in the dark, 5°C cold van on board and were then live filtered (LMD) or fixed for 24 hours, then filtered (BONCAT). The results of LMD genomics and BONCAT are currently ongoing and will not be discussed in this chapter.

4.3.3 *Simul-staining and imaging of manganese oxides and microbial cells*

The 50 and 20-mL filter samples were analyzed microscopically to identify *in-situ* MnO_x-cell associations using MnO_x LBB-SYBR simul-staining methods (Cavazos and Glass, 2020). The protocol from Cavazos et al. 2020 was used with the following changes: filters were cut into ¼ sections and first stained with 5 µL of SYBR™ Green I Nucleic Acid Gel Stain, 10,000X concentrate in DMSO diluted to 1:400 concentration (Invitrogen, S7563) and reacted for 15 minutes in the dark. Filters were then rinsed with 5 µL of 0.2-micron filter sterilized 1X PBS and dried in the dark until filters became transparent. The filters were then stained in the dark with 20 µL of 0.04% LBB stain and reacted for ~8 minutes. The filters were then immediately placed under a Zeiss Z.1 microscope and imaged with DIC light under maximum brightness and the GFP (470/525) filter within 45 minutes of staining with colorimetric reagent Leucoberbelin Blue I (LBB) (432199; Sigma-

Aldrich) diluted to 0.04% in glacial acetic acid. Images were analyzed in Fiji (Schindelin et al., 2012) using the protocol outlined in Cavazos et al. (Cavazos and Glass, 2020).

4.3.4 *Sterile Orca Basin media*

Enrichment culture media was created with 2x0.22 sterile filtered Orca Basin water from ~2200 m collected in 10-liter carboys. 500 mL of the sterile 2200 m Orca Basin water was anoxically sparged with helium for 10 minutes after addition of 100 μM NO_3^- . 50 μM of anoxic sparged manganese chloride (244589; Sigma-Aldrich) dissolved in artificial seawater was then added to the anoxic enrichment cultures based on environmentally relevant values from 2200 meters (**Figure 21**). Additional transfers with 100, 150, and 500 μM anoxic sparged manganese chloride (244589; Sigma-Aldrich) dissolved in artificial seawater were performed in the same method as listed above.

4.3.5 *Anoxic enrichment cultures*

The media was then transferred into an anaerobic chamber where 1:10 dilutions were performed with 81 mL of media and 9 mL of anoxic water sample taken from 2200 m (section 4.3.1) into new sterile 160 mL serum bottles. Additional transfers with 100, 150, and 500 μM anoxic sparged manganese chloride (Mn^{2+} ; 244589; Sigma-Aldrich) dissolved in artificial seawater were performed in the same method as listed above. Anoxic enrichment transfer cultures were taken out of the anaerobic chamber and sparged with either a specialty 95% CH_4 /5% CO_2 gas mixture or a 100% He gas for 5 minutes to replace the headspace, and then sparged to overpressure. The overpressure culture bottles were stored in the dark on their side in a 5°C environmental chamber. Subsamples for NO_3^- and

MnO_x were taken in the anaerobic chamber, and bottles were re-sparged to overpressure with respective gases after each subsampling timepoint.

4.3.6 *Scanning electron microscopy coupled with energy dispersive x-ray spectroscopy*

150 µM Mn²⁺ enrichment cultures (25 mL) from 100% He and 95% CH₄/5% CO₂ were extracted in an anoxic chamber (97% N₂/3% H₂) and filtered onto GTTP Isopore membrane 0.2 µm pore size, hydrophilic polycarbonate membrane, 25 mm diameter filters (Millipore Sigma, GTTP02500) with a Geotech hand pump (Fondriest Environmental; 87500001) inside the chamber. The sample atop filters were then transferred with 100 µL sterile milli-Q water onto standard SEM pin stub mounts with ø12mm conductive carbon tabs already attached to the mounts. Samples were left in the chamber overnight to dry completely. The morphology of the sample was characterized using Scanning Electron Microscopy coupled with Energy Dispersive X-Ray Spectroscopy (SEM-EDX, Hitachi SU8230). Prior to analysis, the sample was coated with a thin layer of gold using the Hummer 6 Sputterer equipped with a gold target.

4.3.7 *X-ray Absorption Spectroscopy*

25-mL samples from 150 µM Mn²⁺ enrichment cultures from 100% He and 95% CH₄-5% CO₂ were extracted in an anaerobic chamber and filtered onto GTTP Isopore membrane 0.2 µm pore size, hydrophilic polycarbonate membrane, 25 mm diameter filters (Millipore Sigma, GTTP02500) with a Geotech hand pump (Fondriest Environmental; 87500001). Samples were then examined for visible particles, and then folded 4 times and mounted onto a plastic mounting set for Synchrotron X-ray Absorption Spectroscopy (XAS) was performed at Beamline 11-2 of the Stanford Synchrotron Radiation Lightsource

(SSRL) at the SLAC National Accelerator Laboratory (Menlo Park, CA, USA). The beamline is equipped with collimating and focusing optics, a liquid-nitrogen-cooled Si(220) monochromator, and a 100-pixel monolithic solid-state Ge detector array. The identification of Mn oxide species was achieved through linear combination fitting of Mn K-edge XANES data.

4.3.8 *Nitrate, nitrite, and nitrous oxide quantification*

Enrichment transfers were sampled to check for nitrate reduction and nitrite production and reduction using Griess assays (García-Robledo et al., 2014), and nitrous oxide production using the gas-chromatography electron current detector setting on a SRI Multiple Gas Analyzer (GC-ECD; #5; SRI Instruments). Briefly, bottles tops were sterilized with 75% ethanol diluted with sterile milli-Q water, and headspaces were sampled by removing 1 mL gas headspace using a 1 mL Gastight Model 1001 Luer Lock (TLL) Instrument Syringe (81320, Hamilton) and a 27-gauge needle (Exel International® Hypodermic Needles, Air-Tite Products; 76290-484). The sample was injected into the GC-ECD to measure peak and area at ~1.6 min according to manufacture protocols and lab calibrations for nitrous oxide. A gas standard curve was made with Scott nitrous oxide gas 1 ppm standard bottle (501514; Scott Gas standards).

For Griess analysis of nitrite/nitrate, enrichment cultures were sampled in an anaerobic chamber (3% H₂ gas, O₂ < 15 ppm) where 1 mL of culture was extracted using a sterile 26-gauge needle (Exel International® Hypodermic Needles, Air-Tite Products; 76290-572), sterile 3-mL syringe, and 0.22 µm filtered into sterile 1.5 mL tubes. Bottles were re-gassed to overpressure after each sampling with their respective gases. 100 µL of

Griess reagent (equal parts NED and sulfanilamide) was added to each 1 ml filtered sample and reacted in the dark for 15 minutes, then measured spectrophotometrically with a 1 mL sterile cuvette on a UV-Vis spectrometer at 540 nm (García-Robledo et al., 2014). 100 ml of vanadium chloride was then added to samples and reacted for 30 minutes in a 60°C water bath to induce nitrate reduction to nitrite. Samples were then again measured spectrophotometrically with 1 mL sterile cuvette at 540 nm. Standard curves were made with artificial sodium nitrate and sodium nitrite in artificial seawater for NO_2^- , NO_2^- -V, NO_3^- -V following methods by García-Robledo et al. (2014).

4.3.9 *Manganese oxide quantification*

Manganese (IV) oxides were detected using the colorimetric reagent Leucoberbelin Blue I (LBB) (432199; Sigma-Aldrich) diluted to 0.04% in glacial acetic acid (Richardson et al., 1988; Jones et al., 2019). Sampling was performed concurrently with sampling for Griess analysis in an anaerobic chamber (3% H_2 gas, $\text{O}_2 < 15$ ppm). 1 ml of culture was extracted using a sterile 26-gauge needle (Exel International® Hypodermic Needles, Air-Tite Products; 76290-572) and sterile 3-mL syringed into sterile 1.5 ml tubes. Bottles were re-gassed to overpressure after each sampling with their respective gases. 150 μL of 0.04% LBB was added to the 1 mL samples and incubated in the dark for 15 minutes. Reacted samples with oxidized LBB were then measured on a UV-Vis spectrometer at 620 nm wavelength in a 1 mL sterile cuvette. Oxidized LBB was calibrated using KMnO_4 (014307.22; ThermoFisher) standards dissolved in artificial seawater.

4.3.10 *Oxygen measurements*

Oxygen was tracked in anoxic culture enrichments for rate measurements of nitrate drawdown and MnO_x production using contactless self-adhesive sterilized oxygen sensor spots (OXSP5-ADH-STER; PyroScience) attached to the side of 160 mL sterile bottles. Blank optical fiber PICFIB2 cables with a PICO-connector were used to measure oxygen spots in 160 mL serum bottles and was connected to a FireSting-O₂ optical oxygen meter connected to a PC for continuous readouts and timepoint measurements. Upper and 0% saltwater calibrations were performed using standard protocols in the PyroScience handbook.

4.3.11 16S rRNA Sequencing

16S rRNA sequencing was performed on all enrichment cultures using a DNeasy PowerWater Kit (Qiagen, 14900-100-NF). Briefly, 25 mL of sample was collected in an anaerobic chamber with sterile 50 mL Falcon[®] Centrifuge Tubes (CLS352070) and filtered onto GTTP Isopore membrane 0.2 µm pore size, hydrophilic polycarbonate membrane, 25 mm diameter filters (Millipore Sigma, GTTP02500) using ~5 Hg vacuum filtration with a 1225 Sampling Manifold (Millipore Sigma; xx2702550). The samples were then processed, and DNA was extracted using the standard Qiagen kit protocol. DNA was sequenced at Livermore National laboratory using Illumina MiSeq sequencing and overlapped at the facility. 16S rRNA sequences were then quality checked and identity-mapped using the Paprica pipeline (Bowman and Ducklow, 2015). The phylogenetic trees were also created using the Paprica pipeline (Bowman and Ducklow, 2015).

4.3.12 Metagenomics

4.3.12.1 Sample collection

4 L brine samples were collected from CTD-mounted Niskin bottles at sampling location P5 (N'27°00.274 W'91°25.107) for depths of 2193, 2202, 2220, 2225, 2235, 2236, and 2246 meters. Samples were concentrated using a large volume concentration (LVC) system (FluidPrep EasyElute Large Volume Concentration Kit, InnovaPrep CC01117) equipped with high-performance tubing (inner diameter 0.25 inches, Masterflex MFLX9641924) and a peristaltic pump (Alexis Peristaltic Pump, Proactive Environmental Products 76548). Especially viscous samples were diluted with autoclaved 18 megaohm water to enable effective concentration. 50-100 mL concentrate was eluted from each sample, which was further concentrated using a concentrating pipette (CP) (InnovaPrep CP Select Concentrating Pipette) with ultrafilter tips (InnovaPrep CC08003-10) and elution foam (EasyElute Elution Buffer – PBS and EasyElute Elution Buffer – Tris, InnovaPrep HC08018-P and HC08018-T). 200-400 µL final concentrate was eluted from each sample, and eluent was stored in 1x DNA/RNA Shield (Zymo Research R1200) in a 3:1 shield-to-sample volumetric ratio. Samples were stored at 4°C until ready for laboratory extraction.

4.3.12.2 DNA extraction

DNA was extracted from stored samples using the ZymoBIOMICS DNA Microprep Kit (Zymo Research, D4301) with the following modifications to efficiently extract high molecular weight DNA from these low-biomass samples. Samples were transferred into the kit's lysis tubes, then were agitated with a handheld lysis device (TerraLyzer, Zymo Research S6022) for 3 minutes each. All centrifugation steps were done at 16,000 x g and were sometimes repeated to ensure a clear supernatant. The III-F Filter step was skipped. Following the final wash step, samples were subjected to an additional “dry spin” for 1 minute to ensure that any residual buffer had been removed. The

DNase/RNase Free Water was heated to 60°C before adding to column matrix, then samples were incubated for 3 minutes before elution. The II-μHRC Filter/HRC Prep Solution steps were skipped. When needed, samples were gently mixed via pipetting.

Following extraction, DNA concentration was measured with the Qubit 1x dsDNA HS Assay Kit (Invitrogen Q33231). Quality was measured with a Nanodrop. Length was measured using the Lonza Flash Gel System with a 1.2% agarose cassette (Lonza 57023) and a 1 kb ladder (New England Biolabs, Inc. N3239S). Samples were stored in 1x DNA/RNA Shield (Zymo Research R1200) in a 3:1 shield-to-sample volumetric ratio and kept at 4°C until sequencing.

4.3.12.3 Library preparation and nanopore sequencing

Stored samples were purified and concentrated for sequencing using the Genomic DNA Clean & Concentrator™ Kit-10 (Zymo Research D4010). The full volumes of remaining DNA (sample masses ranging from 128.7 – 712.8 ng) were prepared for sequencing following the Ligation Sequencing gDNA with Native Barcoding Kit 24 v14 protocol (NBE_9169_v114_revP_15Sep2022, Oxford Nanopore Technologies) and using the Native Barcoding Kit 24 V14 (Oxford Nanopore Technologies SQK-NBD114.24). Each sample (e.g. each depth or blank) was assigned to its own barcode. Barcoded samples were pooled and loaded into a MinION R10.4.1 flow cell (Oxford Nanopore Technologies FLO-MIN114), then sequenced on the Mk1C (Oxford Nanopore Technologies) running MinKNOW v23.04.5 for 72 hours. Two sequencing runs were done: the first contained DNA extracted from 3 water samples and 2 blanks, and the second contained DNA

extracted from 4 water samples and 2 blanks. New flow cells were used for each sequencing run.

4.3.12.4 Basecalling

Pod5 files resulting from sequencing were base called on a Google Collab instance using dorado v0.8.0 (Oxford Nanopore Technologies) with the model dna_r10.4.1_e8.2_400bps_sup@v5.0.0 and separated into barcode-specific FASTQ and BAM files using the dorado demux command.

4.3.12.5 MAG assembly

MAGs were assembled using Nanophase, a pipeline designed for constructing MAGs from nanopore-generated long-read sequences (Liu et al., 2022). This tool involves several bioinformatic tools, including metaFlye (Kolmogorov et al., 2020), MetaBAT2(Kang et al., 2019), MaxBin2 (Wu et al., 2015), MetaWRAP (Uritskiy et al., 2018), SemiBin (Pan et al., 2022), minimap2 (Li, 2018), Racon (Vaser et al., 2017), medaka (<https://github.com/nanoporetech/medaka>), GNU Parallel (<https://pubmed.ncbi.nlm.nih.gov/21572440/>, <https://doi.org/10.5281/zenodo.5233953>), CheckM, Prodigal, GTDB-Tk and fastANI.

4.3.12.6 Long-read assembly

Long read fastq files for each depth were passed into Nanophase using default parameters. Assembly was conducted separately for each sampling depth. For each MAG, GC content and genome size were checked to ensure that they were in accordance with similar genomes on the GTDB-TK database.

4.3.13 Metatranscriptomics

RNA for metatranscriptomics was collected in triplicate for each depth, kept on ice upon collection and immediately filtered with a filter manifold onto 0.45-micron filters. Filters were immediately folded into sterile cryotubes (FisherSci; 10-500-26) and suspended with 1 mL of RNAlater (ThermoFisher; AM7020) in each vial. The vial was rolled gently to spread RNAlater across filter. Filters were then stored at -80°C until sequencing at the Lawrence Livermore National Laboratory. RNA sequencing results were loaded into KBase for downstream analysis (Arkin et al., 2018). We focused on metatranscriptomic data from ~2200 meters. Sequencing reads were aligned to long reference prokaryotic genome sequences from metagenomics (above) using Bowtie2 - v2.3.2 (Langmead and Salzberg, 2012). Transcripts from RNA-seq were aligned using StringTie - v2.1.5.

4.4 Results

4.4.1 Orca Basin redoxcline geochemistry

The Orca Basin is located along the Texas-Louisiana continental slope (26°56'N, 91°19'W) (Addy and Behrens, 1980) and was sampled in June-July 2023 on the R/V *Point Sur*. This study focused on samples from Orca Basin's redoxcline, from 2195-2220 meters (m) depth below sea level, and immediately above the DHAB brine, which lies below ~2225 (**Figure 21a**). Above the redoxcline, dissolved O₂ declined from 6 μM at 2050 m to undetectable (<1 μM) at 2195 m, and nitrate declined from ~22 μM at 2050 m to ~3 μM at 2195 m (**Figure 21b**). Nitrate further declined through the redoxcline, dropping to <1 μM at 2220 m. Dissolved Mn²⁺ rose through the redoxcline, from undetectable at 2195 m to ~80 μM at 2220 m. The 2023 Mn²⁺ data overlapped exactly with 1998 Mn²⁺ data from Van

Cappellen et al. (1998). Based on the consistent overlap of Mn^{2+} data, we can assume that the Mn(IV) peak ($\sim 400 \text{ nmol L}^{-1}$) at 2200 m reported in ref. (Van Cappellen et al., 1998) from 1998 occurred at the same depth in 2023. We confirmed the presence of particulate Mn(IV) at 2200 m in 2023 by staining filters with leucoberbelin blue (LBB) as an MnO_x indicator (Figure 21c).

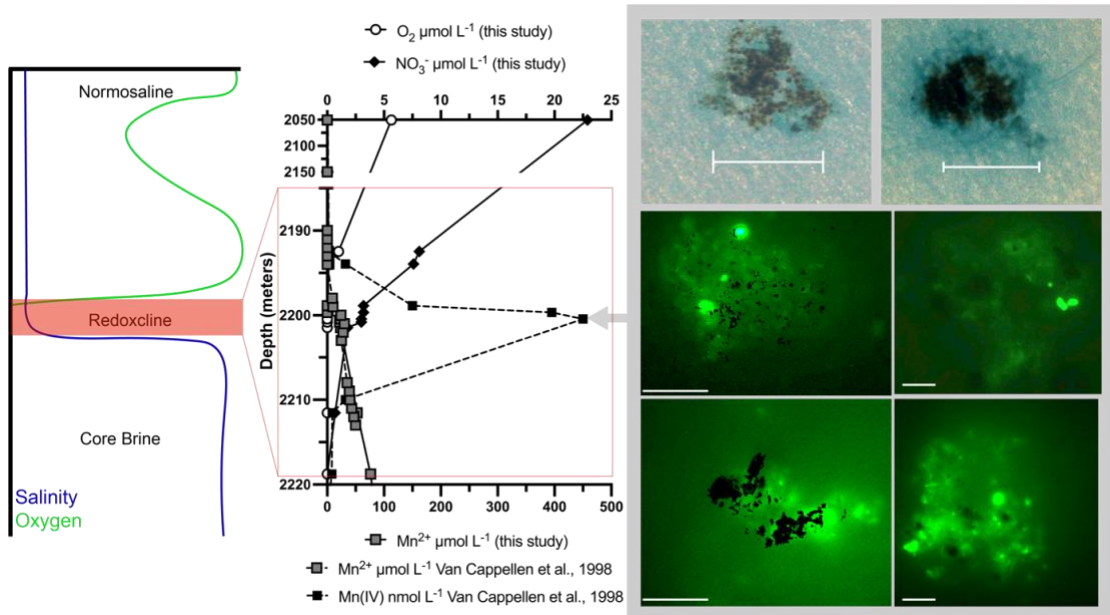


Figure 21. Orca Basin redoxcline depth profile. (a) Left: simplified schema of Orca basin water column oxygen and salinity shifts from normosaline, redoxcline, and core brine. (b) Middle: dissolved oxygen (above), nitrate (above), and dissolved Mn^{2+} (below) measured during cruise in 2023, and particulate Mn(IV) (below) and Mn^{2+} (below) (Van Cappellen et al., 1998). (c) Microscopy of samples collected at 2200 meters are shown on the right. Top right: leucoberbelin blue-stained MnO_x particles are visible as dark particles surrounded by blue haloes. Bottom right: simul-staining with leucoberbelin blue and SYBR green stain; MnO_x particles appear black when overlaid with SYBR cell images. Scale bar is 5 microns for simul-staining images and 30 microns for LBB images.

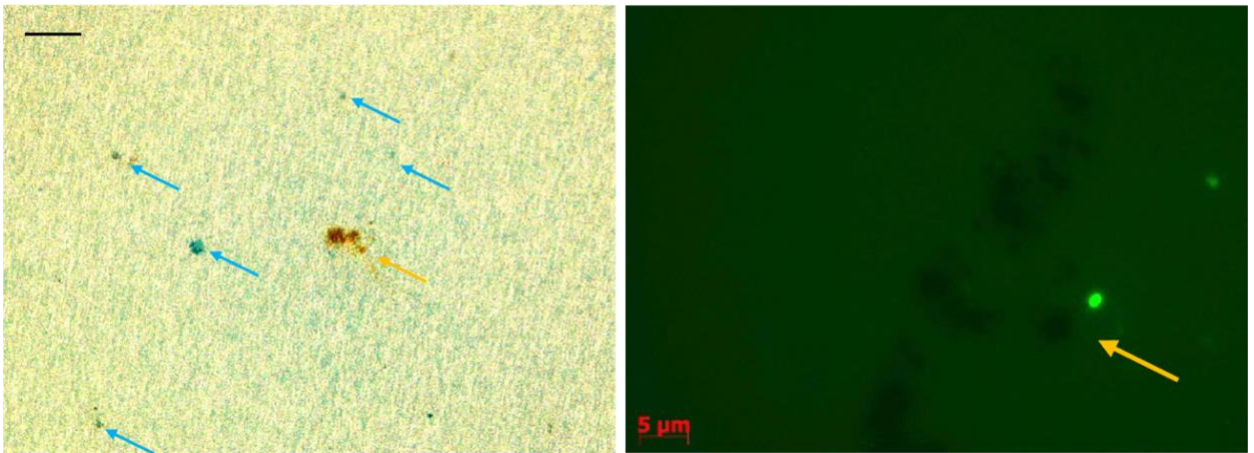
4.4.2 Manganese particles co-located with cells are only detected at 2200 m

Simultaneous staining (simul-staining) (Cavazos and Glass, 2020) of filters from 2200 m with SYBR green DNA stain and LBB staining shows SYBR-green stained cells

(1-5 microns) co-located with LBB+ MnO_x particles (**Figure 21c**). LBB+ MnO_x particles are 3 to 5-micron large but form conglomerates up to ~30 micron wide. Cells appear as biofilm-like matrices that encompass LBB+ MnO_x particles. Overall, no LBB+ MnO_x particles were detected without the co-presence of cells (**Figure 21c**).

Iron oxides are present on filters at 2200 m as brown-red particles but were not spatially associated with cells (**Figure 22a**). LBB+ MnO_x particles were not detected in the DHAB brine (2300 meters) despite increased particulate matter overall (**Figure 22b**). Further, cells and particles were not co-located at 2300 m, and cell counts were lower in the DHAB brine than at the Mn(IV) peak (**Figure 22b**).

2200 meters



2300 meters

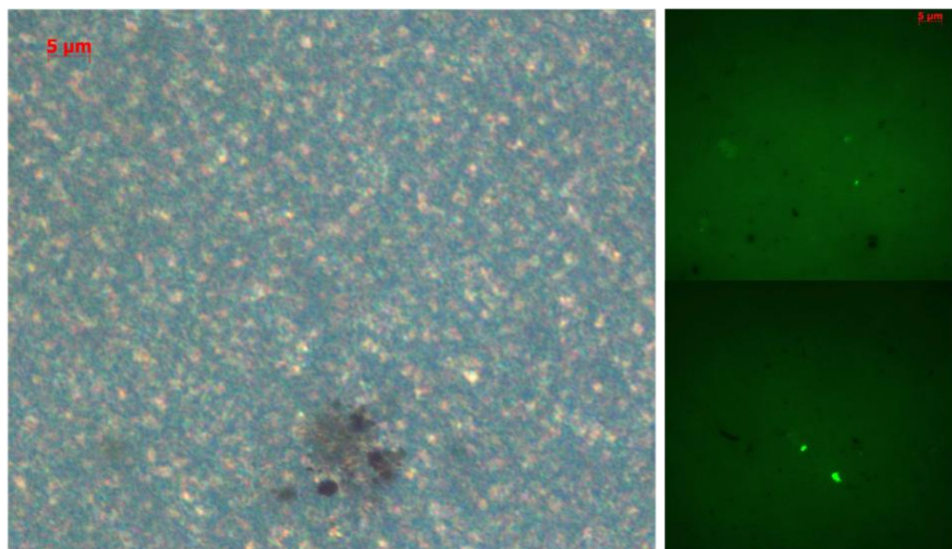


Figure 22. DIC and SYBR microscopy images of cells from 2200 m and 2300 m samples. Top left, DIC 10x microscopy image of filter sample collected from 2200 m with LBB staining. LBB+ particles are indicated with blue arrows and appear as dark particles with a blue “halo” around them. Iron oxides are indicated with yellow arrows and appear as red-brown particles. Scale bar is 50 microns. Top right, fluorescent 100x microscopy image of filter sample collected from 2200 m simultaneously stained with LBB and SYBR. Iron oxides are dark particles indicated with yellow arrow. Bottom left, DIC 100x microscopy image of filter sample collected from 2300 m core brine with LBB staining. No blue “halos” were detected but dark particles were frequently noted. Bottom right, microscopy of samples collected from the core

brine (2300 m) simul-stained with LBB and SYBR. Dark particles were abundant but none were LBB+ nor were any associated with cells.

4.4.3 Manganese particles produced by culture transfers are likely δ -MnO₂ and coated in cellular biofilms

Enrichment cultures established by anoxic sampling at 2200 m were incubated for ~20 days and used for culture transfers. Particles from 45-day culture transfers analyzed by X-ray Absorption Near Edge Spectroscopy (XANES) have an edge-position maximum at ~6563 eV, corresponding to Mn(IV) (**Figure 23a**). Quantitative analysis of the spectra additionally supports δ -MnO₂ as the only detected manganese particle in enrichment cultures (**Figure 24**). Low amounts of particles were successfully transferred onto the filter for XANES analysis which may interfere with the ability to detect additional manganese particles. Scanning electron microscopy-energy dispersive X-ray spectroscopy (SEM-EDX) identified minerals containing manganese with rod-shaped and cocci-shaped particles approximately the size of microbial cells (0.5-1 micron; **Figure 23**). We presume the observed filamentous matrices covering some particles to be cellular biofilms (**Figure 23b**). Two distinct morphologies of particles were found: node-particles and stacked layers, (**Figure 23b, 23c**). Significant amounts of fluorine were detected in SEM-EDX analysis as well, but the origin is unknown.

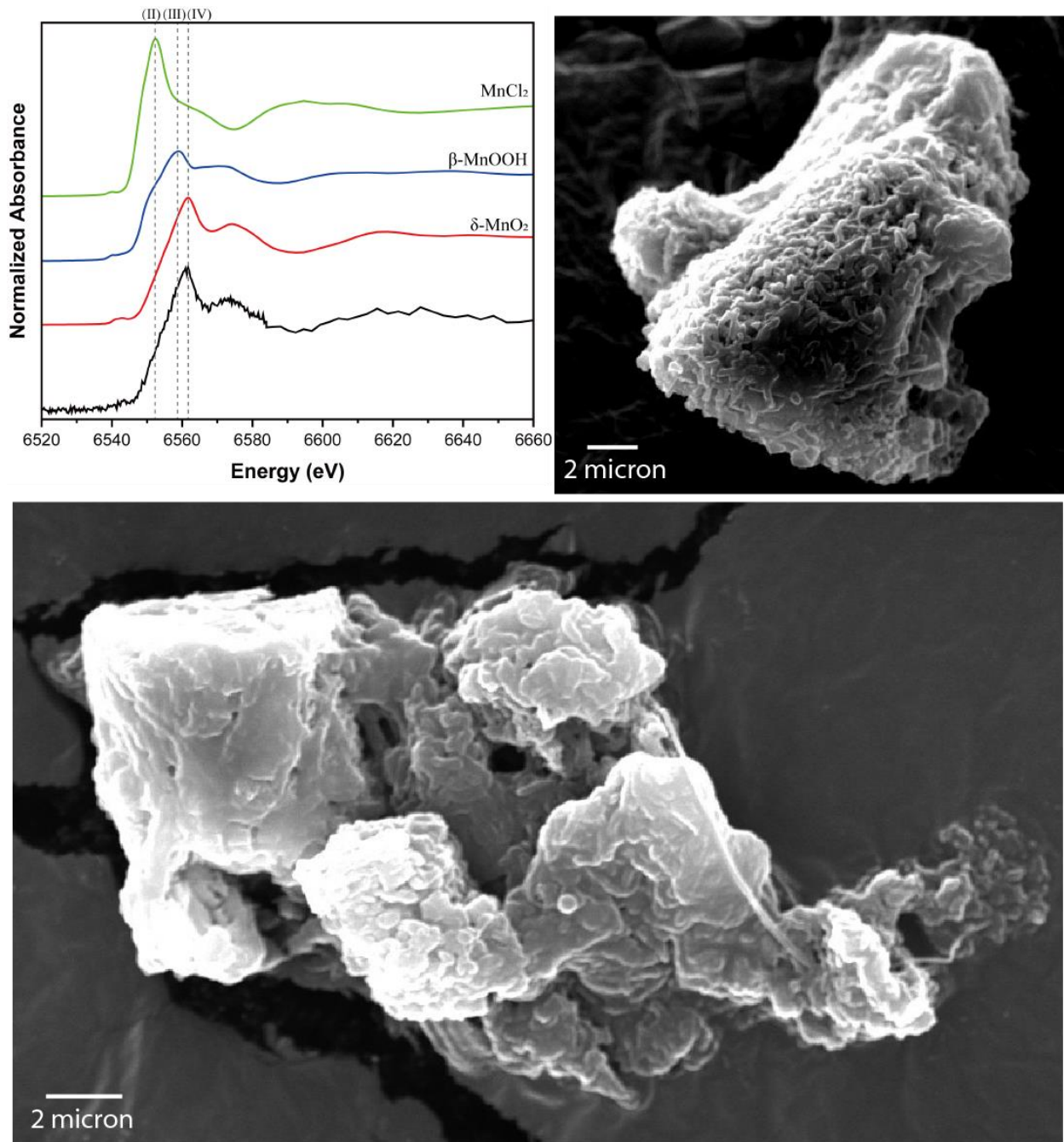


Figure 23. XANES peak data and SEM-EDX images from 2200-meter culture transfer sample 150 μM Mn^{2+} . (a) Red, blue, and green lines correspond to representative samples of $\delta\text{-MnO}_2$, $\beta\text{-MnOOH}$, and MnCl_2 , respectively. Bottom black line is the edge maximum position for enrichment sample. Dashed lines indicated edge maxima for each state of Mn. (b) Representative SEM-EDX image of a node-like particle containing manganese. Filamentous material covering node-like particles are presumed to be rod-shaped cells. (c) Representative SEM-EDX image of a stacked particle containing manganese. Rod and cocci-type material is seen within the stacked

particle and presumed to be cells. XANES k-edge data and SEM-EDX image correspond to the same enrichment culture bottle (150 $\mu\text{M Mn}^{2+}$ and He headspace).

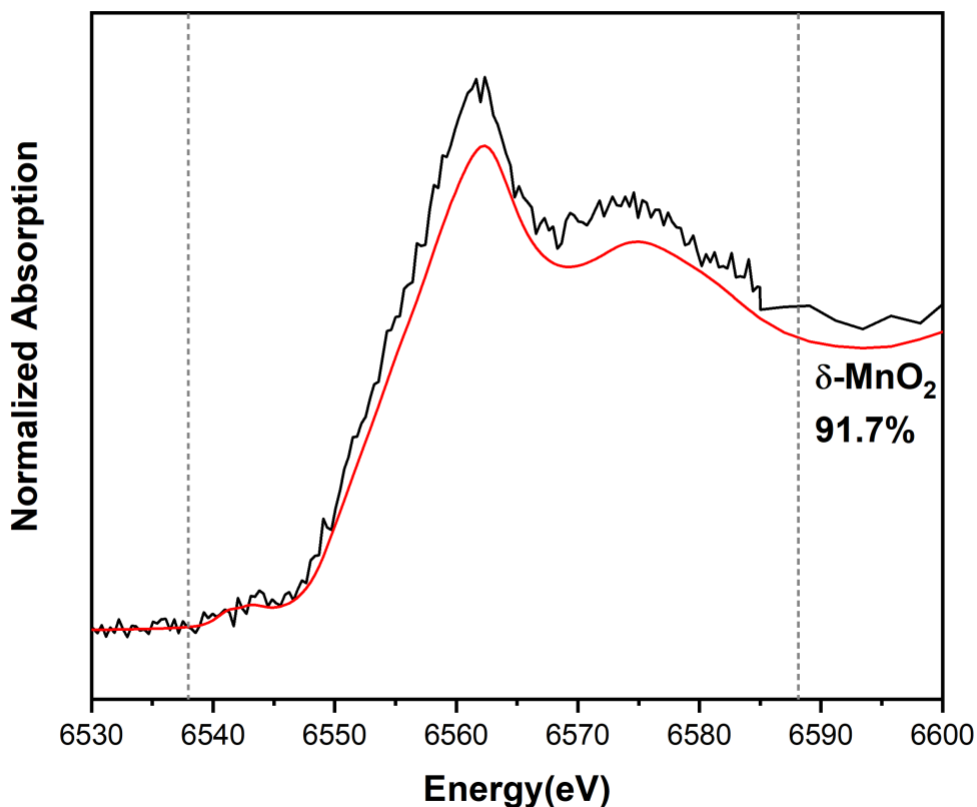


Figure 24. Quantitative XANES data of culture transfer sample from 2200-meter culture transfer sample 150 $\mu\text{M Mn}^{2+}$. Energy versus normalized absorbance plotted from XANES data collected from representative of 2200-meter enrichment cultures (black line). Pure sample of $\delta\text{-MnO}_2$ plotted as energy versus normalized absorbance is plotted alongside our sample in red. Fit of these two lines is 91.7%.

4.4.4 Low-suboxic enrichments from 2200 meters consume nitrate and produce manganese oxides

Culture transfers were set up to measure MnO_x production under gas headspaces with addition of NO_3^- and Mn^{2+} . Oxygen conditions in sterile enrichment bottles with no

culture addition were measured in the low-suboxic range (0.5-1 μM oxygen). Addition of culture to the enrichment bottles with NO_3^- and Mn^{2+} caused no change in low-suboxic range measurements.

Enrichment cultures produced MnO_x when supplemented with environmentally relevant values of Mn^{2+} (50 μM) and an excess of NO_3^- (**Figure 25**). Additional transfers from original enrichment cultures produce MnO_x over a range of Mn^{2+} and NO_3^- concentrations (**Figure 25; Figure 26**). MnO_x production is higher with a 95% $\text{CH}_4/5\%$ CO_2 headspace than with 100% He headspace (**Figure 26**). Total production of MnO_x in enrichments occurred at equivalent amounts to Mn(IV) measured in the redoxcline (Van Cappellen et al., 1998) (**Figure 21; Figure 26**).

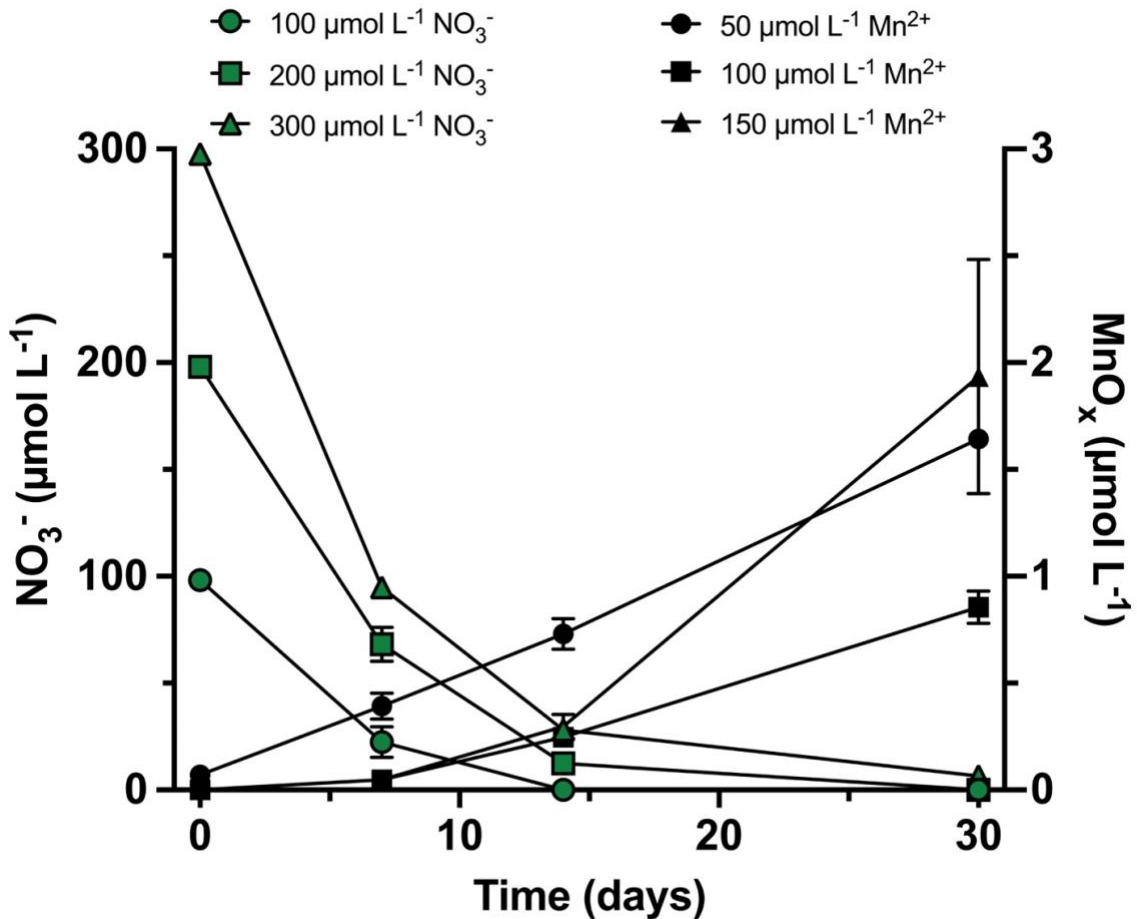


Figure 25. NO_3^- reduction and MnO_x production rates in suboxic enrichment cultures containing inoculant from Orca Basin 2200 meters water samples. Duplicate bottles were taken for each concentration of NO_3^- and Mn^{2+} and are shown with standard error. Nitrate drawdown is represented with green symbols and MnO_x production is represented with black symbols. The rates of drawdown and production for the 100 μM NO_3^- and 50 μM Mn^{2+} condition is shown with circles, the 200 μM NO_3^- and 100 μM Mn^{2+} condition is shown with squares, and 300 μM NO_3^- and 150 μM Mn^{2+} condition is shown with triangles. All enrichment cultures plotted contain $\text{CH}_4\text{-CO}_2$ headspaces. Some sample points do not contain error bars which indicate values that fell within standard error from each other.

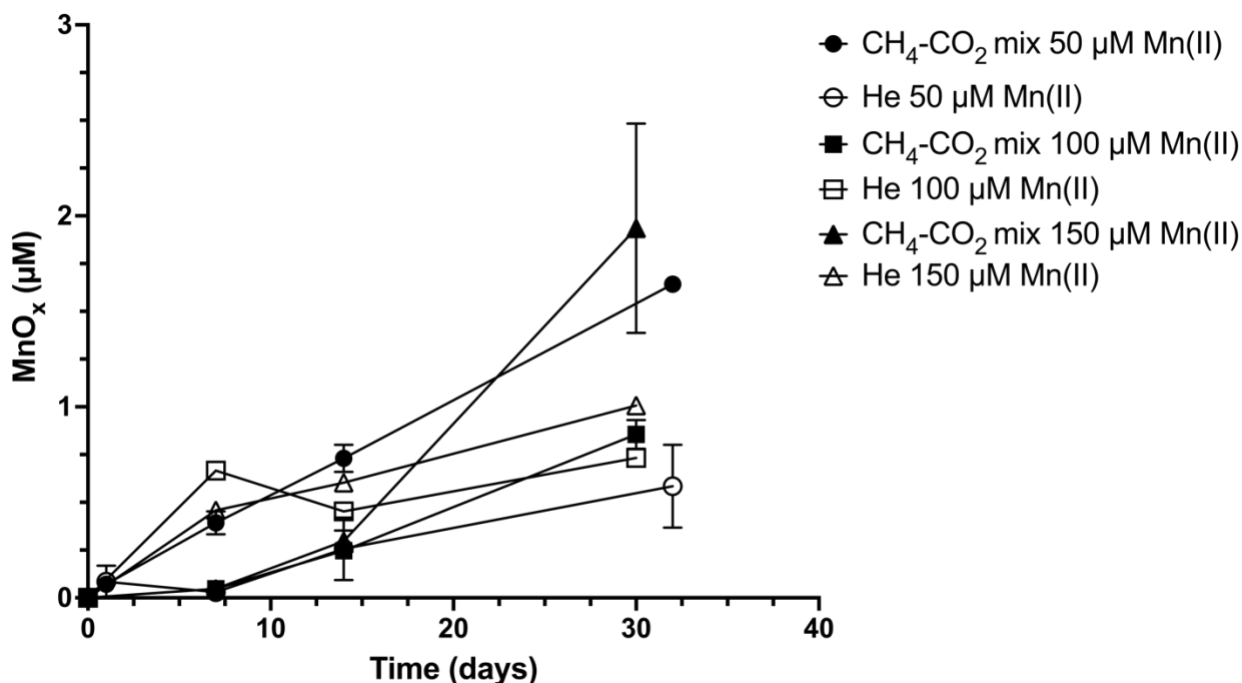
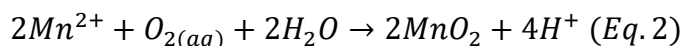


Figure 26. MnO_x production in suboxic enrichment cultures containing inoculant from Orca Basin (2200 meter depth). MnO_x production in the 50 µM Mn²⁺ and 100 µM NO₃⁻ condition is represented by circular symbols, the 100 µM Mn²⁺ and 200 µM NO₃⁻ condition by squares, and the 150 µM Mn²⁺ and 300 µM NO₃⁻ condition by triangles. Helium gas headspaces are open symbols, and 95% CH₄-5% CO₂ gas headspaces are filled in black symbols. Values are shown with standard error (SEM).

The equation for oxidation of Mn²⁺ with O₂ producing MnO₂ is thermodynamically feasible at the given pH for our enrichment cultures (LaRowe et al., 2021):



The mass balance of required O₂ supporting MnO₂ production is 1:2, which supports MnO₂ production for the 100 µM Mn²⁺ bottle cultures in both headspaces (**Figure 25; Figure 26**). However, the MnO₂ production in 95% CH₄/5% CO₂ for 50 and 150 µM Mn²⁺ additions are slightly greater than the measured O₂ tensions present in the bottle cultures (**Figure 25; Figure 26**).

4.4.5 *MnO_x* producing transfers from ~2200 meters are dominated by *Marinobacter* and *Idiomarina* spp

The microbial community in enrichment cultures given a range of NO₃⁻ and Mn²⁺ is dominated by species of *Marinobacter* after 60 days (**Figure 27**). *Marinobacter adhaerens* and *Marinobacter salarius* are the dominant species across all enrichment cultures. Species of *Idiomarina* and *Alcanivorax* are also enriched in bottle cultures after 60 days. Overall, 100 μM bottle culture additions of Mn²⁺ with 200 μM nitrate correlate with the highest abundance of *Marinobacter salarius*, regardless of gas headspace. However, there is no clear correlation between Mn²⁺ concentration and the microbial community diversity. The 150 μM Mn²⁺ condition with 95% CH₄-5% CO₂ headspace contained significantly lower cell counts overall and was excluded from further analysis (**Figure 27a**). The 95% CH₄/5% CO₂ gas headspace enrichment cultures show *Marinobacter salarius* is the dominant microorganism for a less diverse community in 100 μM Mn²⁺ versus 50 μM Mn²⁺. The 500 μM Mn²⁺ condition maintains a more diverse community (**Figure 27a**). The 100% He headspace bottles all contained a higher number of detected species of *Marinobacter* overall, particularly in the 500 μM Mn²⁺ condition versus the 500 μM Mn²⁺ 95% CH₄-5% CO₂ condition (**Figure 27b**). 100% helium gas headspace enrichment cultures show *Marinobacter salarius* is a dominant microorganism across all Mn²⁺ concentrations, as well as an uncultured species of *Marinobacter*; sp. NP-4. *Idiomarina* are also much more dominant in 100% He headspaces (**Figure 27b**). Sequencing of the microbial community from original seawater samples above, at, and below the redoxcline did not detect the presence of *Marinobacter* in the top 50 most abundant species.

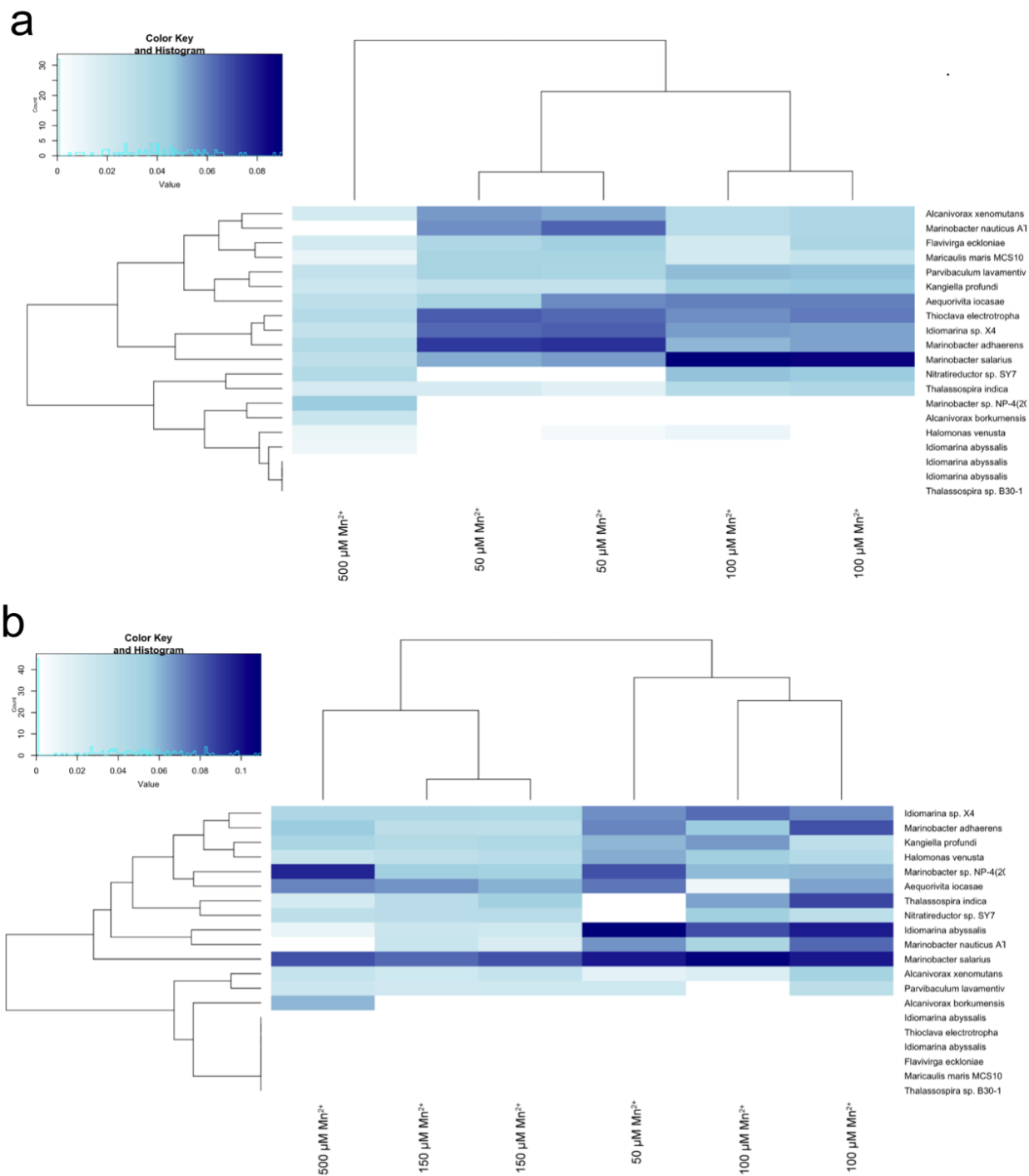


Figure 27. 16S rRNA phylogenetic trees constructed of enrichment cultures across both gas headspaces (95% CH₄/5% CO₂ versus 100% He) and all Mn²⁺ addition concentrations. (a) 95% CH₄/5% CO₂ gas headspace enrichment cultures show

***Marinobacter salarius* is the dominate microorganism. (b) 100% helium gas headspace enrichment cultures show *Marinobacter salarius* is a dominant microorganism across all Mn²⁺ concentrations, as well as an uncultured species, *Marinobacter* sp. NP-4. The top twenty most abundant species are shown for each gas headspace condition (a;b).**

4.4.6 *Nitrospirota* are present and transcriptionally active at ~2200 meters

Candidatus Manganitrophaceae of the *Nitrospirota* phylum was detected between ~2200 and ~2240 meters only (**Figure 27**). A metagenomic assembled genome was assembled for *Ca.* Manganitrophaceae from 2200 meters. *Ca.* Manganitrophaceae is transcriptionally active at ~2200 meters, including genes reported involved in chemolithoautotrophic manganese oxidation, PCC-1 (Yu and Leadbetter, 2020). Additional confirmed and proposed enzymes involved in manganese oxidation were also transcriptionally active at ~2200 meters belonging to other bacteria, including Methylococcales (**Table 3**). Putative manganese-oxidizing multicopper oxidase MnxG is additionally transcriptionally active on an assembled MAG at and above 2200 meters (Table X; 20-65 transcripts per million). GTDB taxonomy identifies the MnxG active MAG as phylum, Nitrospirota; family, JAADHI01.

Table 3. Transcription of Mn²⁺-oxidizing genes in Orca Basin. Protein-type and transcription per million (TPM) for each depth where proteins were detected with metatranscriptomics.

Protein	TPM	2201.5 meters	2201.46 meters	2201.46 meters	2193.96 meters	2193.96 meters	2193.96 meters	2192.48 meters	2192.48 meters	2192.48 meters
manganese-oxidizing multicopper oxidase MnxG [Nitrospira sp.]	4935	22	16	10	62	47	28	43	44	21
Putative beta-barrel porin-2, OmpL-like	--	--	--	--	164	164	164	--	--	--

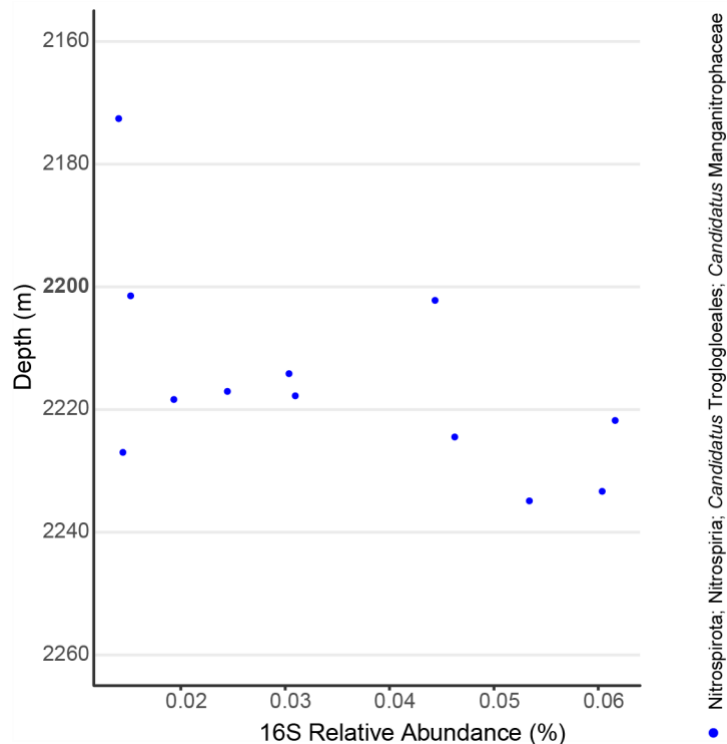


Figure 28. Relative abundance of Nitrospirota; Ca. Manganitrophaceae in Orca Basin. 16S rRNA relative abundance of species detected in Orca Basin depth. Data compiled from station P5 in Orca Basin.

4.5 Discussion

Redox conditions supporting detectable concentrations of biotic MnO_x formation may be constrained to extreme marine environments where there is abundant Mn²⁺ and a sharply stratified redoxcline (Glockzin et al., 2014). DHABs are globally widespread extreme environments in oceans containing a sharp redoxcline caused by tectonic activity exposing evaporitic deposits (Merlino et al., 2018; Varrella et al., 2020). The Orca Basin DHAB contains a ‘metabolic crumb’ indicating significant Mn²⁺ oxidation to insoluble MnO_x particles corresponding with oxygen below our limits of detection in the redoxcline (**Figure 21**). We focused on this MnO_x ‘crumb’ that occurs at ~2200 meters to identify the

microorganisms present, understand their associations with oxidized manganese, and see if we could observe MnO_x production in enrichment cultures *ex-situ*.

We detected a known chemolithoautotrophic Mn²⁺-oxidizing bacteria, *Candidatus* Manganitrophaceae of the Nitrospirota phylum, and found it to be transcriptionally active at ~2200 meters. *Candidatus* Manganitrophaceae is the first characterized chemolithoautotrophic manganese-oxidizing bacterium isolated from a laboratory water system (Yu and Leadbetter, 2020). To our knowledge, this is the first report of the detection of *Ca.* Manganitrophaceae in an environmental system, as well as transcriptional activity. We identified PCC-1 and MnxG, previously postulated to support Mn²⁺-oxidation by *Ca.* Manganitrophaceae, on our Orca Basin MAG and found them to be actively transcribed at ~2200 meters (Geszvain et al., 2012)(**Table 3**). PCC-1 is a porin-cytochrome *c* protein complex used in chemolithotroph oxidation of Fe²⁺ and is highly expressed by *Ca.* Manganitrophaceae during growth on Mn²⁺ (Yu and Leadbetter, 2020). We propose that this candidate species is actively contributing to Mn²⁺ oxidation in Orca basin at ~2200 meters, where Mn(IV) peaks.

16S sequencing of enrichment cultures supplied with Mn²⁺ and NO₃⁻ indicate the dominance of *Marinobacter* species. *Marinobacter* have previously been isolated from manganese nodule-containing basalt rocks and were shown to grow on plates supplemented with Mn²⁺ as the electron donor (Templeton et al., 2005). The supplemented nitrate in enrichment cultures is likely used as both the sole nitrogen source by *Marinobacter* as well as an additional electron acceptor supporting denitrification in the cells. *Marinobacter* are widely abundant in the Gulf of Mexico, particularly due to the significant amount of crude-oil in the water column from extractions and previous oil spills (Karthikeyan et al., 2020a).

Marinobacter species dominated the open ocean, sediments, and beach sands following the Deepwater horizon blowout, which impacted the entire North bend of the Gulf of Mexico (Kostka et al., 2011; Gutierrez et al., 2013; Yang et al., 2016).

My finding of cellular biofilm-LBB+ MnO_x associations at ~2200 meters support a biogenic origin of MnO_x. Marine Mn²⁺-oxidizing have been previously found to colonize the manganese nodules that are produced (Templeton et al., 2005). LBB+ MnO_x particles were found exclusively at the ~2200 m Mn(IV) peak in Orca Basin. Further, all detected LBB+ MnO_x particles contained SYBR-green stained cellular conglomerates also exclusive to the Mn(IV) peak in Orca Basin (**Figure 21**). Further examination of the LBB+ MnO_x particles and cell communities suggest that manganese containing particles are covered in a cellular biofilm, and that manganese particles are likely δ-MnO₂. Indeed, Mn²⁺-oxidizing bacteria colonizing ferromanganese crusts and oxides often form biofilm matrices (Stein et al., 2001; Templeton et al., 2005; Yli-Hemminki et al., 2014; Yu and Leadbetter, 2020).

Anaerobic MnO_x formation by bacteria has been postulated for oxygen-depleted marine systems where quantities of MnO_x are significant, suggesting nitrate as an oxidant (Murray et al., 1995; Aller et al., 1998; Robbins et al., 2023). Yet, any mechanism of marine bacteria capable of proposed anaerobic manganese oxidation remain unknown (Canfield et al., 2005). However, the MnO_x production occurring in transfer cultures from ~2200 meters, and supplied with Mn²⁺ and NO₃⁻, can be explained stoichiometrically by measured low sub-oxic conditions (**Figure 25, 26, 27, Eq. 2**). MnO_x production did occur in 150 μM Mn²⁺ bottle conditions beyond what the measured O₂ could stoichiometrically support, but MnO_x carry-over during 1:10 dilution transfers may account for this discrepancy. It was

previously reported that Mn^{2+} oxidation occurs at oxygen tensions as low as 5 μM (Tebo, 1991; Clement et al., 2009). In transfer cultures from ~2200 meters of the Orca Basin, manganese oxidation occurs at oxygen tensions as low as 0.5 μM ; 10x lower than previously reported. I propose that Orca Basin microbes, including detected *Marinobacter* species from transfer cultures, use oxygen at 0.5 μM to 25 nM levels to oxidize Mn^{2+} to MnO_2 . This measured production of MnO_x in low-suboxic enrichment cultures and detection of known Mn^{2+} -oxidizing bacteria collectively suggest a low-suboxic (Berg et al., 2022) biological formation mechanism for manganese oxides by denitrifying *Marinobacter* species in Orca Basin. However, Mn^{2+} oxidation has not been identified as an energy-generating process in *Marinobacter*, who may be effective manganese oxidizers via iron siderophores catalyzing sequestration of Mn^{2+} for oxidation (Templeton et al., 2005; Amin et al., 2009; Homann et al., 2009; Geszvain et al., 2012; Wang et al., 2012).

4.6 Conclusion

Sedimentary manganese oxide (MnO_x) enrichments are a potential signature for early Earth oxygenation and biological aerobic respiration (Nealson, 2006; Johnson et al., 2013; Robbins et al., 2023). We found evidence for a microbial origin of $\delta\text{-MnO}_2$ from Mn^{2+} in Orca Basin where oxygen is below our limits of detection, nitrate is being depleted, and Mn(IV) peaks. We detected Mn^{2+} -oxidation occurring at O_2 between 0.5 μM to 25 nM; 10x lower than the suboxic (~5 μM) levels of oxygen previously reported for the Black Sea (Clement et al., 2009). *Marinobacter* species can oxidize Mn^{2+} in transfer cultures, but the NO_3^- in sterile seawater media may have influenced their dominance *ex-situ*. Our finding of novel *Ca. Manganothraceae* directly sequenced from the ~2200 m Mn(IV) peak in

Orca Basin suggests that several organisms employing diverse metabolic lifestyles are contributing to manganese oxide formation and manganese cycling.

Further, we suggest that biologic MnO₂ is formed around the cells producing the mineral. Biotic MnO_x is highly insoluble and usually physically associated with Mn²⁺-oxidizing cells (Hansel, 2017). Insoluble, cell-associated biotic MnO_x has also been found to be morphologically distinct from abiotically formed Mn(IV) structures, which may make these minerals a potential biosignature for Mn²⁺-oxidizing bacteria (Robbins et al., 2023). Microbial community composition and diversity are different between manganese oxide nodules and the surrounding sediment at the Clarion-Clipperton Fracture Zone (CCFZ) (Mogollón et al., 2016; Cho et al., 2018). Bacteria capable of growing on media enriched with Mn²⁺ as the sole electron donor under suboxic plate conditions have been identified directly above the anoxic brine of Orca Basin (Van Cappellen et al., 1998). However, there has been no comprehensive understanding in Orca Basin of the microbial community on MnO_x particles nor any genomic sequencing for microbes physically attached to MnO_x formed *in-situ*. Future work focuses on metagenomic sequencing of cells physically attached to LBB+ MnO_x particles and will provide a comprehensive method to isolate and sequence cells that are physically attached to MnO_x particles providing a comprehensive understanding of the microbial community colonizing MnO_x particles *in-situ* at Orca basin.

CHAPTER 5. CONCLUSIONS AND FUTURE DIRECTIONS

5.1 Novel bacteria contribute to nitrogen loss in anoxic marine systems

In this dissertation, I sought to understand the contributions of marine nitrogen loss by microbes that use diverse electron donors in anoxic marine systems. Anoxic marine systems are areas of intense biological nitrogen loss (DeVries et al. 2013; Merlino et al. 2018). Some anoxic marine systems are extremely well studied, such as the ETNP ODZ, but the identity of the microbes that catalyze nitrogen loss in ODZs are still being elucidated. Understanding mechanisms of nitrogen loss are essential to constrain greenhouse gas fluxes in anoxic marine systems, which are expanding under climate change. Further, the oxyclines in anoxic marine systems are serve as intriguing natural systems to study microbial evolution in extant ancestors to primordial ocean microbes.

I identified three novel species of bacteria that are likely contributing to nitrogen loss in the ETNP ODZ and Orca Basin DHAB. The ETNP ODZ contains high transcription of genes in the same family as the nitric oxide dismutase (*nod*) gene from *Methylomirabilota* has been reported in the anoxic core. We sought to identify the microbe(s) responsible for the abundant transcription of nitric oxide dismutase (*nod*) in the ETNP ODZ. We found that the most abundantly transcribed *nod* genes in the Eastern Tropical North Pacific ODZ belong to a new order (UBA11136) of Alphaproteobacteria. Molecular oxygen for aerobic respiration may originate from nitric oxide dismutation via cryptic oxygen cycling. Molecular oxygen for aerobic respiration may originate from nitric oxide dismutation via cryptic oxygen cycling. Intriguingly, UBA11136 constitutes a deep branching clade of Alphaproteobacteria that has recently been implicated in a new model for eukaryogenesis

(Esposti 2023) It is now hypothesized that eukaryogenesis originated in the primordial ocean with a marine Alphaproteobacteria whose lineage is remanent in modern-day oxyclines (Geiger, Sanchez-Flores, Padilla-Gomez, and Degli Esposti 2023; Cevallos and Degli Esposti 2022).

5.2 Methanol, formaldehyde and formate utilization in the ETNP ODZ

We infer from metagenomics and transcriptomics that UBA11136 is an aerobic bacteria using formaldehyde and formate as a source of electrons, with additional electrons possibly from sulfide oxidation in chapter 2. Our results implicate Alphaproteobacteria order UBA11136 as a significant player in marine nitrogen loss and highlight their potential in one-carbon, nitrogen, and sulfur metabolism in ODZs. In chapter 3, we found that under anaerobic cultures with a methane headspace as the sole carbon source and nitrate as the sole nitrogen source, *M. pacificus* spp. nov. expresses lanthanide-dependent pyrroloquinoline quinone alcohol dehydrogenase, ExaF, and formate dehydrogenase, Fdh, as well as the full suite of proteins for denitrification. We postulate that *M. pacificus* is oxidizing methanol or ethanol, formed in the headspace by an unknown mechanism, to formate and using the electrons from formate to catalyze denitrification. Our results provide a new *Marinobacter* species that may be relevant for ODZs and elucidate a mechanism for anaerobic 1-carbon oxidation coupled to denitrification for the *Marinobacter* species.

Our results from Chapter 2 and 3 suggest methanol, ethanol, and formaldehyde in the ETNP ODZ is essential to providing formate used in denitrification. Oxidized formate provides electrons driving nitrate reduction and subsequent nitrogen loss (Yamamoto and

Ishimoto, 1977). Methanol is the most likely potential 1-carbon substrate that could be abundant in the ETNP ODZ produced by phytoplankton (Mincer and Aicher, 2016). 1-carbon oxidation of methanol and formaldehyde to formate-driven denitrification may be more abundant in the ETNP ODZ than previously considered.

5.3 Manganese oxidation in Orca Basin

Manganese cycling bacteria have previously been detected above and below an Mn(IV) oxide (MnO_x) peak (~2200 meters) in the Orca basin DHAB along the Texas-Louisiana continental slope. However, biotic MnO_x occurs at O₂ < 1 μM (presumed anoxia), and nitrate depletion (~22 μM to ~3 μM), which led us to explore potential anaerobic manganese oxidation occurring with nitrate reduction in Chapter 4. In enrichment cultures from ~2200 meters, we found that microbial cells consume nitrate and produce δ-MnO_x covered in biofilms. *Marinobacter* species dominated enrichment cultures amended with nitrate and Mn²⁺ over ~40 days of dark incubation from ~2200 meters in Orca Basin. We further assembled a transcriptionally active MAG of novel chemolithotroph Mn²⁺-oxidizer, *Ca. Manganitrophaceae* at ~2200 meters. Our active MAG transcribes PCC-1, which is a highly transcribed porin cytochrome *c* during growth of *Ca. Manganitrophaceae* on Mn²⁺ (Yu and Leadbetter, 2020). We surmise that multiple species of anaerobic, nitrate-utilizing bacteria are likely contributing to manganese oxidation at ~2200 meters in Orca Basin through several mechanisms.

5.4 Low-suboxic seawater amended with nitrate selects for *Marinobacter* spp.

We isolated a novel *Marinobacter* species and detected several other species from enrichment cultures in the ETNP ODZ and Orca Basin DHAB in Chapter 3 and 4. Both

enrichment cultures were amended with relatively high quantities of nitrate compared to *in-situ* values. Oxygen conditions in bottles were maintained between 1 μM to 50 nM O_2 . The “opportunotroph” lifestyle of *Marinobacter*, which exclusively are found in saline water, likely primes this phylum to dominant enrichment cultures given nitrate (Handley and Lloyd 2013b). *Marinobacter* contain large genomes, can build all amino acids, and grow both anaerobically and aerobically. The anaerobic mechanism of 1-carbon oxidation by *Marinobacter* had not yet been described. We postulate that methanol, ethanol, or formaldehyde is oxidized to formate by lanthanide and PQQ-dependent ExaF protein found in methylotrophs. Formate is then oxidized to yield electrons that are shuttled to catalyze denitrification in *Marinobacter pacificus*. Further, *Marinobacter* contain several outer-cell mechanisms for detoxification and are well-described iron chelators (Amin et al., 2009). The abundant *Marinobacter* species detected in Orca Basin enrichment Mn^{2+} amended cultures in Chapter 4 may use a mechanisms similar to their iron-detoxification siderophores to mitigate toxic levels of manganese (Hansel, 2017).

5.5 Future directions

The lack of cultured representatives of this novel Alphaproteobacterial clade prevents us from comparing our results to known biochemical functions or metabolisms, in Chapter 2. Future work in isolating and characterizing UBA11136 will shed light on its function in the modern-day ETNP ODZ, including potential oxygen generation from nitric oxide dismutation.

Future work with laser-microdissection metagenomic sequencing in collaboration with Lawrence Livermore lab will provide a comprehensive method to isolate cells that are

physically attached to MnO_x particles. Bacteria capable of growing on media enriched with Mn²⁺ as the sole electron donor under suboxic plate conditions have been identified directly above the anoxic brine of Orca Basin (Van Cappellen et al., 1998). However, there has been no comprehensive understanding in Orca Basin of the microbial community on MnO_x particles nor any genomic sequencing for microbes physically attached to MnO_x formed *in-situ*. Microbial community composition and diversity are distinctly different between manganese oxide nodules and the surrounding sediment at the Clarion-Clipperton Fracture Zone (CCFZ) (Cho et al., 2018).

REFERENCES

- Acinas, S.G., Ferrera, I., Sarmiento, H., Diez-Vives, C., Forn, I., Ruiz-Gonzalez, C. et al. (2015) Validation of a new catalysed reporter deposition-fluorescence in situ hybridization probe for the accurate quantification of marine Bacteroidetes populations. *Environ Microbiol* **17**: 3557-3569.
- Addy, S.K., and Behrens, E.W. (1980) Time of accumulation of hypersaline anoxic brine in Orca basin (Gulf of Mexico). *Marine Geology* **37**: 241-252.
- Aldunate, M., Henríquez-Castillo, C., Ji, Q., Lueders-Dumont, J., Mulholland, M.R., Ward, B.B. et al. (2020) Nitrogen assimilation in picocyanobacteria inhabiting the oxygen-deficient waters of the eastern tropical North and South Pacific. *Limnology and Oceanography* **65**: 437-453.
- Aller, R.C., Hall, P.O.J., Rude, P.D., and Aller, J.Y. (1998) Biogeochemical heterogeneity and suboxic diagenesis in hemipelagic sediments of the Panama Basin. *Deep Sea Research Part I: Oceanographic Research Papers* **45**: 133-165.
- Alonge, M., Lebeigle, L., Kirsche, M., Jenike, K., Ou, S., Aganezov, S. et al. (2022) Automated assembly scaffolding using RagTag elevates a new tomato system for high-throughput genome editing. *Genome Biology* **23**: 258.
- Amin, S.A., Green, D.H., Hart, M.C., Küpper, F.C., Sunda, W.G., and Carrano, C.J. (2009) Photolysis of iron–siderophore chelates promotes bacterial–algal mutualism. *Proceedings of the National Academy of Sciences* **106**: 17071-17076.
- Amin, S.A., Green, D.H., Gärdes, A., Romano, A., Trimble, L., and Carrano, C.J. (2012) Siderophore-mediated iron uptake in two clades of *Marinobacter* spp. associated with phytoplankton: the role of light. *BioMetals* **25**: 181-192.
- Anstett, J., Plominsky, A.M., DeLong, E.F., Kiesser, A., Jürgens, K., Morgan-Lang, C. et al. (2023) A compendium of bacterial and archaeal single-cell amplified genomes from oxygen deficient marine waters. *Scientific Data* **10**: 332.
- Arkin, A.P., Cottingham, R.W., Henry, C.S., Harris, N.L., Stevens, R.L., Maslov, S. et al. (2018) KBase: The United States Department of Energy Systems Biology Knowledgebase. *Nature Biotechnology* **36**: 566-569.
- Babbin, A.R., Keil, R.G., Devol, A.H., and Ward, B.B. (2014) Organic matter stoichiometry, flux, and oxygen control nitrogen loss in the ocean. *Science* **344**: 406-408.
- Babbin, A.R., Bianchi, D., Jayakumar, A., and Ward, B.B. (2015) Rapid nitrous oxide cycling in the suboxic ocean. *Science* **348**: 1127-1129.
- Backer, H., and Schoell, M. (1972) New Deeps with Brines and Metalliferous Sediments in the Red Sea. *Nature Physical Science* **240**: 153-158.

Berg, J.S., Ahmerkamp, S., Pjevac, P., Hausmann, B., Milucka, J., and Kuypers, M.M.M. (2022) How low can they go? Aerobic respiration by microorganisms under apparent anoxia. *FEMS Microbiology Reviews* **46**.

Bertagnolli, A.D., and Stewart, F.J. (2018) Microbial niches in marine oxygen minimum zones. *Nature Reviews Microbiology* **16**: 723-729.

Bertagnolli, A.D., Konstantinidis, K.T., and Stewart, F.J. (2020) Non-denitrifier nitrous oxide reductases dominate marine biomes. *Environ Microbiol Rep* **12**: 681-692.

Bhattarai, H.R., Wanek, W., Siljanen, H.M.P., Ronkainen, J.G., Liimatainen, M., Hu, Y. et al. (2021) Denitrification is the major nitrous acid production pathway in boreal agricultural soils. *Communications Earth & Environment* **2**: 54.

Bianchi, D., Weber, T.S., Kiko, R., and Deutsch, C. (2018) Global niche of marine anaerobic metabolisms expanded by particle microenvironments. *Nature Geoscience* **11**: 263-268.

Blöthe, M., Wegorzewski, A., Müller, C., Simon, F., Kuhn, T., and Schippers, A. (2015) Manganese-cycling microbial communities inside deep-sea manganese nodules. *Environmental science & technology* **49**: 7692-7700.

Bodenmiller, D.M., and Spiro, S. (2006) The *yjeB* (*nsrR*) gene of *Escherichia coli* encodes a nitric oxide-sensitive transcriptional regulator. *J Bacteriol* **188**: 874-881.

Bolster, K.M., Heller, M.I., Mulholland, M.R., and Moffett, J.W. (2022) Iron and manganese accumulation within the Eastern Tropical North Pacific oxygen deficient zone. *Geochimica et Cosmochimica Acta* **334**: 259-272.

Bonin, P., and Raymond, N. (1990) Effects of oxygen on denitrification in marine sediments. *Hydrobiologia* **207**: 115-122.

Boratyn, G.M., Thierry-Mieg, J., Thierry-Mieg, D., Busby, B., and Madden, T.L. (2019) Magic-BLAST, an accurate RNA-seq aligner for long and short reads. *BMC Bioinf* **20**: 405.

Borin, S., Mapelli, F., Rolli, E., Song, B., Tobias, C., Schmid, M.C. et al. (2013) Anammox bacterial populations in deep marine hypersaline gradient systems. *Extremophiles* **17**: 289-299.

Botz, R., Schmidt, M., Wehner, H., Hufnagel, H., and Stoffers, P. (2007) Organic-rich sediments in brine-filled Shaban-and Kebrit deeps, northern Red Sea. *Chemical Geology* **244**: 520-553.

Bourbonnais, A., Chang, B.X., Sonnerup, R.E., Doney, S.C., and Altabet, M.A. (2023) Marine N₂O cycling from high spatial resolution concentration, stable isotopic and isotopomer measurements along a meridional transect in the eastern Pacific Ocean. *Frontiers in Marine Science* **10**.

- Bowman, J.S., and Ducklow, H.W. (2015) Microbial Communities Can Be Described by Metabolic Structure: A General Framework and Application to a Seasonally Variable, Depth-Stratified Microbial Community from the Coastal West Antarctic Peninsula. *PLOS ONE* **10**: e0135868.
- Bracco, A., Paris, C.B., Esbaugh, A.J., Frasier, K., Joye, S.B., Liu, G. et al. (2020) Transport, Fate and Impacts of the Deep Plume of Petroleum Hydrocarbons Formed During the Macondo Blowout. *Frontiers in Marine Science* **7**.
- Brettin, T., Davis, J.J., Disz, T., Edwards, R.A., Gerdes, S., Olsen, G.J. et al. (2015) RASTtk: a modular and extensible implementation of the RAST algorithm for building custom annotation pipelines and annotating batches of genomes. *Sci Rep* **5**: 8365.
- Bristow, L.A., Dalsgaard, T., Tiano, L., Mills, D.B., Bertagnolli, A.D., Wright, J.J. et al. (2016) Ammonium and nitrite oxidation at nanomolar oxygen concentrations in oxygen minimum zone waters. *Proc Natl Acad Sci U S A* **113**: 10601-10606.
- Bristow, L.A., Callbeck, C.M., Larsen, M., Altabet, M.A., Dekaezemacker, J., Forth, M. et al. (2017) N₂ production rates limited by nitrite availability in the Bay of Bengal oxygen minimum zone. *Nature Geoscience* **10**: 24-29.
- Busecke, J.J.M., Resplandy, L., Ditkovsky, S.J., and John, J.G. (2022) Diverging Fates of the Pacific Ocean Oxygen Minimum Zone and Its Core in a Warming World. *AGU Advances* **3**: e2021AV000470.
- Cabello-Yeves, P.J., Callieri, C., Picazo, A., Mehrshad, M., Haro-Moreno, J.M., Roda-Garcia, J.J. et al. (2021) The microbiome of the Black Sea water column analyzed by shotgun and genome centric metagenomics. *Environ Microbiome* **16**: 5.
- Cai, Y., Yang, K., Qiu, C., Bi, Y., Tian, B., and Bi, X. (2023) A Review of Manganese-Oxidizing Bacteria (MnOB): Applications, Future Concerns, and Challenges. *Int J Environ Res Public Health* **20**.
- Callbeck, C.M., Canfield, D.E., Kuypers, M.M.M., Yilmaz, P., Lavik, G., Thamdrup, B. et al. (2021) Sulfur cycling in oceanic oxygen minimum zones. *Limnol Oceanogr* **66**: 2360-2392.
- Canfield, D.E., and Kraft, B. (2022) The ‘oxygen’ in oxygen minimum zones. *Environmental Microbiology* **24**: 5332-5344.
- Canfield, D.E., Erik, K., and Bo, T. (2005) The Iron and Manganese Cycles. In *Advances in Marine Biology*. Canfield, D.E., Kristensen, E., and Thamdrup, B. (eds): Academic Press, pp. 269-312.
- Cavazos, A.R., and Glass, J.B. (2020) Simul-staining manganese oxides and microbial cells. *Limnology and Oceanography: Methods* **18**: 362-373.

- Cepeda-Morales, J., Beier, E., Gaxiola-Castro, G., Lavín, M., and Godínez, V. (2009) Effect of the oxygen minimum zone on the second chlorophyll maximum. *Ciencias Marinas* **35**: 389-403.
- Cevallos, M.A., and Degli Esposti, M. (2022) New Alphaproteobacteria thrive in the depths of the ocean with oxygen gradient. *Microorganisms* **10**: 455.
- Chaumeil, P.A., Mussig, A.J., Hugenholtz, P., and Parks, D.H. (2022) GTDB-Tk v2: memory friendly classification with the genome taxonomy database. *Bioinformatics* **38**: 5315-5316.
- Chavez, F.P., and Messié, M. (2009) A comparison of Eastern Boundary Upwelling Ecosystems. *Progress in Oceanography* **83**: 80-96.
- Chen, J.H., Yu, L.J., Boussac, A., Wang-Otomo, Z.Y., Kuang, T., and Shen, J.R. (2019) Properties and structure of a low-potential, penta-heme cytochrome c(552) from a thermophilic purple sulfur photosynthetic bacterium *Thermochromatium tepidum*. *Photosynth Res* **139**: 281-293.
- Chen, K.H., Wu, H.H., Ke, S.F., Rao, Y.T., Tu, C.M., Chen, Y.P. et al. (2012) Bacteriohemerythrin bolsters the activity of the particulate methane monooxygenase (pMMO) in *Methylococcus capsulatus* (Bath). *J Inorg Biochem* **111**: 10-17.
- Cheng, X., McCreary, J.P., Qiu, B., Qi, Y., Du, Y., and Chen, X. (2018) Dynamics of Eddy Generation in the Central Bay of Bengal. *Journal of Geophysical Research: Oceans* **123**: 6861-6875.
- Cho, H., Kim, K.-H., Son, S.K., and Hyun, J.-H. (2018) Fine-scale Microbial Communities Associated with Manganese Nodules in Deep-sea Sediment of the Korea Deep Ocean Study Area in the Northeast Equatorial Pacific. *Ocean Science Journal* **53**: 337-353.
- Chronopoulou, P.-M., Shelley, F., Pritchard, W.J., Maanoja, S.T., and Trimmer, M. (2017) Origin and fate of methane in the Eastern Tropical North Pacific oxygen minimum zone. *The ISME Journal* **11**: 1386-1399.
- Cita, M.B. (2006) Exhumation of Messinian evaporites in the deep-sea and creation of deep anoxic brine-filled collapsed basins. *Sedimentary Geology* **188**: 357-378.
- Clement, B.G., Luther, G.W., and Tebo, B.M. (2009) Rapid, oxygen-dependent microbial Mn(II) oxidation kinetics at sub-micromolar oxygen concentrations in the Black Sea suboxic zone. *Geochimica et Cosmochimica Acta* **73**: 1878-1889.
- Cline, J.D., and Richards, F.A. (1972) Oxygen deficient conditions and nitrate reduction in the Eastern Tropical North Pacific Ocean. *Limnology and Oceanography* **17**: 885-900.

- Cramm, R., Pohlmann, A., and Friedrich, B. (1999) Purification and characterization of the single-component nitric oxide reductase from *Ralstonia eutropha* H16. *FEBS letters* **460**: 6-10.
- D'Asaro, E., Altabet, M., Kumar, N.S., and Ravichandran, M. (2020) Structure of the Bay of Bengal oxygen deficient zone. *Deep Sea Research Part II: Topical Studies in Oceanography* **179**: 104650.
- Dalsgaard, T., Stewart, F.J., Thamdrup, B., De Brabandere, L., Revsbech, N.P., Ulloa, O. et al. (2014) Oxygen at nanomolar levels reversibly suppresses process rates and gene expression in anammox and denitrification in the oxygen minimum zone off northern Chile. *mBio* **5**: e01966.
- Dellwig, O., Schnetger, B., Brumsack, H.-J., Grossart, H.-P., and Umlauf, L. (2012) Dissolved reactive manganese at pelagic redoxclines (part II): Hydrodynamic conditions for accumulation. *Journal of Marine Systems* **90**: 31-41.
- Deutsch, C., Brix, H., Ito, T., Frenzel, H., and Thompson, L. (2011) Climate-Forced Variability of Ocean Hypoxia. *Science* **333**: 336-339.
- DeVries, T., Deutsch, C., Rafter, P.A., and Primeau, F. (2013) Marine denitrification rates determined from a global 3-D inverse model. *Biogeosciences* **10**: 2481-2496.
- Diercks, A., Ziervogel, K., Sibert, R., Joye, S.B., Asper, V., and Montoya, J.P. (2019) Vertical marine snow distribution in the stratified, hypersaline, and anoxic Orca Basin (Gulf of Mexico). *Elementa: Science of the Anthropocene* **7**.
- Duteil, O., Frenger, I., and Getzlaff, J. (2021) The riddle of eastern tropical Pacific Ocean oxygen levels: the role of the supply by intermediate-depth waters. *Ocean Sci* **17**: 1489-1507.
- Eddebbar, Y.A., Whitt, D.B., Verdy, A., Mazloff, M.R., Subramanian, A.C., and Long, M.C. (2024) Eddy-Mediated Turbulent Mixing of Oxygen in the Equatorial Pacific. *Journal of Geophysical Research: Oceans* **129**: e2023JC020588.
- Eddebbar, Y.A., Subramanian, A.C., Whitt, D.B., Long, M.C., Verdy, A., Mazloff, M.R., and Merrifield, M.A. (2021) Seasonal Modulation of Dissolved Oxygen in the Equatorial Pacific by Tropical Instability Vortices. *Journal of Geophysical Research: Oceans* **126**: e2021JC017567.
- Ehrenreich, P., Behrends, A., Harder, J., and Widdel, F. (2000) Anaerobic oxidation of alkanes by newly isolated denitrifying bacteria. *Arch Microbiol* **173**.
- Elbon, C.E., Stewart, F.J., and Glass, J.B. (2024) Novel Alphaproteobacteria transcribe genes for nitric oxide transformation at high levels in a marine oxygen-deficient zone. *Applied and Environmental Microbiology* **90**: e02099-02023.

- Espinoza-Morriberon, D., Echevin, V., and Colas, F. (2018) Interannual and decadal variability of the primary productivity and Oxygen Minimum Zone in the Peruvian Upwelling System. In.
- Esposti, M.D. (2023) Eukaryotes inherited inositol lipids from bacteria: implications for the models of eukaryogenesis. *FEBS Letters* **597**: 2484-2496.
- Ettwig, K.F., Speth, D.R., Reimann, J., Wu, M.L., Jetten, M.S., and Keltjens, J.T. (2012) Bacterial oxygen production in the dark. *Frontiers in microbiology* **3**: 273.
- Ettwig, K.F., Butler, M.K., Le Paslier, D., Pelletier, E., Mangenot, S., Kuypers, M.M.M. et al. (2010) Nitrite-driven anaerobic methane oxidation by oxygenic bacteria. *Nature* **464**: 543-548.
- Evans, N., Tichota, J., Moffett, J.W., and Devol, A.H. (2023a) Prolific nitrite reoxidation across the Eastern Tropical North Pacific Ocean. *Limnology and Oceanography* **68**: 1719-1733.
- Evans, N., Tichota, J., Ruef, W., Moffett, J., and Devol, A. (2023b) Rapid Expansion of Fixed Nitrogen Deficit in the Eastern Pacific Ocean Revealed by 50-Year Time Series. *Global Biogeochemical Cycles* **37**: e2022GB007575.
- Evans, N., Boles, E., Kwiecinski, J.V., Mullen, S., Wolf, M., Devol, A.H. et al. (2020) The role of water masses in shaping the distribution of redox active compounds in the Eastern Tropical North Pacific oxygen deficient zone and influencing low oxygen concentrations in the eastern Pacific Ocean. *Limnology and Oceanography* **65**: 1688-1705.
- Flintrop, C.M., Rogge, A., Miksch, S., Thiele, S., Waite, A.M., and Iversen, M.H. (2018) Embedding and slicing of intact in situ collected marine snow. *Limnology and Oceanography: Methods* **16**: 339-355.
- Font, E., Swart, S., Bruss, G., Sheehan, P.M.F., Heywood, K.J., and Queste, B.Y. (2024) Ventilation of the Arabian Sea Oxygen Minimum Zone by Persian Gulf Water. *Journal of Geophysical Research: Oceans* **129**: e2023JC020668.
- Forte, E., Urbani, A., Saraste, M., Sarti, P., Brunori, M., and Giuffrè, A. (2001) The cytochrome cbb3 from *Pseudomonas stutzeri* displays nitric oxide reductase activity. *Eur J Biochem* **268**: 6486-6491.
- Frey, C., Bange, H.W., Achterberg, E.P., Jayakumar, A., Löscher, C.R., Arévalo-Martínez, D.L. et al. (2020) Regulation of nitrous oxide production in low-oxygen waters off the coast of Peru. *Biogeosciences* **17**: 2263-2287.
- Fuchsman, C.A., Devol, A.H., Saunders, J.K., McKay, C., and Rocap, G. (2017) Niche Partitioning of the N Cycling Microbial Community of an Offshore Oxygen Deficient Zone. *Frontiers in Microbiology* **8**.

- Fuchsman, C.A., Palevsky, H.I., Widner, B., Duffy, M., Carlson, M.C., Neibauer, J.A. et al. (2019) Cyanobacteria and cyanophage contributions to carbon and nitrogen cycling in an oligotrophic oxygen-deficient zone. *The ISME Journal* **13**: 2714-2726.
- Fujiwara, T., and Fukumori, Y. (1996) Cytochrome cb-type nitric oxide reductase with cytochrome c oxidase activity from *Paracoccus denitrificans* ATCC 35512. *Journal of bacteriology* **178**: 1866-1871.
- Ganesh, S., Parris, D.J., DeLong, E.F., and Stewart, F.J. (2014) Metagenomic analysis of size-fractionated picoplankton in a marine oxygen minimum zone. *ISME J* **8**: 187-211.
- Ganesh, S., Bristow, L.A., Larsen, M., Sarode, N., Thamdrup, B., and Stewart, F.J. (2015) Size-fraction partitioning of community gene transcription and nitrogen metabolism in a marine oxygen minimum zone. *The ISME Journal* **9**: 2682-2696.
- Garcia-Robledo, E., Padilla, C.C., Aldunate, M., Stewart, F.J., Ulloa, O., Paulmier, A. et al. (2017) Cryptic oxygen cycling in anoxic marine zones. *Proceedings of the National Academy of Sciences* **114**: 8319-8324.
- García-Robledo, E., Corzo, A., and Papaspyrou, S. (2014) A fast and direct spectrophotometric method for the sequential determination of nitrate and nitrite at low concentrations in small volumes. *Marine Chemistry* **162**: 30-36.
- Gaye, B., Nagel, B., Dähnke, K., Rixen, T., and Emeis, K.-C. (2013) Evidence of parallel denitrification and nitrite oxidation in the ODZ of the Arabian Sea from paired stable isotopes of nitrate and nitrite. *Global Biogeochemical Cycles* **27**: 1059-1071.
- Gazitúa, M.C., Vik, D.R., Roux, S., Gregory, A.C., Bolduc, B., Widner, B. et al. (2021) Potential virus-mediated nitrogen cycling in oxygen-depleted oceanic waters. *The ISME Journal* **15**: 981-998.
- Geiger, O., Sanchez-Flores, A., Padilla-Gomez, J., and Esposti, M.D. (2023) Multiple approaches of cellular metabolism define the bacterial ancestry of mitochondria. *Sci Adv* **9**: eadh0066.
- Geszvain, K., Butterfield, C., Davis, R.E., Madison, A.S., Lee, S.W., Parker, D.L. et al. (2012) The molecular biogeochemistry of manganese(II) oxidation. *Biochem Soc Trans* **40**: 1244-1248.
- Glass, J.B., Elbon, C.E., and Williams, L.D. (2023) Something old, something new, something borrowed, something blue: the anaerobic microbial ancestry of aerobic respiration. *Trends in Microbiology* **31**: 135-141.
- Glass, J.B., Kretz, C.B., Ganesh, S., Ranjan, P., Seston, S.L., Buck, K.N. et al. (2015) Meta-omic signatures of microbial metal and nitrogen cycling in marine oxygen minimum zones. *Frontiers in Microbiology* **6**: 998.

- Glockzin, M., Pollehne, F., and Dellwig, O. (2014) Stationary sinking velocity of authigenic manganese oxides at pelagic redoxclines. *Marine Chemistry* **160**: 67-74.
- Goericke, R., Olson, R., and Shalapyonok, A. (2000) A novel niche for *Prochlorococcus* sp. in low-light suboxic environments in the Arabian Sea and the Eastern Tropical North Pacific. *Deep Sea Research Part I: Oceanographic Research Papers* **47**: 1183-1205.
- Gómez Alvarez, E., Amedro, D., Afif, C., Gligorovski, S., Schoemaeker, C., Fittschen, C. et al. (2013) Unexpectedly high indoor hydroxyl radical concentrations associated with nitrous acid. *Proceedings of the National Academy of Sciences* **110**: 13294-13299.
- Good, N.M., Moore, R.S., Suriano, C.J., and Martinez-Gomez, N.C. (2019) Contrasting in vitro and in vivo methanol oxidation activities of lanthanide-dependent alcohol dehydrogenases XoxF1 and ExaF from *Methylobacterium extorquens* AM1. *Sci Rep* **9**: 4248.
- Good, N.M., Vu, H.N., Suriano, C.J., Subuyuj, G.A., Skovran, E., and Martinez-Gomez, N.C. (2016) Pyrroloquinoline Quinone Ethanol Dehydrogenase in *Methylobacterium extorquens* AM1 Extends Lanthanide-Dependent Metabolism to Multicarbon Substrates. *Journal of Bacteriology* **198**: 3109-3118.
- Green, E.J., and Carritt, D.E. (1967) Oxygen Solubility in Sea Water: Thermodynamic Influence of Sea Salt. *Science* **157**: 191-193.
- Gutierrez, T., Singleton, D.R., Berry, D., Yang, T., Aitken, M.D., and Teske, A. (2013) Hydrocarbon-degrading bacteria enriched by the Deepwater Horizon oil spill identified by cultivation and DNA-SIP. *The ISME Journal* **7**: 2091-2104.
- Hach, P.F., Marchant, H.K., Krupke, A., Riedel, T., Meier, D.V., Lavik, G. et al. (2020) Rapid microbial diversification of dissolved organic matter in oceanic surface waters leads to carbon sequestration. *Scientific Reports* **10**: 13025.
- Handley, K., and Lloyd, J. (2013) Biogeochemical implications of the ubiquitous colonization of marine habitats and redox gradients by *Marinobacter* species. *Frontiers in Microbiology* **4**.
- Hansel, C.M. (2017) Chapter Two - Manganese in Marine Microbiology. In *Advances in Microbial Physiology*. Poole, R.K. (ed): Academic Press, pp. 37-83.
- Hansen, H.P., and Koroleff, F. (1999) Determination of nutrients. In *Methods of Seawater Analysis*, pp. 159-228.
- Helm, K.P., Bindoff, N.L., and Church, J.A. (2011) Observed decreases in oxygen content of the global ocean. *Geophysical Research Letters* **38**.
- Henríquez-Castillo, C., Plominsky, A.M., Ramírez-Flandes, S., Bertagnolli, A.D., Stewart, F.J., and Ulloa, O. (2022) Metaomics unveils the contribution of *Alteromonas*

bacteria to carbon cycling in marine oxygen minimum zones. *Frontiers in Marine Science* **9**.

Henson, M.W., Lanclos, V.C., Pitre, D.M., Weckhorst, J.L., Lucchesi, A.M., Cheng, C. et al. (2020) Expanding the diversity of bacterioplankton isolates and modeling isolation efficacy with large-scale dilution-to-extinction cultivation. *Appl Environ Microbiol* **86**: e00943-00920.

Hernandez, D., and Rowe, J.J. (1987) Oxygen regulation of nitrate uptake in denitrifying *Pseudomonas aeruginosa*. *Appl Environ Microbiol* **53**: 745-750.

Hoang, D.T., Chernomor, O., Haeseler, A.v., Minh, B.Q., and Vinh, L.S. (2017) UFBoot2: improving the ultrafast bootstrap approximation. *Mol Biol Evol* **35**: 518–522.

Homann, V.V., Sandy, M., Tincu, J.A., Templeton, A.S., Tebo, B.M., and Butler, A. (2009) Loihichelins A–F, a Suite of Amphiphilic Siderophores Produced by the Marine Bacterium *Halomonas* LOB-5. *Journal of Natural Products* **72**: 884-888.

Howat, A.M., Vollmers, J., Taubert, M., Grob, C., Dixon, J.L., Todd, J.D. et al. (2018) Comparative Genomics and Mutational Analysis Reveals a Novel XoxF-Utilizing Methylophile in the Roseobacter Group Isolated From the Marine Environment. *Frontiers in Microbiology* **9**.

Hsu, K.J. (1973) The origin of the Mediterranean evaporites. *Initial reports of the deep sea drilling project* **13**: 1203-1231.

Hu, Q.-Q., Zhou, Z.-C., Liu, Y.-F., Zhou, L., Mbadinga, S.M., Liu, J.-F. et al. (2019) High microbial diversity of the nitric oxide dismutation reaction revealed by PCR amplification and analysis of the nod gene. *International Biodeterioration & Biodegradation* **143**: 104708.

Huang, L., Liu, X., Rensing, C., Yuan, Y., Zhou, S., and Nealson, K.H. (2022) Light-independent anaerobic microbial oxidation of manganese driven by an electrosynthetic coculture. *The ISME Journal* **17**: 163-171.

Ito, T., and Deutsch, C. (2013) Variability of the oxygen minimum zone in the tropical North Pacific during the late twentieth century. *Global Biogeochemical Cycles* **27**: 1119-1128.

Jackson, M.P., and Hudec, M.R. (2017) *Salt tectonics: Principles and practice*: Cambridge University Press.

Jain, C., Rodriguez, R.L., Phillippy, A.M., Konstantinidis, K.T., and Aluru, S. (2018) High throughput ANI analysis of 90K prokaryotic genomes reveals clear species boundaries. *Nat Commun* **9**: 5114.

- Ji, Q., Babbin, A.R., Jayakumar, A., Oleynik, S., and Ward, B.B. (2015) Nitrous oxide production by nitrification and denitrification in the Eastern Tropical South Pacific oxygen minimum zone. *Geophysical Research Letters* **42**: 10,755-710,764.
- Ji, Q., Buitenhuis, E., Suntharalingam, P., Sarmiento, J.L., and Ward, B.B. (2018) Global Nitrous Oxide Production Determined by Oxygen Sensitivity of Nitrification and Denitrification. *Global Biogeochemical Cycles* **32**: 1790-1802.
- Johnson, J.E., Webb, S.M., Thomas, K., Ono, S., Kirschvink, J.L., and Fischer, W.W. (2013) Manganese-oxidizing photosynthesis before the rise of cyanobacteria. *Proceedings of the National Academy of Sciences* **110**: 11238-11243.
- Johnson, K.S., Coale, K.H., Berelson, W.M., and Gordon, R.M. (1996) On the formation of the manganese maximum in the oxygen minimum. *Geochimica et Cosmochimica Acta* **60**: 1291-1299.
- Jones, M.R., Luther, G.W., Mucci, A., and Tebo, B.M. (2019) Concentrations of reactive Mn(III)-L and MnO₂ in estuarine and marine waters determined using spectrophotometry and the leuco base, leucoberberlin blue. *Talanta* **200**: 91-99.
- Joye, S.B. (2015) Deepwater Horizon, 5 years on. *Science* **349**: 592-593.
- Joye, S.B., Samarkin, V.A., Orcutt, B.N., MacDonald, I.R., Hinrichs, K.-U., Elvert, M. et al. (2009) Metabolic variability in seafloor brines revealed by carbon and sulphur dynamics. *Nature Geoscience* **2**: 349-354.
- Jürgens, K., and Taylor, G.T. (2018) Microbial ecology and biogeochemistry of oxygen-deficient water columns. *Microbial Ecology of the Oceans, 3rd Edn, edited by: Gasol, JM and Kirchman, DL, John Wiley & Sons, Inc NJ, USA*: 231-288.
- Kalvelage, T., Jensen, M.M., Contreras, S., Revsbech, N.P., Lam, P., Günter, M. et al. (2011) Oxygen sensitivity of anammox and coupled N-cycle processes in oxygen minimum zones. *PLoS One* **6**: e29299.
- Kalvelage, T., Lavik, G., Lam, P., Contreras, S., Arteaga, L., Löscher, C.R. et al. (2013) Nitrogen cycling driven by organic matter export in the South Pacific oxygen minimum zone. *Nature Geoscience* **6**: 228-234.
- Kalyuzhnaya, M.G., Yang, S., Rozova, O.N., Smalley, N.E., Clubb, J., Lamb, A. et al. (2013) Highly efficient methane biocatalysis revealed in a methanotrophic bacterium. *Nature Communications* **4**: 2785.
- Kang, D.D., Li, F., Kirton, E., Thomas, A., Egan, R., An, H., and Wang, Z. (2019) MetaBAT 2: an adaptive binning algorithm for robust and efficient genome reconstruction from metagenome assemblies. *PeerJ* **7**: e7359.
- Karstensen, J., Stramma, L., and Visbeck, M. (2008) Oxygen minimum zones in the eastern tropical Atlantic and Pacific oceans. *Progress in Oceanography* **77**: 331-350.

- Karthikeyan, S., Rodriguez-R, L.M., Heritier-Robbins, P., Hatt, J.K., Huettel, M., Kostka, J.E., and Konstantinidis, K.T. (2020a) Genome repository of oil systems: An interactive and searchable database that expands the catalogued diversity of crude oil-associated microbes. *Environmental Microbiology* **22**: 2094-2106.
- Karthikeyan, S., Rodriguez, R.L., Heritier-Robbins, P., Hatt, J.K., Huettel, M., Kostka, J.E., and Konstantinidis, K.T. (2020b) Genome repository of oil systems: An interactive and searchable database that expands the catalogued diversity of crude oil-associated microbes. *Environ Microbiol* **22**: 2094-2106.
- Katoh, K., Rozewicki, J., and Yamada, K.D. (2019) MAFFT online service: multiple sequence alignment, interactive sequence choice and visualization. *Briefings in bioinformatics* **20**: 1160-1166.
- Kawasaki, T., Matsumura, Y., and Hasumi, H. (2022) Deep water pathways in the North Pacific Ocean revealed by Lagrangian particle tracking. *Scientific Reports* **12**: 6238.
- Kaye, J.Z., Sylvan, J.B., Edwards, K.J., and Baross, J.A. (2011) Halomonas and Marinobacter ecotypes from hydrothermal vent, seafloor and deep-sea environments. *FEMS Microbiology Ecology* **75**: 123-133.
- Keeling, R.E., Körtzinger, A., and Gruber, N. (2010) Ocean deoxygenation in a warming world. *Ann Rev Mar Sci* **2**: 199-229.
- Keltjens, J.T., Pol, A., Reimann, J., and Op den Camp, H.J. (2014) PQQ-dependent methanol dehydrogenases: rare-earth elements make a difference. *Appl Microbiol Biotechnol* **98**: 6163-6183.
- Kessler, W.S. (2006) The circulation of the eastern tropical Pacific: A review. *Progress in Oceanography* **69**: 181-217.
- Khmelenina, V.N., Colin Murrell, J., Smith, T.J., and Trotsenko, Y.A. (2018) Physiology and Biochemistry of the Aerobic Methanotrophs. In *Aerobic Utilization of Hydrocarbons, Oils and Lipids*. Rojo, F. (ed). Cham: Springer International Publishing, pp. 1-25.
- Kits, K.D., Klotz, M.G., and Stein, L.Y. (2015a) Methane oxidation coupled to nitrate reduction under hypoxia by the Gammaproteobacterium *Methylomonas denitrificans*, sp. nov. type strain FJG1. *Environmental Microbiology* **17**: 3219-3232.
- Kits, K.D., Campbell, D.J., Rosana, A.R., and Stein, L.Y. (2015b) Diverse electron sources support denitrification under hypoxia in the obligate methanotroph *Methylomicrobium album* strain BG8. *Frontiers in Microbiology* **6**.
- Kolmogorov, M., Bickhart, D.M., Behsaz, B., Gurevich, A., Rayko, M., Shin, S.B. et al. (2020) metaFlye: scalable long-read metagenome assembly using repeat graphs. *Nature Methods* **17**: 1103-1110.

- Koo, C.W., and Rosenzweig, A.C. (2021) Biochemistry of aerobic biological methane oxidation. *Chemical Society Reviews* **50**: 3424-3436.
- Kostka, J.E., Prakash, O., Overholt, W.A., Green, S.J., Freyer, G., Canion, A. et al. (2011) Hydrocarbon-degrading bacteria and the bacterial community response in gulf of Mexico beach sands impacted by the deepwater horizon oil spill. *Appl Environ Microbiol* **77**: 7962-7974.
- Kraft, B., Strous, M., and Tegetmeyer, H.E. (2011) Microbial nitrate respiration—genes, enzymes and environmental distribution. *Journal of biotechnology* **155**: 104-117.
- Kraft, B., Jehmlich, N., Larsen, M., Bristow, L.A., Könneke, M., Thamdrup, B., and Canfield, D.E. (2022) Oxygen and nitrogen production by an ammonia-oxidizing archaeon. *Science* **375**: 97-100.
- Kremling, K. (1999) Determination of the major constituents. In *Methods of Seawater Analysis*, pp. 229-251.
- Kwieceński, J.V., and Babbín, A.R. (2021) A High-Resolution Atlas of the Eastern Tropical Pacific Oxygen Deficient Zones. *Global Biogeochemical Cycles* **35**: e2021GB007001.
- Lampitt, R.S. (2001) Marine Snow*. In *Encyclopedia of Ocean Sciences (Second Edition)*. Steele, J.H. (ed). Oxford: Academic Press, pp. 686-694.
- Langmead, B., and Salzberg, S.L. (2012) Fast gapped-read alignment with Bowtie 2. *Nat Methods* **9**: 357-359.
- Lappan, R., Shelley, G., Islam, Z.F., Leung, P.M., Lockwood, S., Nauer, P.A. et al. (2023) Molecular hydrogen in seawater supports growth of diverse marine bacteria. *Nature Microbiology* **8**: 581-595.
- LaRowe, D.E., Carlson, H.K., and Amend, J.P. (2021) The Energetic Potential for Undiscovered Manganese Metabolisms in Nature. *Front Microbiol* **12**: 636145.
- Lavin, P., González, B., Santibáñez, J.F., Scanlan, D.J., and Ulloa, O. (2010) Novel lineages of *Prochlorococcus* thrive within the oxygen minimum zone of the eastern tropical South Pacific. *Environ Microbiol Rep* **2**: 728-738.
- Lay, C.Y., Mykytczuk, N.C., Niederberger, T.D., Martineau, C., Greer, C.W., and Whyte, L.G. (2012) Microbial diversity and activity in hypersaline high Arctic spring channels. *Extremophiles* **16**: 177-191.
- Lenton, T.M., and Watson, A.J. (2000a) Redfield revisited: 2. What regulates the oxygen content of the atmosphere? *Global Biogeochemical Cycles* **14**: 249-268.
- Lenton, T.M., and Watson, A.J. (2000b) Redfield revisited: 1. Regulation of nitrate, phosphate, and oxygen in the ocean. *Global Biogeochemical Cycles* **14**: 225-248.

- Leu, A.O., Eppley, J.M., Burger, A., and DeLong, E.F. (2022) Diverse Genomic Traits Differentiate Sinking-Particle-Associated versus Free-Living Microbes throughout the Oligotrophic Open Ocean Water Column. *mBio* **13**: e0156922.
- Li, H. (2018) Minimap2: pairwise alignment for nucleotide sequences. *Bioinformatics* **34**: 3094-3100.
- Lieberman, R.L., and Rosenzweig, A.C. (2005) Crystal structure of a membrane-bound metalloenzyme that catalyses the biological oxidation of methane. *Nature* **434**: 177-182.
- Lin, H., Ascher, D.B., Myung, Y., Lamborg, C.H., Hallam, S.J., Gionfriddo, C.M. et al. (2021) Mercury methylation by metabolically versatile and cosmopolitan marine bacteria. *ISME J* **15**: 1810-1825.
- Lipschultz, F., Wofsy, S.C., Ward, B.B., Codispoti, L.A., Friedrich, G., and Elkins, J.W. (1990) Bacterial transformations of inorganic nitrogen in the oxygen-deficient waters of the Eastern Tropical South Pacific Ocean. *Deep Sea Research Part A Oceanographic Research Papers* **37**: 1513-1541.
- Liu, L., Yang, Y., Deng, Y., and Zhang, T. (2022) Nanopore long-read-only metagenomics enables complete and high-quality genome reconstruction from mock and complex metagenomes. *Microbiome* **10**: 209.
- Liu, T., Qiu, Y., Lin, X., Ni, X., Wang, L., Li, H., and Jing, C. (2024) Dissolved Oxygen Recovery in the Oxygen Minimum Zone of the Arabian Sea in Recent Decade as Observed by BGC-Argo Floats. *Geophysical Research Letters* **51**: e2024GL108841.
- Liu, Y., Ai, G.-M., Miao, L.-L., and Liu, Z.-P. (2016) Marinobacter strain NNA5, a newly isolated and highly efficient aerobic denitrifier with zero N₂O emission. *Bioresource Technology* **206**: 9-15.
- Loginova, A.N., Thomsen, S., and Engel, A. (2016) Chromophoric and fluorescent dissolved organic matter in and above the oxygen minimum zone off Peru. *Journal of Geophysical Research: Oceans* **121**: 7973-7990.
- Lorenson, T.D., Cooper, A.K., Hart, P.E., and Winters, W.J. (2002) Geologic Setting and Context of Cores Taken During the IMAGES VIII/PAGE 127 Cruise of the RV Marion Dufresne in the Northern Gulf of Mexico.
- Luesken, F.A., Wu, M.L., Op den Camp, H.J.M., Keltjens, J.T., Stunnenberg, H., Francoijs, K.-J. et al. (2012) Effect of oxygen on the anaerobic methanotroph ‘Candidatus Methyloirabilis oxyfera’: kinetic and transcriptional analysis. *Environmental Microbiology* **14**: 1024-1034.
- Lutterbeck, H.E., Arévalo-Martínez, D.L., Löscher, C.R., and Bange, H.W. (2018) Nitric oxide (NO) in the oxygen minimum zone off Peru. *Deep Sea Res Part II Top Stud Oceanogr* **156**: 148-154.

- Luyten, J., Pedlosky, J., and Stommel, H. (1983) The ventilated thermocline. *Journal of Physical Oceanography* **13**: 292-309.
- Manz, W., Amann, R., Ludwig, W., Wagner, M., and Schleifer, K.-H. (1992) Phylogenetic oligodeoxynucleotide probes for the major subclasses of Proteobacteria: problems and solutions. *Systematic and Applied Microbiology* **15**: 593-600.
- Margolskee, A., Frenzel, H., Emerson, S., and Deutsch, C. (2019) Ventilation Pathways for the North Pacific Oxygen Deficient Zone. *Global Biogeochemical Cycles* **33**: 875-890.
- Martin, J.E., and Waters, L.S. (2022) Regulation of Bacterial Manganese Homeostasis and Usage During Stress Responses and Pathogenesis. *Frontiers in Molecular Biosciences* **9**.
- Mattes, T.E., Burke, S., Rocap, G., and Morris, R.M. (2022) Two metatranscriptomic profiles through low-dissolved-oxygen waters (DO, 0 to 33 μ M) in the Eastern Tropical North Pacific Ocean. *Microbiol Resour Announc* **11**: e01201-01221.
- McKay, L.J., Gutierrez, T., and Teske, A.P. (2016) Development of a group-specific 16S rRNA-targeted probe set for the identification of *Marinobacter* by fluorescence in situ hybridization. *Deep Sea Research Part II: Topical Studies in Oceanography* **129**: 360-367.
- Merino, N., Aronson, H.S., Bojanova, D.P., Feyhl-Buska, J., Wong, M.L., Zhang, S., and Giovannelli, D. (2019) Living at the extremes: extremophiles and the limits of life in a planetary context. *Frontiers in microbiology* **10**: 780.
- Merlino, G., Barozzi, A., Michoud, G., Ngugi, D.K., and Daffonchio, D. (2018) Microbial ecology of deep-sea hypersaline anoxic basins. *FEMS Microbiology Ecology* **94**.
- Mestre, M., Ruiz-González, C., Logares, R., Duarte, C.M., Gasol, J.M., and Sala, M.M. (2018) Sinking particles promote vertical connectivity in the ocean microbiome. *Proceedings of the National Academy of Sciences* **115**: E6799-E6807.
- Miller, A.R., Densmore, C.D., Degens, E.T., Hathaway, J.C., Manheim, F.T., McFarlin, P.F. et al. (1965) Hot brines and recent iron deposits in deeps of the Red Sea. In *Open-File Report*. Reston, VA.
- Mincer, T.J., and Aicher, A.C. (2016) Methanol production by a broad phylogenetic array of marine phytoplankton. *PloS one* **11**: e0150820.
- Moffett, J.W., Goepfert, T.J., and Naqvi, S.W.A. (2007) Reduced iron associated with secondary nitrite maxima in the Arabian Sea. *Deep Sea Research Part I: Oceanographic Research Papers* **54**: 1341-1349.

- Mogollón, J.M., Mewes, K., and Kasten, S. (2016) Quantifying manganese and nitrogen cycle coupling in manganese-rich, organic carbon-starved marine sediments: Examples from the Clarion-Clipperton fracture zone. *Geophysical Research Letters* **43**: 7114-7123.
- Morris, J.J., Kirkegaard, R., Szul, M.J., Johnson, Z.I., and Zinser, E.R. (2008) Facilitation of Robust Growth of *Prochlorococcus* Colonies and Dilute Liquid Cultures by *Helper*; Heterotrophic Bacteria. *Applied and Environmental Microbiology* **74**: 4530-4534.
- Müller, V., and Hess, V. (2017) The Minimum Biological Energy Quantum. *Frontiers in Microbiology* **8**.
- Murray, J.W., Codispoti, L.A., and Friederich, G.E. (1995) Oxidation-Reduction Environments. In *Aquatic Chemistry*: American Chemical Society, pp. 157-176.
- Murrell, J.C., Gilbert, B., and McDonald, I.R. (2000) Molecular biology and regulation of methane monooxygenase. *Archives of Microbiology* **173**: 325-332.
- Naqvi, W. (1991) Geographical extent of denitrification in the Arabian Sea in relation to some physical processes. *Oceanologica Acta* **14**: 281-290.
- Narvekar, J., Roy Chowdhury, R., Gaonkar, D., Kumar, P.K.D., and Prasanna Kumar, S. (2021) Observational evidence of stratification control of upwelling and pelagic fishery in the eastern Arabian Sea. *Scientific Reports* **11**: 7293.
- Nealson, K. (2006) The Prokaryotes. In, pp. 222-231.
- Neretin, L.N., Pohl, C., Jost, G., Leipe, T., and Pollehne, F. (2003) Manganese cycling in the Gotland deep, Baltic Sea. *Marine Chemistry* **82**: 125-143.
- Nguyen, L.T., Schmidt, H.A., von Haeseler, A., and Minh, B.Q. (2015) IQ-TREE: a fast and effective stochastic algorithm for estimating maximum-likelihood phylogenies. *Mol Biol Evol* **32**: 268-274.
- Niederberger, T.D., Perreault, N.N., Tille, S., Lollar, B.S., Lacrampe-Couloume, G., Andersen, D. et al. (2010) Microbial characterization of a subzero, hypersaline methane seep in the Canadian High Arctic. *The ISME Journal* **4**: 1326-1339.
- Nigro, L.M., Elling, F.J., Hinrichs, K.-U., Joye, S.B., and Teske, A. (2020) Microbial ecology and biogeochemistry of hypersaline sediments in Orca Basin. *PLOS ONE* **15**: e0231676.
- Niks, D., and Hille, R. (2019) Molybdenum- and tungsten-containing formate dehydrogenases and formylmethanofuran dehydrogenases: Structure, mechanism, and cofactor insertion. *Protein Sci* **28**: 111-122.
- Nurk, S., Meleshko, D., Korobeynikov, A., and Pevzner, P.A. (2017) metaSPAdes: a new versatile metagenomic assembler. *Genome Res* **27**: 824-834.

- Oldham, V., Owings, S., Jones, M., Tebo, B., and Luther, G. (2015) Evidence for the presence of strong Mn(III)-binding ligands in the water column of the Chesapeake Bay. *Marine Chemistry* **171**.
- Oldham, V.E., Jones, M.R., Tebo, B.M., and Luther, G.W. (2017) Oxidative and reductive processes contributing to manganese cycling at oxic-anoxic interfaces. *Marine Chemistry* **195**: 122-128.
- Pachiadaki, M.G., Yakimov, M.M., LaCono, V., Leadbetter, E., and Edgcomb, V. (2014) Unveiling microbial activities along the halocline of Thetis, a deep-sea hypersaline anoxic basin. *The ISME Journal* **8**: 2478-2489.
- Pack, M.A., Heintz, M.B., Reeburgh, W.S., Trumbore, S.E., Valentine, D.L., Xu, X., and Druffel, E.R. (2015) Methane oxidation in the eastern tropical North Pacific Ocean water column. *Journal of Geophysical Research: Biogeosciences* **120**: 1078-1092.
- Padilla, C.C., Bertagnolli, A.D., Bristow, L.A., Sarode, N., Glass, J.B., Thamdrup, B., and Stewart, F.J. (2017) Metagenomic Binning Recovers a Transcriptionally Active Gammaproteobacterium Linking Methanotrophy to Partial Denitrification in an Anoxic Oxygen Minimum Zone. *Frontiers in Marine Science* **4**.
- Padilla, C.C., Bristow, L.A., Sarode, N., Garcia-Robledo, E., Gómez Ramírez, E., Benson, C.R. et al. (2016) NC10 bacteria in marine oxygen minimum zones. *The ISME Journal* **10**: 2067-2071.
- Pan, S., Zhu, C., Zhao, X.-M., and Coelho, L.P. (2022) A deep siamese neural network improves metagenome-assembled genomes in microbiome datasets across different environments. *Nature Communications* **13**: 2326.
- Parks, D.H., Chuvochina, M., Rinke, C., Mussig, A.J., Chaumeil, P.-A., and Hugenholtz, P. (2021) GTDB: an ongoing census of bacterial and archaeal diversity through a phylogenetically consistent, rank normalized and complete genome-based taxonomy. *Nucleic Acids Research* **50**: D785-D794.
- Patel, A., Noble, R.T., Steele, J.A., Schwalbach, M.S., Hewson, I., and Fuhrman, J.A. (2007) Virus and prokaryote enumeration from planktonic aquatic environments by epifluorescence microscopy with SYBR Green I. *Nat Protoc* **2**: 269-276.
- Pautot, G., Guennoc, P., Coutelle, A., and Lyberis, N. (1984) Discovery of a large brine deep in the northern Red Sea. *Nature* **310**: 133-136.
- Peng, W., Qu, X., Shaik, S., and Wang, B. (2021) Deciphering the oxygen activation mechanism at the CuC site of particulate methane monooxygenase. *Nature Catalysis* **4**: 266-273.
- Pernthaler, A., Pernthaler, J., and Amann, R. (2002) Fluorescence in situ hybridization and catalyzed reporter deposition for the identification of marine bacteria. *Appl Environ Microbiol* **68**: 3094-3101.

- Pernthaler, J., Glöckner, F.-O., Schlönhuber, W., and Amann, R. (2001) Fluorescence in situ hybridization (FISH) with rRNA-targeted oligonucleotide probes. *Methods in Enzymology* **30**: 207-226.
- Pilcher, R.S., and Blumstein, R.D. (2007) Brine volume and salt dissolution rates in Orca Basin, northeast Gulf of Mexico. *AAPG Bulletin* **91**: 823-833.
- Polat, M., Liisberg, J.B., Krogsbøll, M., Blunier, T., and Johnson, M.S. (2021) Photochemical method for removing methane interference for improved gas analysis. *Atmos Meas Tech* **14**: 8041-8067.
- Raghoebarsing, A.A., Pol, A., van de Pas-Schoonen, K.T., Smolders, A.J.P., Ettwig, K.F., Rijpstra, W.I.C. et al. (2006) A microbial consortium couples anaerobic methane oxidation to denitrification. *Nature* **440**: 918-921.
- Ramachandran, A., and Walsh, D.A. (2015) Investigation of XoxF methanol dehydrogenases reveals new methylotrophic bacteria in pelagic marine and freshwater ecosystems. *FEMS Microbiology Ecology* **91**.
- Reid, J.L. (1965) Intermediate Waters of the Pacific Ocean. *Limnology and Oceanography* **11**: 313-316.
- Reis, P.C.J., Tsuji, J.M., Weiblen, C., Schiff, S.L., Scott, M., Stein, L.Y., and Neufeld, J.D. (2024) Enigmatic persistence of aerobic methanotrophs in oxygen-limiting freshwater habitats. *The ISME Journal* **18**.
- Revsbech, N.P., Larsen, L.H., Gundersen, J., Dalsgaard, T., Ulloa, O., and Thamdrup, B. (2009) Determination of ultra-low oxygen concentrations in oxygen minimum zones by the STOX sensor. *Limnology and Oceanography: Methods* **7**: 371-381.
- Richardson, D.J., Butt, J.N., Fredrickson, J.K., Zachara, J.M., Shi, L., Edwards, M.J. et al. (2012) The 'porin-cytochrome' model for microbe-to-mineral electron transfer. *Mol Microbiol* **85**: 201-212.
- Richardson, L.L., Aguilar, C., and Nealson, K.H. (1988) Manganese oxidation in pH and O₂ microenvironments produced by phytoplankton. *Limnology and Oceanography* **33**: 352-363.
- Rieck, A., Herlemann, D.P.R., Jürgens, K., and Grossart, H.-P. (2015) Particle-Associated Differ from Free-Living Bacteria in Surface Waters of the Baltic Sea. *Frontiers in Microbiology* **6**.
- Rimoldi, B., Alexander, J., and Morris, S. (1996) Experimental turbidity currents entering density-stratified water: analogues for turbidites in Mediterranean hypersaline basins. *Sedimentology* **43**: 527-540.

- Robbins, L.J., Fakhraee, M., Smith, A.J.B., Bishop, B.A., Swanner, E.D., Peacock, C.L. et al. (2023) Manganese oxides, Earth surface oxygenation, and the rise of oxygenic photosynthesis. *Earth-Science Reviews* **239**: 104368.
- Robinson, C. (2019) Microbial Respiration, the Engine of Ocean Deoxygenation. *Frontiers in Marine Science* **5**.
- Rodriguez-R, L.M., and Konstantinidis, K.T. (2016) The enveomics collection: a toolbox for specialized analyses of microbial genomes and metagenomes. *PeerJ Preprints* **4**: e1900v1901.
- Ross, M.O., and Rosenzweig, A.C. (2017) A tale of two methane monooxygenases. *J Biol Inorg Chem* **22**: 307-319.
- Ruff, S.E., Schwab, L., Vidal, E., Hemingway, J.D., Kraft, B., and Murali, R. (2024) Widespread occurrence of dissolved oxygen anomalies, aerobic microbes, and oxygen-producing metabolic pathways in apparently anoxic environments. *FEMS Microbiology Ecology* **100**.
- Ruiz-Perez, C.A., Bertagnolli, A.D., Tsementzi, D., Woyke, T., Stewart, F.J., and Konstantinidis, K.T. (2021) Description of *Candidatus Mesopelagibacter carboxydoxydans* and *Candidatus Anoxipelagibacter denitrificans*: Nitrate-reducing SAR11 genera that dominate mesopelagic and anoxic marine zones. *Syst Appl Microbiol* **44**: 126185.
- Saager, P.M., De Baar, H.J., and Burkill, P.H. (1989) Manganese and iron in Indian Ocean waters. *Geochimica et Cosmochimica Acta* **53**: 2259-2267.
- Sackett, W.M., Brooks, J.M., Bernard, B.B., Schwab, C.R., Chung, H., and Parker, R.A. (1979) A carbon inventory for Orca Basin brines and sediments. *Earth and Planetary Science Letters* **44**: 73-81.
- Sacks, L., and Barker, H. (1949) The influence of oxygen on nitrate and nitrite reduction. *Journal of Bacteriology* **58**: 11-22.
- Salomonsson, L., Reimann, J., Toshi, T., Krause, N., Gonska, N., Shiro, Y., and Ådelroth, P. (2012) Proton transfer in the quinol-dependent nitric oxide reductase from *Geobacillus stearothermophilus* during reduction of oxygen. *Biochimica et Biophysica Acta (BBA) - Bioenergetics* **1817**: 1914-1920.
- Sanford, R.A., Wagner, D.D., Wu, Q., Chee-Sanford, J.C., Thomas, S.H., Cruz-García, C. et al. (2012) Unexpected nondenitrifier nitrous oxide reductase gene diversity and abundance in soils. *Proceedings of the National Academy of Sciences* **109**: 19709-19714.
- Sansone, F.J., Popp, B.N., Gasc, A., Graham, A.W., and Rust, T.M. (2001) Highly elevated methane in the eastern tropical North Pacific and associated isotopically enriched fluxes to the atmosphere. *Geophysical Research Letters* **28**: 4567-4570.

- Sarma, V.V.S.S. (2002) An evaluation of physical and biogeochemical processes regulating the oxygen minimum zone in the water column of the Bay of Bengal. *Global Biogeochemical Cycles* **16**: 46-41-46-10.
- Sarma, V.V.S.S., and Udaya Bhaskar, T.V.S. (2018) Ventilation of Oxygen to Oxygen Minimum Zone Due to Anticyclonic Eddies in the Bay of Bengal. *Journal of Geophysical Research: Biogeosciences* **123**: 2145-2153.
- Sawyer, D.E., Mason, R.A., Cook, A.E., and Portnov, A. (2019) Submarine Landslides Induce Massive Waves in Subsea Brine Pools. *Sci Rep* **9**: 128.
- Schindelin, J., Arganda-Carreras, I., Frise, E., Kaynig, V., Longair, M., Pietzsch, T. et al. (2012) Fiji: an open-source platform for biological-image analysis. *Nature Methods* **9**: 676-682.
- Schinke, H., and Matthäus, W. (1998) On the causes of major Baltic inflows —an analysis of long time series. *Continental Shelf Research* **18**: 67-97.
- Schmidt, M., Al-Farawati, R., and Botz, R. (2015) Geochemical Classification of Brine-Filled Red Sea Deeps. In, pp. 219-233.
- Schmidtko, S., Stramma, L., and Visbeck, M. (2017) Decline in global oceanic oxygen content during the past five decades. *Nature* **542**: 335-339.
- Schmitz, R.A., Peeters, S.H., Mohammadi, S.S., Berben, T., van Erven, T., Iosif, C.A. et al. (2023) Simultaneous sulfide and methane oxidation by an extremophile. *Nat Commun* **14**: 2974.
- Schorn, S., Graf, J.S., Littmann, S., Hach, P.F., Lavik, G., Speth, D.R. et al. (2024) Persistent activity of aerobic methane-oxidizing bacteria in anoxic lake waters due to metabolic versatility. *Nature Communications* **15**: 5293.
- Sheehan, P.M.F., Webber, B.G.M., Sanchez-Franks, A., Matthews, A.J., Heywood, K.J., and Vinayachandran, P.N. (2020) Injection of Oxygenated Persian Gulf Water Into the Southern Bay of Bengal. *Geophysical Research Letters* **47**: e2020GL087773.
- Shi, L., Fredrickson, J.K., and Zachara, J.M. (2014) Genomic analyses of bacterial porin-cytochrome gene clusters. *Front Microbiol* **5**: 657.
- Shokes, R.F., Trabant, P.K., Presley, B.J., and Reid, D.F. (1977) Anoxic, Hypersaline Basin in the Northern Gulf of Mexico. *Science* **196**: 1443-1446.
- Simon, J., Gross, R., Einsle, O., Kroneck, P.M., Kroger, A., and Klimmek, O. (2000) A NapC/NirT-type cytochrome c (NrfH) is the mediator between the quinone pool and the cytochrome c nitrite reductase of *Wolinella succinogenes*. *Mol Microbiol* **35**: 686-696.
- Sousa, F.L., Alves, R.J., Ribeiro, M.A., Pereira-Leal, J.B., Teixeira, M., and Pereira, M.M. (2012) The superfamily of heme–copper oxygen reductases: Types and

evolutionary considerations. *Biochimica et Biophysica Acta (BBA) - Bioenergetics* **1817**: 629-637.

Speth, D.R., Lagkouravdos, I., Wang, Y., Qian, P.-Y., Dutilh, B.E., and Jetten, M.S. (2017) Draft genome of *Scalindua rubra*, obtained from the interface above the discovery deep brine in the Red Sea, sheds light on potential salt adaptation strategies in anammox bacteria. *Microbial ecology* **74**: 1-5.

Stan-Lotter, H., and Fendrihan, S. (2012) Adaption of microbial life to environmental extremes. *Springer* **10**: 978-973.

Stein, L.Y., La Duc, M.T., Grundl, T.J., and Nealson, K.H. (2001) Bacterial and archaeal populations associated with freshwater ferromanganous micronodules and sediments. *Environ Microbiol* **3**: 10-18.

Steinsdóttir, H.G., Gómez-Ramírez, E., Mhatre, S., Schauburger, C., Bertagnolli, A.D., Pratte, Z.A. et al. (2022a) Anaerobic methane oxidation in a coastal oxygen minimum zone: spatial and temporal dynamics. *Environmental Microbiology*.

Steinsdóttir, H.G.R., Schauburger, C., Mhatre, S., Thamdrup, B., and Bristow, L.A. (2022b) Aerobic and anaerobic methane oxidation in a seasonally anoxic basin. *Limnology and Oceanography* **67**: 1257-1273.

Stramma, L., Johnson, G.C., Sprintall, J., and Mohrholz, V. (2008) Expanding Oxygen-Minimum Zones in the Tropical Oceans. *Science* **320**: 655-658.

Stüeken, E.E., Long, A., Rochelle-Bates, N., and Teske, A. (2024) Deep-Marine Brine Seeps Stimulate Microbial Nitrogen Cycling: Implications for the Formation of Sediment-Hosted Ore Deposits. *Journal of Geophysical Research: Biogeosciences* **129**: e2024JG008189.

Sun, X., Frey, C., Garcia-Robledo, E., Jayakumar, A., and Ward, B.B. (2021) Microbial niche differentiation explains nitrite oxidation in marine oxygen minimum zones. *The ISME journal* **15**: 1317-1329.

Szeinbaum, N., Nunn, B.L., Cavazos, A.R., Crowe, S.A., Stewart, F.J., DiChristina, T.J. et al. (2020) Novel insights into the taxonomic diversity and molecular mechanisms of bacterial Mn(III) reduction. *Environ Microbiol Rep* **12**: 583-593.

Taylor, G.T., Suter, E.A., Pachiadaki, M.G., Astor, Y., Edgcomb, V.P., and Scranton, M.I. (2018) Temporal shifts in dominant sulfur-oxidizing chemoautotrophic populations across the Cariaco Basin's redoxcline. *Deep Sea Research Part II: Topical Studies in Oceanography* **156**: 80-96.

Tebo, B.M. (1991) Manganese(II) oxidation in the suboxic zone of the Black Sea. *Deep Sea Research Part A Oceanographic Research Papers* **38**: S883-S905.

- Tebo, B.M., and Emerson, S. (1986) Microbial manganese (II) oxidation in the marine environment: a quantitative study. *Biogeochemistry* **2**: 149-161.
- Tebo, B.M., Johnson, H.A., McCarthy, J.K., and Templeton, A.S. (2005) Geomicrobiology of manganese (II) oxidation. *TRENDS in Microbiology* **13**: 421-428.
- Tebo, B.M., Bargar, J.R., Clement, B.G., Dick, G.J., Murray, K.J., Parker, D. et al. (2004) BIOGENIC MANGANESE OXIDES: Properties and Mechanisms of Formation. *Annual Review of Earth and Planetary Sciences* **32**: 287-328.
- Templeton, A., Staudigel, H., and Tebo, B. (2005) Diverse Mn(II)Oxidizing Bacteria Isolated from Submarine Basalts at Loihi Seamount. *Geomicrobiology Journal - GEOMICROBIOL J* **22**: 127-139.
- Thamdrup, B. (2012) New Pathways and Processes in the Global Nitrogen Cycle. *Annual Review of Ecology, Evolution, and Systematics* **43**: 407-428.
- Thamdrup, B., Dalsgaard, T., and Revsbech, N.P. (2012) Widespread functional anoxia in the oxygen minimum zone of the Eastern South Pacific. *Deep Sea Research Part I: Oceanographic Research Papers* **65**: 36-45.
- Thamdrup, B., Steinsdottir, H.G.R., Bertagnolli, A., Padilla, C., Patin, N.V., Garcia-Robledo, E. et al. (2019) Anaerobic methane oxidation is an important sink for methane in the ocean's largest oxygen minimum zone. *Limnology and Oceanography* **64**: 2569-2585.
- Torres, J.J., Grigsby, M.D., and Clarke, M.E. (2012) Aerobic and anaerobic metabolism in oxygen minimum layer fishes: the role of alcohol dehydrogenase. *J Exp Biol* **215**: 1905-1914.
- Torres-Beltrán, M., Hawley, A.K., Capelle, D., Zaikova, E., Walsh, D.A., Mueller, A. et al. (2017) A compendium of geochemical information from the Saanich Inlet water column. *Sci Data* **4**: 170159.
- Trapnell, C., Roberts, A., Goff, L., Pertea, G., Kim, D., Kelley, D.R. et al. (2012) Differential gene and transcript expression analysis of RNA-seq experiments with TopHat and Cufflinks. *Nat Protoc* **7**: 562-578.
- Trefry, J.H., and Presley, B.J. (1982) Manganese fluxes from Mississippi Delta sediments. *Geochimica et Cosmochimica Acta* **46**: 1715-1726.
- Trefry, J.H., Presley, B.J., Keeney-Kennicutt, W.L., and Trocine, R.P. (1984) Distribution and chemistry of manganese, iron, and suspended particulates in Orca Basin. *Geo-Marine Letters* **4**: 125-130.
- Trifinopoulos, J., Nguyen, L.T., von Haeseler, A., and Minh, B.Q. (2016) W-IQ-TREE: a fast online phylogenetic tool for maximum likelihood analysis. *Nucleic Acids Res* **44**: W232-235.

- Tsantilas, K.A., Merrihew, G.E., Robbins, J.E., Johnson, R.S., Park, J., Plubell, D.L. et al. (2024) A framework for quality control in quantitative proteomics. *bioRxiv*.
- Tsementzi, D., Wu, J., Deutsch, S., Nath, S., Rodriguez, R.L., Burns, A.S. et al. (2016) SAR11 bacteria linked to ocean anoxia and nitrogen loss. *Nature* **536**: 179-183.
- Tucker, N.P., Le Brun, N.E., Dixon, R., and Hutchings, M.I. (2010) There's NO stopping NsrR, a global regulator of the bacterial NO stress response. *Trends Microbiol* **18**: 149-156.
- Tully, B.J., Graham, E.D., and Heidelberg, J.F. (2018) The reconstruction of 2,631 draft metagenome-assembled genomes from the global oceans. *Scientific data* **5**: 1-8.
- Ulloa, O., Canfield, D.E., DeLong, E.F., Letelier, R.M., and Stewart, F.J. (2012) Microbial oceanography of anoxic oxygen minimum zones. *Proceedings of the National Academy of Sciences* **109**: 15996-16003.
- Ulloa, O., Henríquez-Castillo, C., Ramírez-Flandes, S., Plominsky, A.M., Murillo, A.A., Morgan-Lang, C. et al. (2021) The cyanobacterium *Prochlorococcus* has divergent light-harvesting antennae and may have evolved in a low-oxygen ocean. *Proceedings of the National Academy of Sciences* **118**: e2025638118.
- Uritskiy, G.V., DiRuggiero, J., and Taylor, J. (2018) MetaWRAP—a flexible pipeline for genome-resolved metagenomic data analysis. *Microbiome* **6**: 158.
- Uzun, M., Alekseeva, L., Krutkina, M., Koziyeva, V., and Grouzdev, D. (2020) Unravelling the diversity of magnetotactic bacteria through analysis of open genomic databases. *Sci Data* **7**: 252.
- Valentine, D.L., Fisher, G.B., Bagby, S.C., Nelson, R.K., Reddy, C.M., Sylva, S.P., and Woo, M.A. (2014) Fallout plume of submerged oil from *Deepwater Horizon*. *Proceedings of the National Academy of Sciences* **111**: 15906-15911.
- Van Cappellen, P., Viollier, E., Roychoudhury, A., Clark, L., Ingall, E., Lowe, K., and Dichristina, T. (1998) Biogeochemical Cycles of Manganese and Iron at the Oxic–Anoxic Transition of a Stratified Marine Basin (Orca Basin, Gulf of Mexico). *Environmental Science & Technology* **32**: 2931-2939.
- Varrella, S., Tangherlini, M., and Corinaldesi, C. (2020) Deep Hypersaline Anoxic Basins as Untapped Reservoir of Polyextremophilic Prokaryotes of Biotechnological Interest. *Mar Drugs* **18**.
- Vaser, R., Sović, I., Nagarajan, N., and Šikić, M. (2017) Fast and accurate de novo genome assembly from long uncorrected reads. *Genome Res* **27**: 737-746.
- Vedamati, J., Chan, C., and Moffett, J. (2014) Distribution of dissolved manganese in the Peruvian Upwelling and Oxygen Minimum Zone. *Geochimica et Cosmochimica Acta* **156**.

- Wallmann, K., Suess, E., Westbrook, G.H., Winckler, G., and Cita, M.B. (1997) Salty brines on the Mediterranean sea floor. *Nature* **387**: 31-32.
- Wang, H., Li, H., Shao, Z., Liao, S., Johnstone, L., Rensing, C., and Wang, G. (2012) Genome Sequence of Deep-Sea Manganese-Oxidizing Bacterium *Marinobacter manganooxydans* MnI7-9. *Journal of Bacteriology* **194**: 899-900.
- Ward, B.B. (2013) How nitrogen is lost. *Science* **341**: 352-353.
- Ward, B.B., and Zafiriou, O.C. (1988) Nitrification and nitric oxide in the oxygen minimum of the eastern tropical North Pacific. *Deep Sea Res Part A Oceanogr Res Pap* **35**: 1127-1142.
- Ward, B.B., Tuit, C.B., Jayakumar, A., Rich, J.J., Moffett, J., and Naqvi, S.W.A. (2008) Organic carbon, and not copper, controls denitrification in oxygen minimum zones of the ocean. *Deep Sea Research Part I: Oceanographic Research Papers* **55**: 1672-1683.
- Wasser, I.M., De Vries, S., Moëgne-Loccoz, P., Schröder, I., and Karlin, K.D. (2002) Nitric oxide in biological denitrification: Fe/Cu metalloenzyme and metal complex NO x redox chemistry. *Chemical Reviews* **102**: 1201-1234.
- Wen, B., Hsu, C., Zeng, W.F., Riffle, M., Chang, A., Mudge, M. et al. (2024) Carafe enables high quality in silico spectral library generation for data-independent acquisition proteomics. *bioRxiv*.
- Whelan, J.K., Oremland, R.S., Tarafa, M., Smith, R., Howarth, R., and Lee, C. (1986) (Table 2) Concentrations of interstitial water, methanes, and other sediment components at DSDP Hole 96-618. In *In supplement to: Whelan, JK et al (1986): Evidence for sulfate-reducing and methane-producing microorganisms in sediments from Sites 618, 619, and 622 In: Bouma, AH; Coleman, JM; Meyer, AW; et al (eds), Initial Reports of the Deep Sea Drilling Project, Washington (US Govt Printing Office), 96, 767-775, <https://doi.org/10.2973/dsdpproc961471986>: PANGAEA.*
- Wiesenburg, D.A., Brooks, J.M., and Bernard, B.B. (1985) Biogenic hydrocarbon gases and sulfate reduction in the Orca Basin brine. *Geochimica et Cosmochimica Acta* **49**: 2069-2080.
- Woehle, C., Roy, A.S., Glock, N., Wein, T., Weissenbach, J., Rosenstiel, P. et al. (2018) A novel eukaryotic denitrification pathway in foraminifera. *Curr Biol* **28**: 2536-2543 e2535.
- Wong, J.C.Y., Raven, J.A., Aldunate, M., Silva, S., Gaitán-Espitia, J.D., Vargas, C.A. et al. (2023) Do phytoplankton require oxygen to survive? A hypothesis and model synthesis from oxygen minimum zones. *Limnology and Oceanography* **68**: 1417-1437.
- Wright, J.J., Konwar, K.M., and Hallam, S.J. (2012) Microbial ecology of expanding oxygen minimum zones. *Nature Reviews Microbiology* **10**: 381-394.

- Wu, Ming L., Ettwig, Katharina F., Jetten, Mike S.M., Strous, M., Keltjens, Jan T., and Niftrik, Laura v. (2011) A new intra-aerobic metabolism in the nitrite-dependent anaerobic methane-oxidizing bacterium Candidatus 'Methyloirabilis oxyfera'. *Biochemical Society Transactions* **39**: 243-248.
- Wu, Y.-W., Simmons, B.A., and Singer, S.W. (2015) MaxBin 2.0: an automated binning algorithm to recover genomes from multiple metagenomic datasets. *Bioinformatics* **32**: 605-607.
- Wu, Y.W., Simmons, B.A., and Singer, S.W. (2016) MaxBin 2.0: an automated binning algorithm to recover genomes from multiple metagenomic datasets. *Bioinformatics* **32**: 605-607.
- Wyrski, K. (1962) The oxygen minima in relation to ocean circulation. In *Deep Sea research and oceanographic abstracts*: Elsevier, pp. 11-23.
- Yamamoto, I., and Ishimoto, M. (1977) Anaerobic growth of *Escherichia coli* on formate by reduction of nitrate, fumarate, and trimethylamine N-oxide. *Zeitschrift für allgemeine Mikrobiologie* **17**: 235-242.
- Yang, S., Chang, B.X., Warner, M.J., Weber, T.S., Bourbonnais, A.M., Santoro, A.E. et al. (2020) Global reconstruction reduces the uncertainty of oceanic nitrous oxide emissions and reveals a vigorous seasonal cycle. *Proc Natl Acad Sci U S A* **117**: 11954-11960.
- Yang, T., Nigro, L.M., Gutierrez, T., D'Ambrosio, L., Joye, S.B., Highsmith, R., and Teske, A. (2016) Pulsed blooms and persistent oil-degrading bacterial populations in the water column during and after the Deepwater Horizon blowout. *Deep Sea Research Part II: Topical Studies in Oceanography* **129**: 282-291.
- Yanpirat, P., Nakatsuji, Y., Hiraga, S., Fujitani, Y., Izumi, T., Masuda, S. et al. (2020) Lanthanide-Dependent Methanol and Formaldehyde Oxidation in *Methylobacterium aquaticum* Strain 22A. *Microorganisms* **8**.
- Yli-Hemminki, P., Jørgensen, K.S., and Lehtoranta, J. (2014) Iron–Manganese Concretions Sustaining Microbial Life in the Baltic Sea: The Structure of the Bacterial Community and Enrichments in Metal-Oxidizing Conditions. *Geomicrobiology Journal* **31**: 263-275.
- Yu, H., and Leadbetter, J.R. (2020) Bacterial chemolithoautotrophy via manganese oxidation. *Nature* **583**: 453-458.
- Yu, N.Y., Wagner, J.R., Laird, M.R., Melli, G., Rey, S., Lo, R. et al. (2010) PSORTb 3.0: improved protein subcellular localization prediction with refined localization subcategories and predictive capabilities for all prokaryotes. *Bioinformatics* **26**: 1608-1615.

- Zallot, R., Oberg, N., and Gerlt, J.A. (2019) The EFI web resource for genomic enzymology tools: leveraging protein, genome, and metagenome databases to discover novel enzymes and metabolic pathways. *Biochemistry* **58**: 4169-4182.
- Zedelius, J., Rabus, R., Grundmann, O., Werner, I., Brodkorb, D., Schreiber, F. et al. (2011) Alkane degradation under anoxic conditions by a nitrate-reducing bacterium with possible involvement of the electron acceptor in substrate activation. *Environmental microbiology reports* **3**: 125-135.
- Zhang, I.H., Sun, X., Jayakumar, A., Fortin, S.G., Ward, B.B., and Babbitt, A.R. (2023) Partitioning of the denitrification pathway and other nitrite metabolisms within global oxygen deficient zones. *ISME Communications* **3**.
- Zheng, R., Wang, C., Wang, H., Qi, H., and Sun, C. (2025) Nitrate-driven dark oxygen production by diverse deep-sea microorganisms. *bioRxiv*: 2025.2003.2010.642362.
- Zhu, B., Wang, J., Bradford, L.M., Ettwig, K., Hu, B., and Lueders, T. (2019) Nitric Oxide Dismutase (nod) Genes as a Functional Marker for the Diversity and Phylogeny of Methane-Driven Oxygenic Denitrifiers. *Front Microbiol* **10**: 1577.
- Zhu, B., Wang, Z., Kanaparthi, D., Kublik, S., Ge, T., Casper, P. et al. (2020) Long-Read Amplicon Sequencing of Nitric Oxide Dismutase (nod) Genes Reveal Diverse Oxygenic Denitrifiers in Agricultural Soils and Lake Sediments. *Microbial Ecology* **80**: 243-247.
- Zhu, B., Bradford, L., Huang, S., Szalay, A., Leix, C., Weissbach, M. et al. (2017) Unexpected diversity and high abundance of putative nitric oxide dismutase (Nod) genes in contaminated aquifers and wastewater treatment systems. *Applied and environmental microbiology* **83**: e02750-02716.
- Zhuang, G.-C., Elling, F.J., Nigro, L.M., Samarkin, V., Joye, S.B., Teske, A., and Hinrichs, K.-U. (2016) Multiple evidence for methylotrophic methanogenesis as the dominant methanogenic pathway in hypersaline sediments from the Orca Basin, Gulf of Mexico. *Geochimica et Cosmochimica Acta* **187**: 1-20.
- Zumft, W.G. (1997) Cell biology and molecular basis of denitrification. *Microbiology and molecular biology reviews* **61**: 533-616.
- Zumft, W.G. (2005) Nitric oxide reductases of prokaryotes with emphasis on the respiratory, heme-copper oxidase type. *Journal of inorganic biochemistry* **99**: 194-215.